UNIVERSITÀ DEL PIEMONTE ORIENTALE

UNIVERSITÀ DEGLI STUDI DEL PIEMONTE ORIENTALE

"AMEDEO AVOGADRO"

Department of Sciences and Technological Innovation

Master's Degree in Chemical Sciences

DEVELOPMENT AND CHARACTERIZATION OF NOVEL CANs (COVALENT ADAPTABLE NETWORKS) BASED ON ACRYLATE-AMINE NETWORKS VIA DYNAMIC CHEMISTRY

SUPERVISOR:

Prof. Michele Laus

CO-SUPERVISORS:

Dott. Riccardo Chiarcos

Dott. Diego Antonioli

CANDIDATE:

Mattia Lippelli

Academic year 2025/2026

Table of contents:

1. Introduction

Since the formulation of Hermann Staudinger's macromolecular hypothesis in 1920, the understanding of how molecular structure determines the macroscopic properties of polymeric materials has revolutionized modern industry[1]. For decades, materials science has operated according to a rigid dichotomy: thermoplastics, consisting of unlinked chains capable of flowing in the molten state to be reprocessed, and thermosets, whose permanently crosslinked networks offer exceptional thermal and mechanical stability at the price of a near-total absence of recyclability[1–4]. However, the current global crisis resulting from the accumulation of plastic waste has made the development of a new generation of materials combining the durability of thermosets with the processability of thermoplastics increasingly urgent[2,4]. In this context, Covalent Adaptable Networks (CANs) have emerged as a transformative paradigm. CANs are polymeric materials where the covalent bonds forming the network are not permanent but can undergo dynamic exchange reactions in response to external stimuli such as heat, light, or pH variations[1–4]. This ability to activate a "dormant plasticity" allows the material to relax internal stresses, repair structural damage, or be completely reshaped, while maintaining the high mechanical performance typical of crosslinked networks[1–4].

From a mechanistic standpoint, reactions within CANs are generally divided into two categories: dissociative and associative[3–5]. In dissociative processes, such as the Diels-Alder reaction, bonds are broken before reforming, leading to a temporary decrease in crosslink density and material viscosity. Conversely, associative mechanisms involve the breaking of a bond occurring simultaneously with the formation of a new one, thereby ensuring constant network connectivity throughout the exchange process. This latter class forms the foundation of vitrimers, introduced by Leibler in 2011, which exhibit a rheological behavior similar to vitreous silica[2–4,6]. A distinctive property of vitrimers is the topology freezing transition temperature (T_v), below which chemical exchanges become negligible on experimental timescales, effectively fixing the material's shape[1,4,7].

1.1 CANs (Covalent Adaptable Networks)

Covalent Adaptable Networks (CANs) are crosslinked polymer structures that incorporate dynamic covalent bonds, capable of undergoing reversible exchange reactions when subjected to specific stimuli, such as thermal, catalytic, photochemical, or pH variations[1-7]. In contrast to conventional thermosetting polymers, which are fundamentally unrecyclable, the dynamic nature of these crosslinks enables the recycling and reprocessing of CANs. This grants them unique properties, including creep resistance at low temperatures and malleability or plasticity at higher temperatures.

In CANs, bond exchange processes are generally slower than the glass transition of the polymer[1,2,5,7,8]. Consequently, polymer relaxation cannot be defined by a single, unique relaxation time value; instead, it must be described by a continuous relaxation time spectrum, $H(\tau, T)$, which is a function of both time and temperature and defines the total fraction of the network that undergoes relaxation at each specific timescale and temperature[8]. In these adaptive networks, this function presents two distinct thermomechanical transitions, which result in two separate relaxation peaks in the $H_{Glass}(\tau, T)$. The first is the glass-to-rubber relaxation, described by the spectrum indicated as $H_{Glass}(\tau, T)$, which involves cooperative motions at the level of polymer segments on a scale of 1-3 nanometers[8]. In particular, in this stage the relaxation of the polymer segments between different crosslinking points occurs and it is related only to the molecular mobility. The second is the rubber-to-liquid relaxation, described by the spectrum indicated as $H_{Network}(\tau, T)$, which is shifted to longer times. This latter transition derives from the chemical exchange of the cross-links and involves mobility on the scale of the entire network mesh[8]. This second phenomenon is related with reaction kinetics and the density of reactive sites present in the material. The flow capacity of these materials is determined by the zero-shear viscosity, denoted as η_0, which in CANs is essentially driven by the covalent exchange of bonds[4,5,8]. The reference literature[8] expresses this viscosity through an integral, where $\eta_0(T)$ is calculated as the integral from negative to positive infinity of the product of the relaxation time τ and the sum of the glass and network

relaxation spectra, integrated over d(ln(τ)) such as is describe in the follwing Eq.1.

$$\eta_0(T) = \int_{-\infty}^{+\infty} \tau[\, H_{Glass}(\ln \tau, T) + H_{Network}(\ln \tau, T)]\, d(\ln(\tau)) \qquad [Eq.1]$$

In this mathematical formulation, $\eta_0(T)$ represents the zero-shear viscosity as a function of temperature T, while τ indicates the relaxation time. The terms $H_{Glass}(\ln \tau, T)$ and $H_{Network}(\ln \tau, T)$ represent the respective contributions to the relaxation spectrum due to the glass transition and the network exchanges. Because the relaxation of the network requires much longer times and dominates the macroscopic flow at elevated temperatures, the glass contribution becomes negligible for the calculation of viscosity[8], allowing the integral to be approximated using only the network contribution, Eq.2.

$$\eta_0(T) = \int_{-\infty}^{+\infty} \tau[\, H_{Network}(\ln \tau, T)]\, d(\ln(\tau)) \qquad [Eq.2]$$

Furthermore, many dynamic networks exhibit a very narrow distribution of relaxation times. Specifically, $H_{Network}(\ln \tau, T)$ is approximately zero for all times not equal to $\tau^*(T)$, where $\tau^*(T)$, is the principal relaxation time of the network[8]. Thanks to this assumption, the viscosity can be approximated as the product of only two terms: the principal relaxation time $\tau^*(T)$ and the rubbery plateau modulus $G_0(T)$, as shown in Eq.3. This plateau modulus is directly proportional to the cross-link density of the material.

$$\eta_0(T) = \tau^*(T) \int_{-\infty}^{+\infty} [\, H_{Network}(\ln \tau, T)]\, d(\ln(\tau)) \approx \tau^*(T) * G_0(T) \qquad [Eq.3]$$

Interestingly, Eq. 3 clearly shows the viscoelastic nature of polymers, in which an applied tension promotes both the molecular flow (the τ* term) and an elastic response (the G_0) term.

1.1.1 Dissociative mechanism

In dissociative networks, bonds break before they can reform[3–5,8]. This introduces a very strong thermodynamic dependence: as the temperature increases, the reaction equilibrium shifts towards dissociation[3–5,8]. This leads to a decrease in the number of crosslinking points that influences both the kinetics of the reaction (τ^* term in Eq. 3) itself and the G_0 term of Eq. 3. The association equilibrium constant (K_a) is defined as Eq.4:

$$K_a = \frac{k_{-1}}{k} \qquad \text{[Eq.4]}$$

where k_{-1} is the bond formation rate and k is the bond scission rate. The K_a dependence on the T is related to the enthalpy of the reversible reaction (ΔH_r^0).

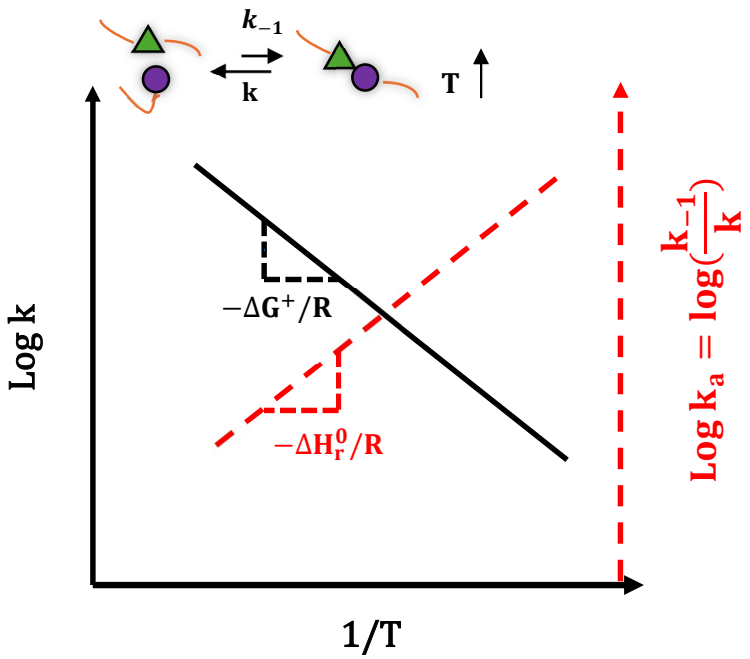

Figure 1. *Overall exchange mechanisms at stake in the network relaxation and corresponding thermodynamic parameters (k being the apparent rate of exchange and* $K_a = \frac{k_{-1}}{k}$ *the apparent association equilibrium constant).*

The upper panel of Fig.1 illustrates the fundamental distinction in the temperature dependence of exchange kinetics and chemical equilibrium for dissociative networks. The exchange rate constant of the reverse reaction ($\log k$, represented by the solid black line) follows an Arrhenius dependence[3–5,8–10], where the slope is governed by the Gibbs free energy of

activation ($\frac{-\Delta G^{++}}{R}$). This indicates that the rate of bond dissociation increases exponentially as the temperature rises (moving to the left along the $\frac{1}{T}$ axis).

The association equilibrium constant ($K_a = \frac{k_{-1}}{k}$, dashed orange line) in dissociative systems is highly sensitive to thermal variations. The slope of this relationship is dictated by the standard enthalpy of reaction ($\frac{-\Delta H_r^0}{R}$)[5,8,9]. Because the reaction of breaking cross-links is typically endothermic, the association equilibrium constant K_a exhibits a positive slope relative to $\frac{1}{T}$. Consequently, as temperature increases, the value of $\log(K_a)$ decreases, shifting the equilibrium toward a dissociated state. This thermodynamic shift results in a significant reduction in the effective cross-link density (ν) of the material[3–5,8–10].

The increase of T then influences the polymer chain mobility, the reversible reaction rate and the crosslinking point density which is in turn linked to both of the two previous factors[5,8]. For these reasons, as the temperature increases the system progresses through various visco-elastic stages, characterized by a sharp decline in cross-link density that leads to the gel point[8], as illustrated in Fig.2. At this critical threshold, the material undergoes a macrostructure change, transitioning from a cross-linked viscoelastic solid to a viscoelastic liquid as the network loses its structural integrity due to excessive bond dissociation[8].

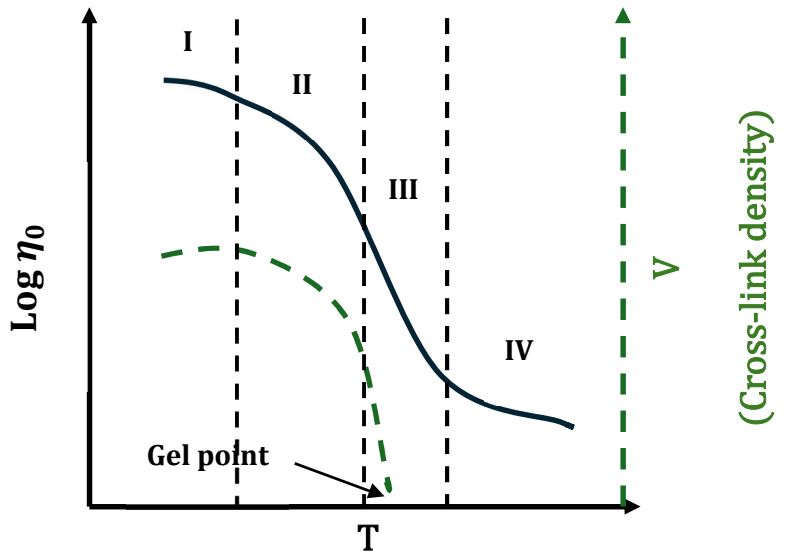

Figure 2. *Evolutions of zero-shear viscosity $\eta_0(T)$ and cross-link density at temperatures above the glass transition.*

In details, several different viscosity regimes are observed as a function of T (see Figure 2).

Regime I (Low-Temperature Latency)[8], in this stage, the degree of dissociation remains negligible, and the network maintains its maximum cross-link density[8]. Although macroscopic properties appear stable, internal structural rearrangements still occur via a subtle, localized dissociation-reassociation mechanism. Rheologically, these materials are virtually indistinguishable from vitrimers; they are characterized by two distinct relaxation spectra $H_{Glass}(\ln\tau, T)$ and $H_{Network}(\ln\tau, T)$ with viscosity being dictated solely by exchange kinetics[5,8].

Regime II (Structural Softening) as temperatures rise, dissociation levels become significant enough to impact the network's integrity[8]. This leads to a noticeable drop in cross-link density, evidenced by a decrease in the amplitude of $H_{Network}(\ln\tau, T)$and its shift toward shorter timescales[8]. Consequently, the temperature dependence of viscosity becomes more pronounced[8]. In this regime, it is crucial to differentiate between the thermal sensitivity of relaxation times and that of zero-shear viscosity.

Regime III (Gel-to-Sol Transition) here, dissociation progresses to the point of reaching the gel transition, triggering a dramatic collapse in zero-shear viscosity[8]. Depending on the architecture of the precursors (whether small

molecules or multifunctional polymers), a sharp decline in T_g may occur, causing $H_{Glass}(\ln \tau, T)$ to shift rapidly toward shorter times[8]. Furthermore, the $H_{Network}(\ln \tau, T)$ spectrum broadens extensively while its intensity continues to diminish[8].

Regime IV (Full Dissociation), this final stage marks the complete removal of any network-related effects as the dissociative bonds are fully broken[8]. However, the system does not always revert to the exact viscosity profile of its non-associating analogues; complex phenomena, such as weak phase segregation or residual interactions, may still influence the rheological behavior of the resulting liquid[8].

Unlike vitrimers, in dissociative networks an increase in temperature causes both shorter bond lifetimes and a decrease in cross-link density (G_0 decreases) [3–5,8–10]. As can be seen in the following graphics Fig.3.

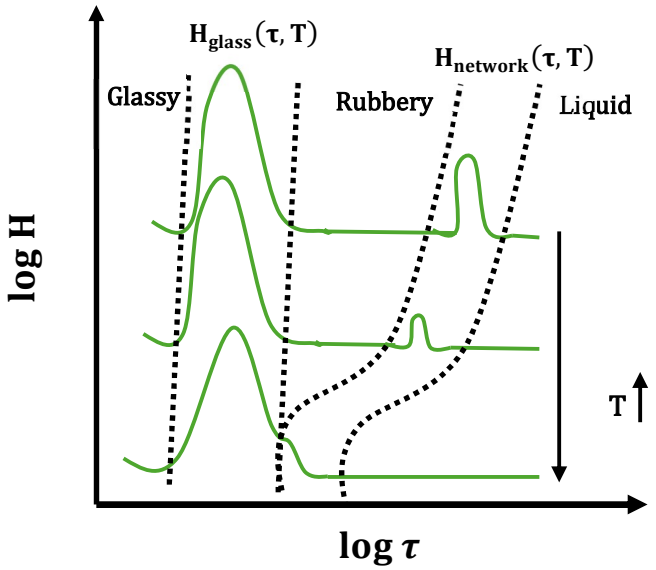

Figure 3. *Typical relaxation time spectra H(τ,T).*

The increase in temperature does not merely accelerate the molecular dynamics, but shifts the thermodynamic equilibrium towards the cleavage of reversible bonds, resulting in a progressive decrease in the active cross-link density[3–5,8–10]. In the relaxation time spectrum, this phenomenon translates into a profound alteration of the $H_{Network}$ peak: parallel to the shift towards shorter relaxation times, a drastic collapse in the peak

amplitude is observed with increasing temperature[8]. This marked drop in the relaxation intensity documents the progressive loss of elastic connectivity of the network, which, at high temperatures, undergoes a reversible de-crosslinking, behaving macroscopically as a viscous fluid, thus differentiating itself clearly and unequivocally from the rheology of vitrimers[8].

In addition, the mechanism of these materials may also not be easily elucidated simply by observing their physical properties; in some cases, materials operating via the dissociative mechanism may have rheological properties indistinguishable from vitrimers. This happens when the rate constant of bond formation is significantly greater than that of bond cleavage, such that the proportion of dissociated bonds is small[3–5,8]. As a result, the viscosity–temperature dependence of these materials still follow Arrhenius' law, and these materials can still be considered vitrimer-like materials[4].

1.1.2 Associative mechanism (*vitrimers)*

In 2011, Leibler and coworkers[4,9] introduced a novel subclass of CANs defined as *vitrimers*. This terminology was chosen because their viscosity decreases gradually with increasing temperature, exhibiting an Arrhenius-type temperature dependence that closely resembles the rheological behavior of vitreous silica[4,9,11,12]. This relationship can be expressed by the following Eq.5:

$$\eta(T) = \eta_0 e^{\frac{E_{att}}{RT}} \qquad \text{[Eq.5]}$$

where η represents the viscosity, η_0 is the pre-exponential factor, E_{att} is the activation energy for the bond exchange reaction, R is the universal gas constant, and T is the absolute temperature, as also shown in Fig.4A and 4B. Eq. 5 cannot be applied with the same confidence to CANs with dissociative mechanism since the dependence of the crosslinking density by the temperature makes the pre-exponential factor also a function of T.

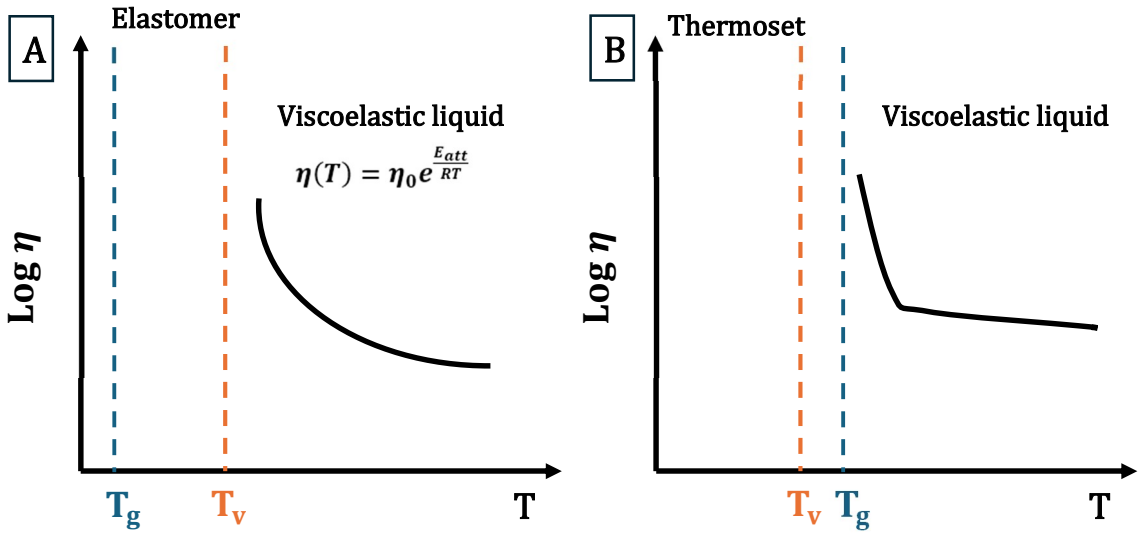

***Figura 4**. (A) Idealised viscosity-temperature relationship of vitrimers with T_g lower than T_v, and (B) T_v lower than T_g.*

The thermomechanical behavior of vitrimers is defined by the interplay between two distinct transition temperatures[3,5,8,13]: the glass transition temperature (T_g) and the topology freezing transition temperature (T_v). While T_g represents the onset of segmental motion within the polymer chains transforming the material from a rigid to a deformable state T_v

marks the point where dynamic bond exchanges become rapid enough to permit macroscopic flow[3–5,8]. Conventionally T_v, is identified as the temperature at which the material reaches a viscosity of 10^{12} Pa · s, shifting from a viscoelastic solid to a viscoelastic liquid[3,8,9].

Crucially, because these two transitions stem from different physical interactions, they are mechanistically independent. The relationship between them dictates the material's state across a temperature gradient. The Fig.4A represent the most common configuration where the vitrimer exists as a rigid solid below T_g, an elastic (rubbery) solid between T_g and T_v, and a viscoelastic liquid above T_v[4,8]. In this liquid regime, the viscosity decrease follows an Arrhenius model, as the rate of flow is governed by the kinetics of the chemical exchange reactions[4,8]. While the Fig.4B represent, this less common behavior occurs when the chemical exchange is thermally ready ($T > T_v$) but physically hindered by the frozen polymer matrix ($T < T_g$). In this state, the network remains fixed because the lack of segmental motion prevents exchange reactions from proceeding[4,8]. Once the temperature surpasses T_g, the material exhibits a sharp drop in viscosity described by the Williams–Landel–Ferry (WLF) equation[3,4,8,13]. With further heating, the system eventually transitions back to a regime where chemical kinetics again control the flow, returning to Arrhenius behavior.

Traditionally, the crosslinks of CANs are dissociative in nature[3,4,8], being broken before reforming in the network. In contrast, the crosslinks of these vitrimers are associative in nature, with their crosslinks being broken only when new bonds are formed.

This has two main effects. Firstly[8], an extended rubbery phase can be observed when heated, as compared to dissociative CANs which transforms from a solid-like state to a liquid-like state more abruptly. In vitrimers, as G_0 varies only weakly with temperature up to the degradation temperature (entropic elasticity), the temperature dependence of the zero-shear viscosity should thus be solely controlled by the kinetics of the bond exchange reaction.

Secondly[8], some groups have also noted a greater creep/solvent resistance for associative CANs.

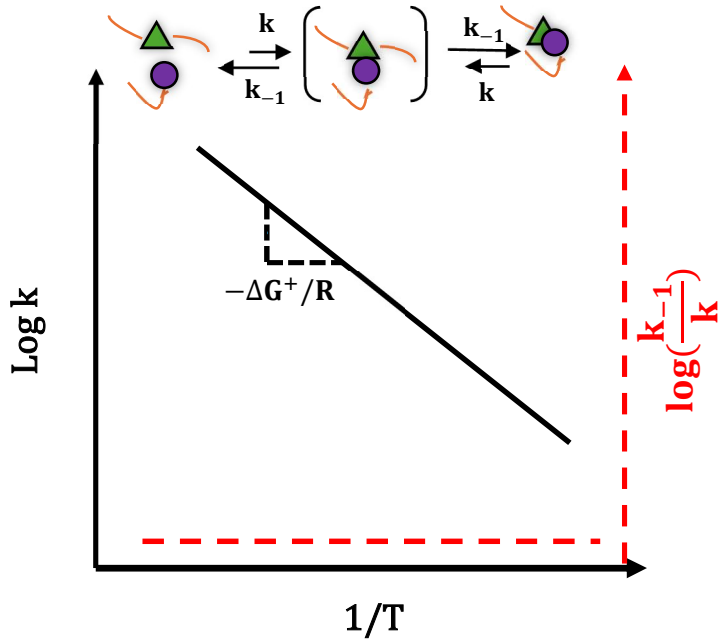

Figure 5. *Overall exchange mechanisms at stake in the network relaxation and corresponding thermodynamic parameters (k being the apparent rate of exchange and* $K_a = \frac{k_{-1}}{k}$ *the apparent association equilibrium constant).*

The upper panel of Fig.5 characterizes the unique temperature dependence of associative CANs, known as vitrimers, where bond exchange occurs through a concertated mechanism a bond is only broken as a new one is simultaneously formed. The exchange rate constant (log k, represented by the solid black line) follows an Arrhenius-like dependence[3,5,8,9,14]. The negative slope of this relationship is governed by the Gibbs free energy of activation ($\frac{-\Delta G^{++}}{R}$), indicating that the rate of bond exchange increases exponentially as the temperature rises (corresponding to lower $\frac{1}{T}$ values). This kinetic control allows the material's viscosity to decrease gradually with temperature, resembling the behavior of vitreous silica[5,8,9]. Crucially, the association equilibrium constant ($\log \frac{k_{-1}}{k}$, dashed orange line) appears as a horizontal line, demonstrating that the chemical equilibrium between bond formation and dissociation is independent of temperature[5,8,9]. This lack of temperature dependence arises because the enthalpy change (ΔH)

of the concerted exchange reaction is typically close to zero. Consequently, the cross-link density (ν) remains essentially constant across the entire temperature range[5,8,9], as shown in Fig.6. This is a defining characteristic of vitrimers, enabling them to flow and be reprocessed as a viscoelastic liquid at elevated temperatures while maintaining the overall topological integrity and stability of the network[9].

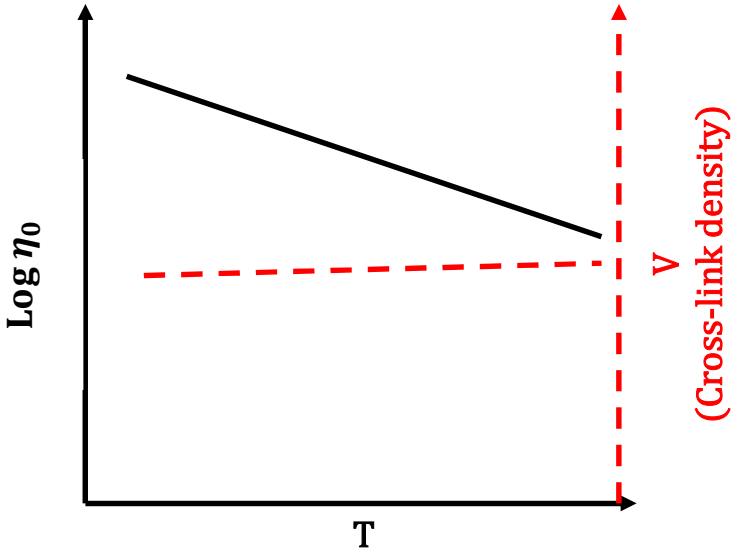

Figure 6. *Evolutions of zero-shear viscosity $\eta_0(T)$ and cross-link density at temperatures above the glass transition.*

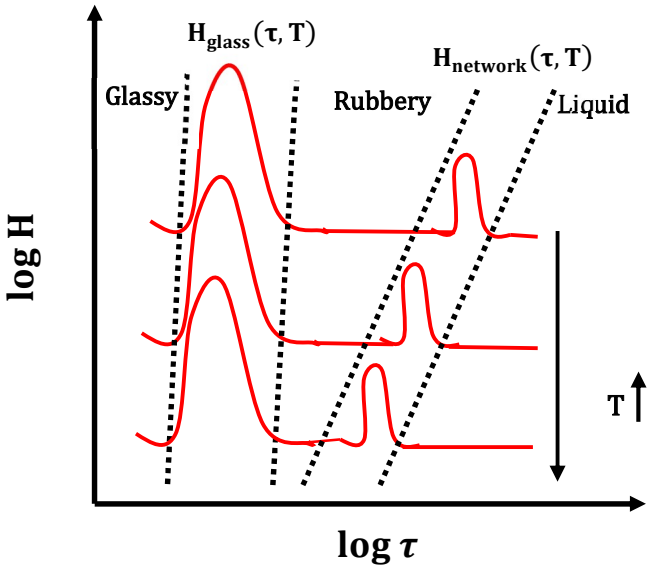

Figure 7. *Typical relaxation time spectra H(τ,T).*

The analysis of the relaxation time spectrum, H(τ), (as represented in Fig. 7) for associative covalent adaptable networks (vitrimers), highlights the remarkable structural stability of the network upon varying the temperature. As expected for an associative mechanism, in which the breaking of a cross-link occurs in a concerted manner with the formation of a new one, the topology and the cross-linking density of the polymer remain constant over time[5,8,9]. This is clearly reflected in the behavior of the relaxation peak associated with the network ($H_{Network}$): as the temperature increases, the peak undergoes a pure translation towards lower relaxation times (τ), indicating an acceleration of the thermally activated exchange kinetics, but its amplitude and the underlying area remain unchanged[8]. Such invariance confirms that the material is able to flow and dissipate applied stresses without experiencing any decrease in the plateau elastic modulus, maintaining the integrity of the three-dimensional network[8].

1.2 CANs Chemical properties

If we look at the chemistry of these processes[5], we can divide the rearrangement mechanisms into two main families: concerted (single-step) mechanisms and stepwise (multi-step) mechanisms, as illustrated in Fig.8. In this framework, the concerted mechanism represents the "ideal" scenario for vitrimers (associative CANs). In this pathway, the formation of the new bond and the breaking of the old one occur simultaneously through an ordered transition state, without the formation of any intermediate species[5]. The significant advantage of this process is that the crosslink density remains perfectly constant throughout the entire relaxation process, behaving analogously to the viscous flow of silica glass[5,8,9]. Conversely, stepwise mechanisms involve the formation of a temporary intermediate state (a "free" bond or a dissociated species) before the new bond is formed[5]. This mechanism can be found in both dissociative CANs (where the intermediate is a stable, broken chain) and some specific associative systems[5]. Unlike the concerted "vitrimeric" process, the stepwise pathway often leads to a transient decrease in crosslink density[5]. Since concerted mechanisms are so rare, in practice we almost always work with stepwise mechanisms, which occur in two distinct steps (bond breaking and bond forming)[5]. The order in which these two steps occur completely changes the properties of the material.

The first case is the associative stepwise mechanism. In this pathway, two polymer chains first 'associate' to form a new covalent bond, and only afterwards does the elimination step occur, breaking the pre-existing bond[2–5,15]. This means that, in the reactive intermediate state, the cross-link density undergoes a temporary increase[5]. Strictly speaking, this deviates from the definition of an 'ideal vitrimer', because heating the material could lead to a fluctuation in connectivity[5]. However, in practical terms, this variation is often negligible: the cross-link density remains practically constant over a wide range of temperatures[5]. For this reason, the associative mechanism is considered the fundamental practical prerequisite for obtaining materials with true vitrimeric properties, which are able to flow when heated without dissolving[2–5,15].

The exact opposite is the dissociative stepwise mechanism. Here, the order is reversed: the pre-existing bond breaks first (dissociation), and only later is a new one formed. During the intermediate state, the network temporarily 'de-cross-links', creating reactive chain ends[5]. This scenario drastically departs from the vitrimer ideal: as the temperature increases, the overall connectivity of the material decreases[2–5,15]. Since it is not limited by the immediate need to encounter another reactive species, this loss of bonds can become quite extensive, also driven by the fact that the de-cross-linked state is thermodynamically favored by entropy[5].

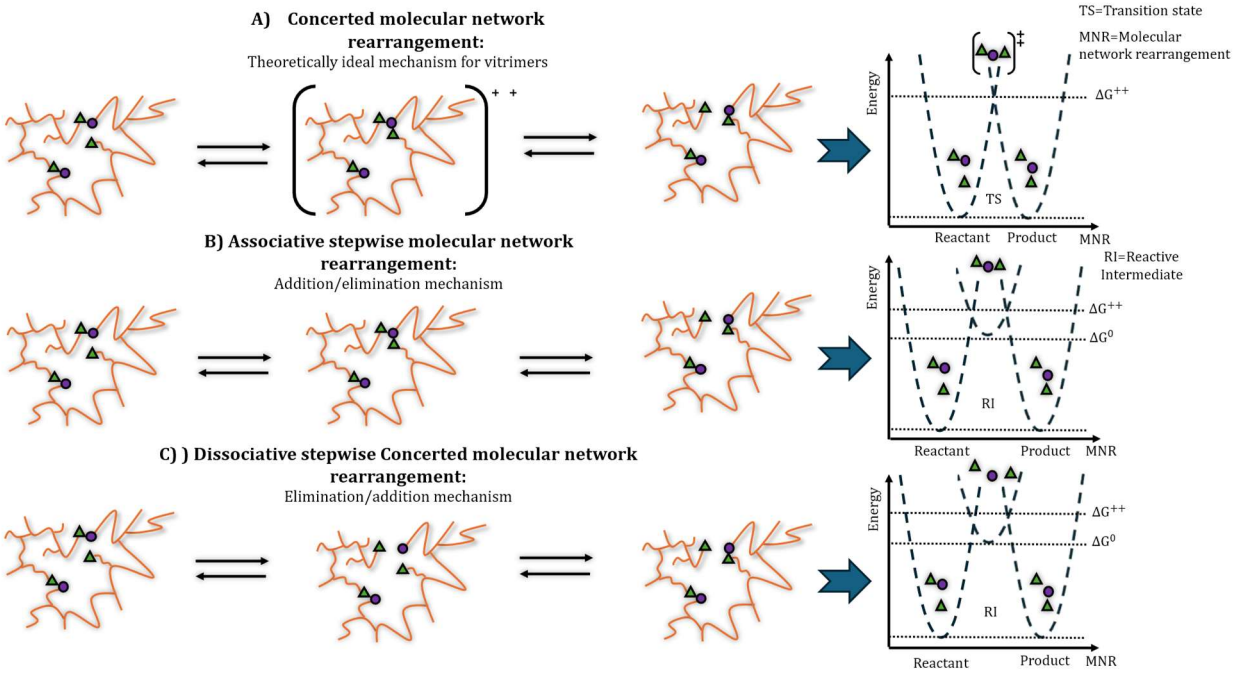

Figure 8. Different types of molecular network rearrangements (MNRs) within covalent networks and their energy profiles.

1.2.1 Associative mechanism chemical properties

This exchange mechanism ensures that the global connectivity and cross-link density of the network remain strictly constant throughout the process[2–5,7,15], preventing the material from undergoing a gel-sol transition and maintaining its insolubility even at high temperatures[7]. These processes are governed by degenerate chemical reactions, in which the reactants and products are chemically identical, resulting in a thermodynamic equilibrium constant equal to one, which makes the degree of cross-linking independent of temperature[2–5,7,15].

Catalyzed transesterification represents the archetype of this class, where a free hydroxyl group attacks an existing ester bond through a coordinated tetrahedral intermediate, typically activated by Lewis acids such as zinc acetate or strong organic bases like triazabicyclodecene (TBD)[1,11,12]. In parallel, the development of systems based on the chemistry of vinylogous compounds, such as urethanes, amides, or diketoenamines, has introduced the possibility of rapid exchanges based on a Michael-type conjugate addition and subsequent elimination mechanism[2–5,15]. These materials often operate without external catalysts because the intrinsic reactivity of the electrophilic carbon in the enaminone system facilitates the attack of free amines[3]. The kinetics of these exchanges can be further modulated by adjusting stoichiometry, such as an excess of free amine or hydroxyl groups, or by introducing internal catalysis through neighboring group participation (NGP)[15].

Another fundamental class of associative reactions involves heteroatom exchange[2–5,15], such as metathesis between boronic esters or boroxines, where the electrophilic nature of boron favors the formation of transient zwitterionic adducts that allow bond shuffling without the need for free nucleophiles. Similarly[2–5,15], silyl ether exchange can proceed via both alcoholysis and direct metathesis catalyzed by acids, offering a strategy to render pre-existing thermoplastic networks like polystyrene or polyethylene malleable. The extension of these concepts to polyionic systems has enabled the use of S_N2-type transalkylation between sulfonium

salts and thioether groups, realizing concerted exchanges that maintain a constant charge and bond density during viscous flow[3,4,16].

Finally, sulfur chemistry offers highly efficient solutions through thiol-thioester exchange, which can be activated even at room temperature via photobases or nucleophiles[15]. In all these associative systems, the activation energy of the process is directly correlated to the barrier of the chemical exchange reaction, allowing the material to flow with an Arrhenian temperature dependence, a characteristic that defines the very essence of vitrimers[4].

Some of the above mentioned reactions are reported in Fig.9.

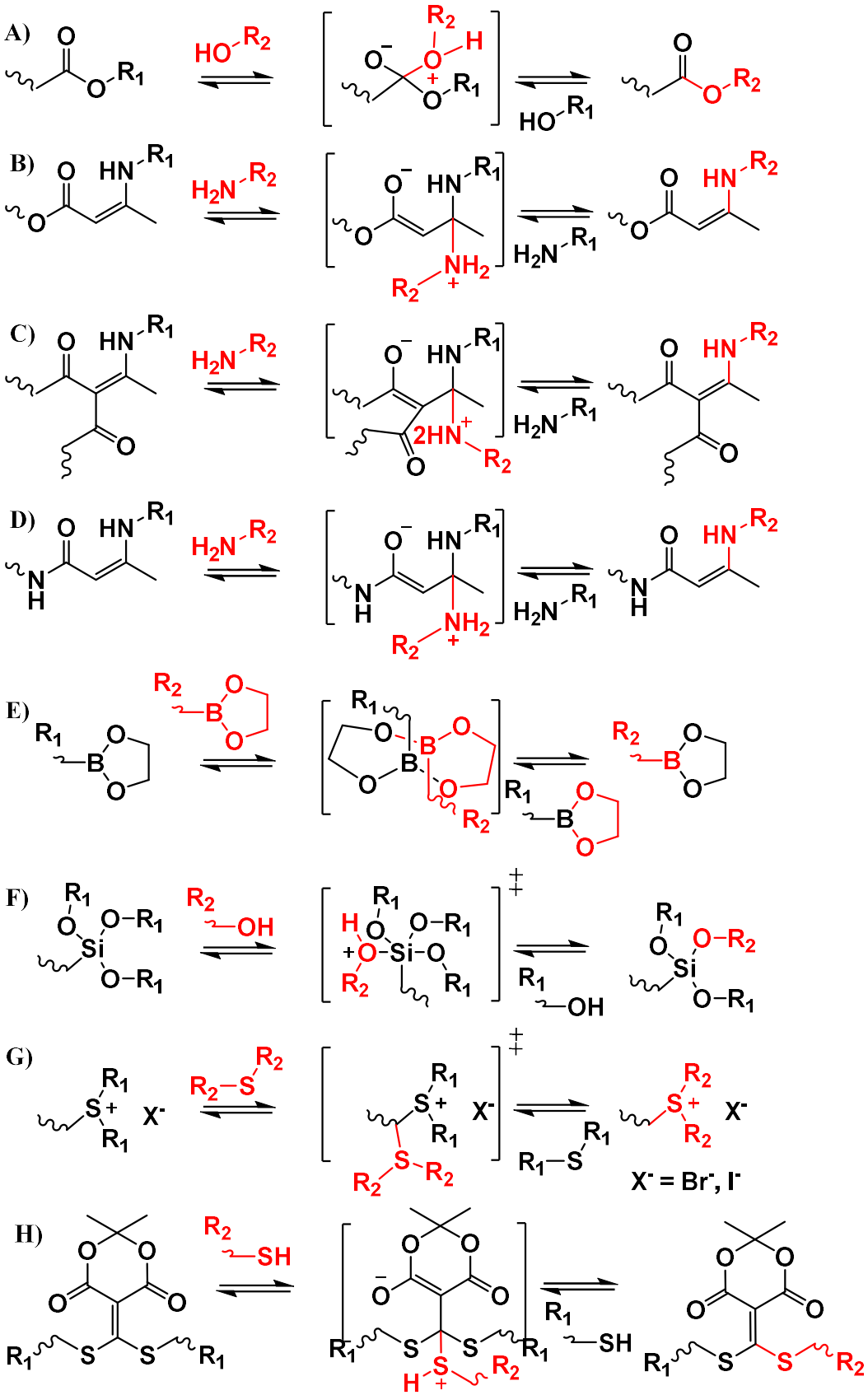

Figure 9. *General mechanism of associative bond exchange. A) Transesterification, B/C/D) Micheal addition on vinylogous compounds, such as urethanes, amides, or diketoenamines, E) Metathesis between boronic esters, F) Silyl ether exchange G) Transalkylation of solfonium salts, H) Transthioetherification of Meldrum's acids.*

1.2.2 Dissociative mechanism chemical properties

Dissociative Covalent Adaptable Networks (CANs) are chemically distinguished by a sequential rearrangement mechanism in which the breaking of an existing covalent bond precedes the formation of a new one, following an elimination-addition pathway[2–5,15]. This process results in a temporary decrease in the crosslink density and connectivity of the network during activation, as chain segments are released as reactive free moieties before recombining[15]. The archetypal reaction of this category is the Diels–Alder (DA) cycloaddition, typically realized between furan and maleimide groups. Chemically, this is an exothermic thermodynamic equilibrium where increasing the temperature shifts the reaction toward the reactants (retro-DA), breaking the sigma bonds to regenerate the original pi-conjugated systems of the diene and dienophile[1]. Another relevant class involves alkoxyamines, derived from nitroxide radical chemistry (NMP), where the C–O bond undergoes homolytic cleavage above 80°C. This generates a transient carbon radical and a stable nitroxide radical that can subsequently recombine to restore connectivity[17].

Dissociative behavior has also been extended to classic polyurethane and polyurea chemistries through the use of blocked isocyanates or hindered urea bonds (HUBs)[18]. In these systems, the presence of bulky substituents on the nitrogen atom distorts the conjugation between the nitrogen lone pair and the carbonyl orbital, facilitating the thermoreversible dissociation of the bond into an isocyanate and an amine or alcohol[1]. Similarly, networks based on the Michael addition of thiols to electrophilic alkenes (such as acrylates or maleimides) can be made dynamic under basic or nucleophilic conditions, where catalyst attack promotes the retro-addition of the thiolate, allowing it to migrate to another electrophilic center[19].

Recent studies have shown that even polyionic systems, such as 1,2,3-triazolium or anilinium salts, operate predominantly through a dissociative pathway mediated by the counterion[15]. In this scenario, a nucleophilic counterion (such as iodide or bromide) attacks the cationic center via an S_N2 nucleophilic substitution, causing the temporary de-alkylation of the crosslinking node and the release of an alkyl halide that can subsequently

react with another free amine or triazole group[1]. Finally, a significant subclass is represented by dissociative CANs mediated by small molecules, where bond cleavage is conditioned by the presence of a condensate, such as water[5]. Networks based on imines, hydrazones, or boronic esters follow a reversible condensation chemistry in which hydrolysis promotes the cleavage of the bond into aldehyde, amine, or acid fragments. In such systems, the reversibility and density of the network are governed by Le Chatelier's principle, where the removal or addition of the molecular mediator shifts the equilibrium between the crosslinked and dissociated states[5]. Some of the above mentioned reactions are reported in Fig.10.

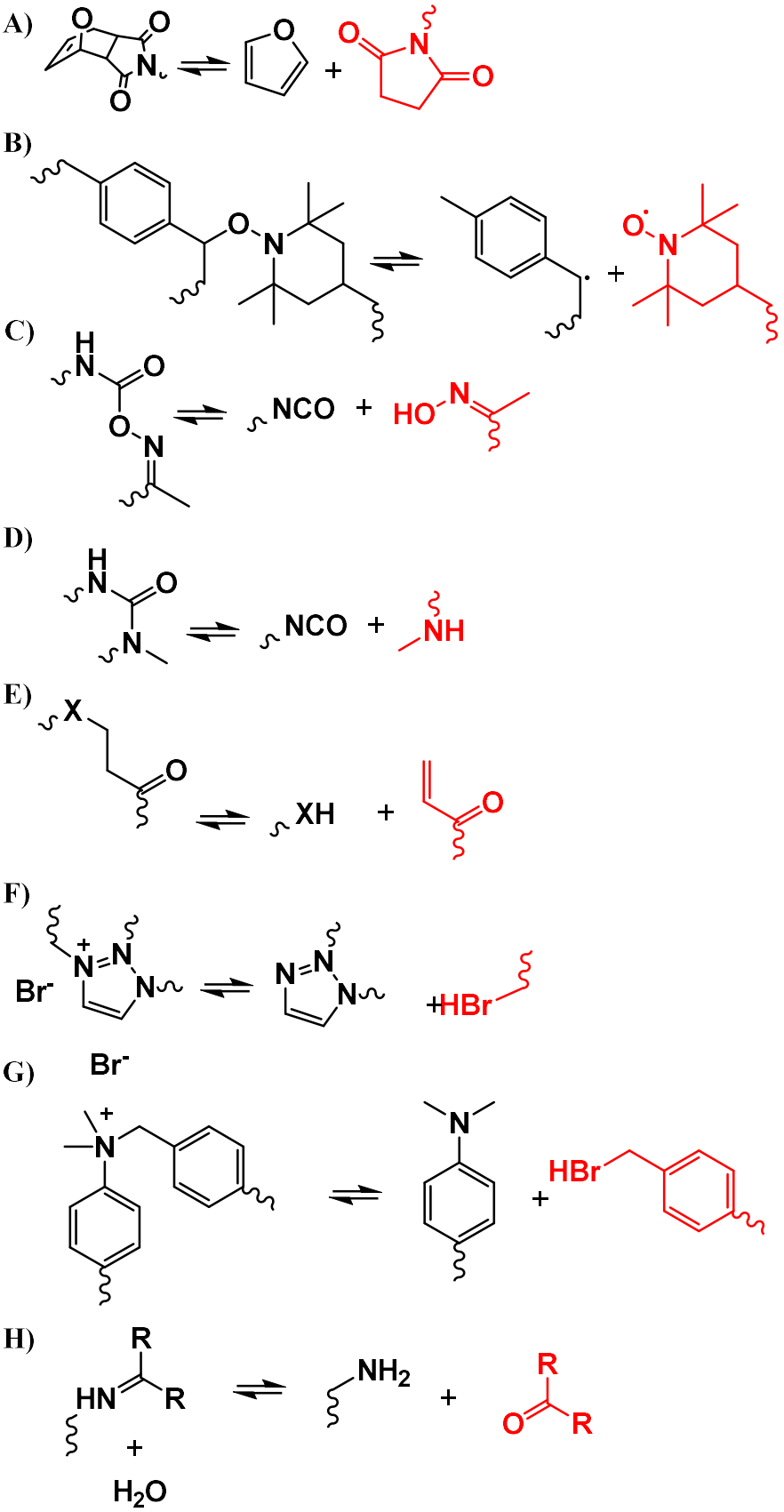

Figure 10. *General mechanism of associative bond exchange. A) Diels-Alder, B) Alkoxyamine dissociation, C) Urethane dissociation, D) Urea dissociation, E) Micheal adduct*

exchange, F) 1,2,3-Triazolium salts nucleophic transalkylation, G) Anilinium salts nucleophic transalkylation, H) Imine transamination.

1.2.3 Transesterification

Among the diverse dynamic covalent chemistries available, transesterification stands out as one of the most extensively investigated and versatile mechanisms; it is widely regarded as a benchmark for its straightforward implementation in industrial processes and its foundational role in the pioneering studies on vitrimers conducted by Leibler and co-workers [9,11,12]. To delve into transesterification mechanisms under uncatalyzed conditions (Fig.11), it is necessary to clearly distinguish between pathways occurring under uncatalyzed conditions, which are dominated by the reactivity of end groups, and catalyzed ones, which exploit various molecular activation strategies[9,11,12]. Although they proceed very slowly and require extended times, uncatalyzed mechanisms are fundamental to understanding the intrinsic reactivity of polymer chains, especially in systems where synthesis metal residues have been previously removed. In these reactions, three main pathways are identified, regulated by the nature of the nucleophiles present[16].

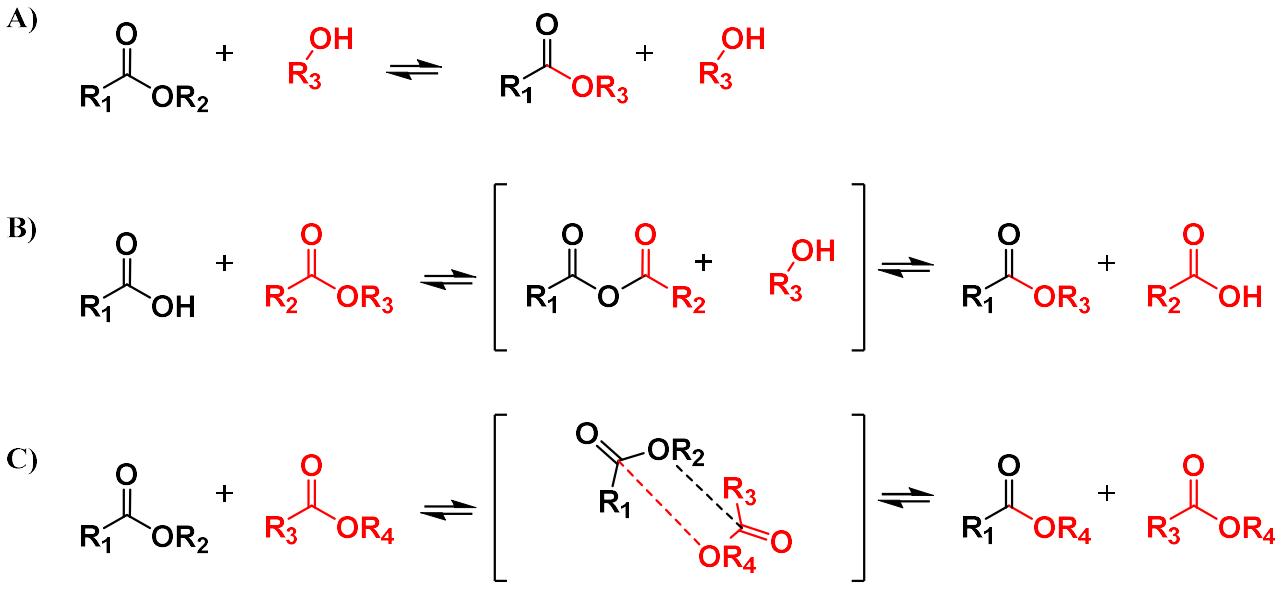

Figure 11. *Primary mechanism for uncatalyzed transesterification. A) Alcoholysis, B) Acidolysis, C) Direct ester exchange.*

Alcoholysis is generally considered the dominant pathway in polyesters devoid of exogenous catalysts due to its higher reaction rate compared to the others[20,21]. In this process, the hydroxyl end groups (-OH) act as nucleophiles, attacking the carbonyl carbon of another ester group and

displacing the leaving group through an S_NAc nucleophilic acyl substitution mechanism[20,21]. A clear example is observed in PET/PEN blends, where studies have shown that the capping of hydroxyl groups can slow down the reaction up to three times, confirming the centrality and vital role of the concentration of these groups[22]. Furthermore, the use of low molecular weight polycaprolactone (PCL) significantly accelerates the process precisely because of its higher concentration of -OH terminals[16].

In epoxy vitrimers (DGEBA), the presence of hydroxyl groups is crucial for transesterification. Without -OH groups, the exchange between two diesters does not occur, even after 24 hours[12].

Transcarbonation is a specific variant of transesterification for polycarbonates (PC). In this system, a hydroxyl nucleophile attacks a carbonate, forming an associative intermediate that reorganizes the network without permanently cleaving it.[23].

A second pathway is acidolysis, which involves the attack of a carboxyl end group (-COOH). Unlike alcoholysis, acidolysis is a more complex and slower process: the carboxyl group initially forms an anhydride intermediate, which subsequently reacts with an alcohol group to form a new ester bond[16]. Studies conducted on PET models have confirmed that an increase in carboxyl groups does not significantly enhance the overall transesterification as much as an increase in hydroxyl groups does[16].

Finally, direct ester exchange (of an associative nature) occurs when the alkoxy parts of two polyesters simultaneously exchange their main chains, leading to the formation of two new copolymeric bonds[24]. It is believed that this process proceeds through a four-center transition state between the carbonyl carbons and the alkoxy oxygens of the two esters (acyl-oxygen cleavage) [24]. This mechanism has been observed in PC/PBT blends, where the exchange between ester and carbonate groups is possible; however, in the absence of catalysts or without the aid of residual metals (such as the titanium derived from PBT synthesis), this exchange proceeds at completely negligible rates and is considered much slower than alcoholysis[16].

The addition of catalysts drastically reduces the activation energy of the process, lowering it from values of about 27-37 kcal/mol to only 17-20 kcal/mol, allowing the reaction to proceed in practical times[9,11,12]. Metal complexes operate primarily through three highly distinct mechanisms[16]. The catalyzed mechanisms have been reported in the following Fig. 14.

It is important to emphasize that the catalytic pathways illustrated in Fig.14 represent fundamental activation principles that are broadly applicable to all variants of transesterification[9,11,12,16,20,21,25–28], including the alcohol-ester (alcoholysis) and ester-ester exchanges. While these mechanisms are depicted for generic reagents, they describe the same transition states and electronic effects that govern the dynamic bond-exchange reactions in Covalent Adaptable Networks, where the high concentration of ester groups and hydroxyl moieties typically present in the polymer backbone dictates the reaction kinetics[9,11,12,16,20,21,25–28].

In the Lewis acid mechanism (carbonyl activation), the metal acts as an electron acceptor through its empty valence orbitals, polarizing the carbonyl group of the ester and making it more susceptible to nucleophilic attack[29]. According to the hard-soft acid-base (HSAB) theory[29], metals with high charge density and small ionic radii ("hard" acids such as Ti^{4+}, La^{3+}, Sn^{4+},) are the most effective in polarizing the carbonyl electron cloud. The main advantage of this mechanism is that it does not typically induce chain scission, proving essential for preserving the high molecular weight and the macroscopic properties of the material. Typical catalysts include titanates, such as titanium tetra-n-butoxide ($Ti(OBu)_4$), which is extremely powerful but prone to causing yellowing[4,5,12]. There are also lanthanide complexes[30], such as samarium acetylacetonate ($Sm(acac)_3$) or lanthanum acetylacetonate ($La(acac)_3$), which offer moderate activity and excellent solubility, making them ideal for precise control in PC/PET blends without excessively degrading the molecular weight. Tin complexes[25], such as dibutyltin dilaurate (DBTDL), are also frequently used to compatibilize PC/PCL blends. Titanium alkoxides ($Ti(Oi-Pr_4)$) are identified as the most efficient catalysts for polycarbonates because they ensure rapid transcarbonation without detectable side reactions[23].

In the Lewis base mechanism (nucleophilic mechanism)[16], the catalyst increases the nucleophilicity of the attacking agent or directly cleaves the polymer chain, generating reactive alkoxides. Within polymers, the ligand of the metal complex can act as a base to cleave chains, generating alkoxide species that initiate and propagate exchange cycles between various groups[16]. Regarding selectivity, in polycarbonate-based vitrimers, the carbonyl adjacent to two electron-withdrawing oxygens is particularly susceptible to attack by nucleophilic ligands, favoring chain scission and the generation of alkoxides rather than carbonyl activation[25,30]. However, an excessive catalyst loading can lead to mechanical degradation due to the severe reduction in molecular weight. This category includes metal alcoholates[26], such as sodium methoxide (NaOMe) and potassium tert-butoxide (KOtBu). NaOMe is very effective in generating polymeric alkoxides but can cause a drastic drop in molecular weight. We also find phosphonium salts, weakly acidic salts that act by cleaving PC chains to generate active hydroxyl groups, and organic bases like TBD (1,5,7-triazabicyclo[4.4.0]dec-5-ene)[31,32], although its use is limited in industrial processes by its strong sensitivity to moisture.

The insertion-coordination mechanism[16], unlike the previous ones, involves the metal ion simultaneously coordinating both the alkoxycarbonyl group (ester) and the nucleophile, bringing them into close spatial proximity within the coordination sphere. The reactants facilitate a coordinated exchange via a four-center transition state involving the acyl oxygen of the ester[9,12]. Ligands act as both initiators and facilitators of coordination: small, linear ligands reduce steric hindrance, easing the access of the polymeric substrate to the metal ion. Moreover, due to the size of the macromolecules, the spatial geometry of the complex is crucial; less hindered geometries (e.g., linear vs. tetrahedral) clearly favor catalytic activity. Typical catalysts include tin octoate (tin(II) 2-ethylhexanoate)[33], very common in ring-opening polymerization (ROP) and "one-pot" chemical recycling of PLA. $Zn(HMDS)_2$ (zinc bis[bis(trimethylsilyl)amide])[27] is also frequently used, acting as a versatile catalyst employed for the synthesis and controlled degradation of

polyesters for the circular economy, as well as zinc acetate ($Zn(OAc)_2$), which is fundamental for the creation of the first epoxy vitrimers where it promotes alcohol-ester exchange in the presence of free -OH groups. $Zn(OAc)_2$ used for epoxy vitrimers, a catalyst loading of 5 mol % reduces the exchange time to only 2 hours, compared to the 15 hours required by uncatalyzed systems[12].

In addition to metal catalysis, the use of Brønsted Acid Catalysis (Protic Acids) represents an innovative platform for polyester vitrimers, allowing rapid exchanges even at room temperature (25 °C), unlike Lewis catalysts that often require temperatures above 100 °C[34]. The network relaxation rate is directly correlated with the pK_a of the acid used: stronger acids induce faster exchanges[34]. Although stronger acids are observed to show higher activation energies (E_a) compared to weak ones, this factor is compensated by more favorable pre-exponential factors, thus still leading to a significantly faster overall stress relaxation[34]. The most powerful typical catalyst in this context is triflic acid (TfOH), which ensures the fastest relaxation times. Variants such as methanesulfonic acid (MSA) and benzenesulfonic acid (BSA) offer exchange kinetics that can be tuned based on their acid strength, while trichloroacetic acid (TCA) is used for systems requiring slower and more controlled exchanges[16].

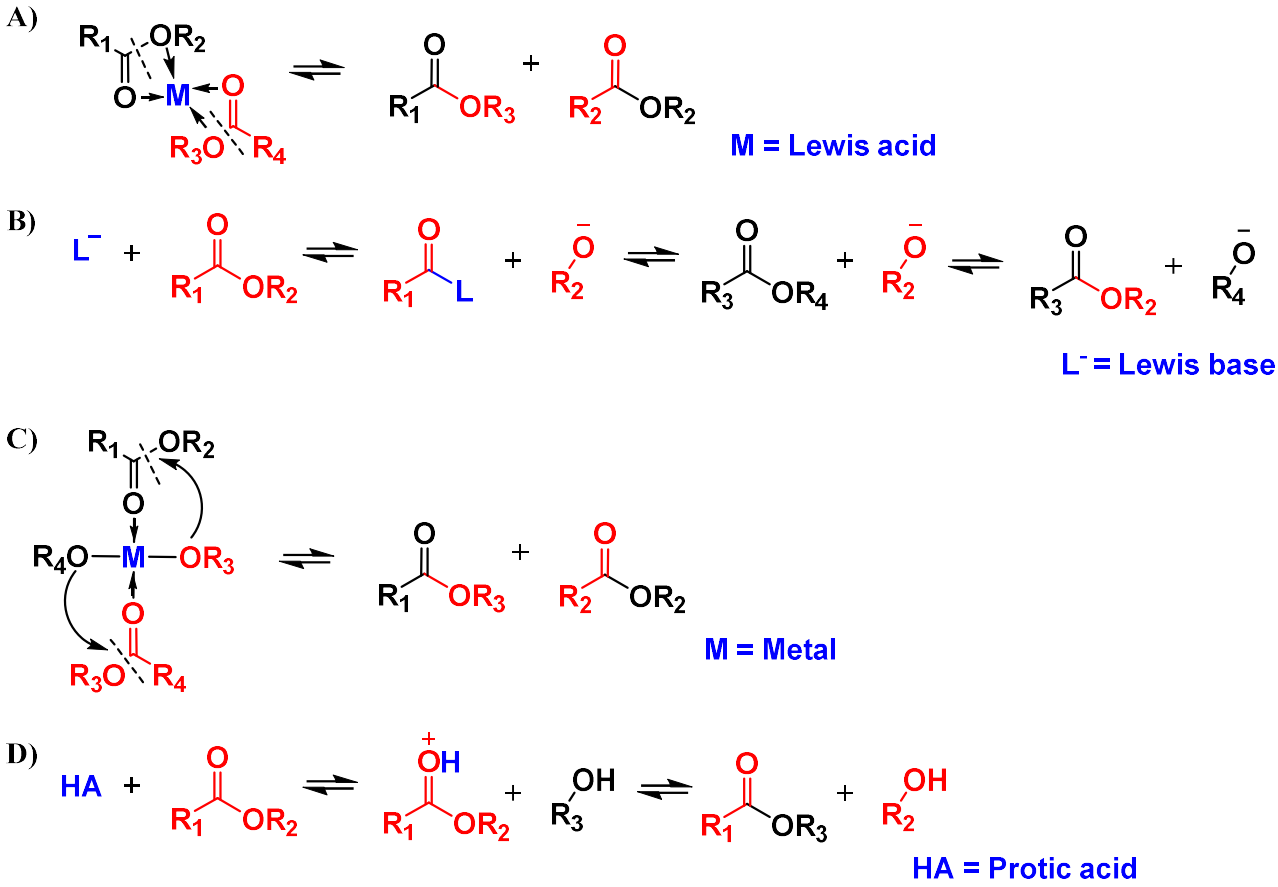

Figure 12. *Catalytic transesterification mechanisms. A) Lewis acid mechanism, B) Lewis base mechanism, C) Insertion coordination mechanism, D) Brønsted Acid mechanism.*

Transesterification inhibitors in applied industrial contexts, such as the production of the commercial PC/PBT blend known as Xenoy, it is strictly necessary to stop the reaction to preserve the polyester's crystallinity and the engineering properties of the material[28]. To achieve this result[28], specific inhibiting agents are used, typically organophosphorus compounds such as phosphoric acid (H_3PO_4) or phosphorous acid (H_3PO_3). These inhibitors act by chelating the metal center (for example, residual titanium), deactivating it effectively[28]. An alternative is triphenyl phosphite (TPP), which acts through a different mechanism by directly blocking the hydroxyl end groups, although it has demonstrated an overall lower effectiveness compared to direct metal chelation[28].

The transesterification mechanism represents the pioneering chemistry originally developed and investigated by Leibler and co-workers for the creation of the very first vitrimeric systems [9,11]. In their seminal works, these networks were synthesized through a straightforward, atom-efficient

curing reaction between carboxylic acids (or anhydrides) and commercial diepoxides, such as diglycidyl ether of bisphenol A (DGEBA), in the presence of a zinc catalyst. From a thermomechanical standpoint, these foundational epoxy vitrimers exhibited excellent mechanical robustness, characterized by high storage moduli in the glassy state (E′ ≈ 2.5 - 3.0 GPa) and a glass transition temperature (T_g) easily tunable between 40 °C and 80 °C depending on the crosslinking density[9,11,12,21]. To illustrate the chemical architecture of these historical benchmarks, a representative schematic of their network topology and catalyst-mediated exchange is reported in Fig.13.

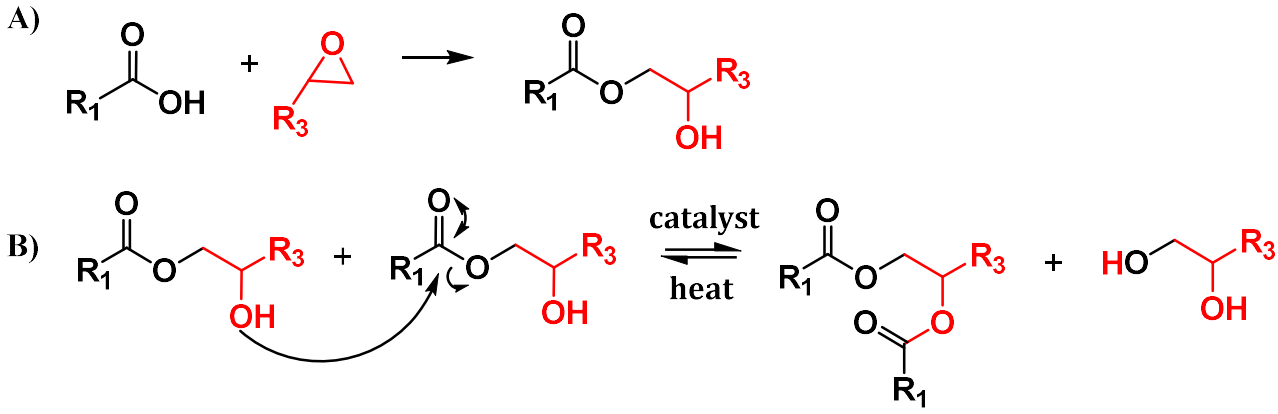

Figura 13. *(a) The nucleophilic addition between epoxides and carboxylic acids yields a characteristic repeating unit that simultaneously contains both an ester group and a free hydroxyl function. (b) At elevated temperatures, these coexisting groups undergo a catalyst-mediated transesterification reaction, enabling dynamic bond exchange within the network.*

1.2.4 Aza-Micheal

Parallel to transesterification, the aza-Michael addition has emerged as a highly attractive pathway for the development of dynamic covalent networks, primarily due to its exceptional reaction efficiency, modularity, and rapid kinetics, which allow for the design of systems that can be processed under milder conditions compared to traditional ester-based vitrimers[3,5,35–37]. The aza-Michael reaction, defined as the nucleophilic addition of a Michael donor (a primary or secondary amine) to a Michael acceptor (a double bond activated by an electron-withdrawing group like an acrylate or acrylamide), represents a fundamental tool for sustainable polymer chemistry[36]. This transformation is highly valued for its 100% atom economy, absence of toxic byproducts, and ability to proceed under mild operating conditions, offering a safer "green" alternative to traditional polyurethane synthesis by avoiding the use of isocyanates[36,38,39]. In the absence of exogenous catalysts and when operating in polar aprotic solvents like THF, the reaction typically proceeds through the formation of an unstable zwitterionic intermediate, resulting from the nucleophilic attack of the amine on the β-carbon of the acrylate[40]. The rate-determining step is the proton transfer from the positively charged ammonium to the negatively charged carbon; since a direct transfer is energetically unfavored, the process is often facilitated by an amine-assisted mechanism where a second amine molecule acts as a "proton shuttle," stabilizing the transition state through a six-membered cyclic structure[40]. This makes the global reaction second-order with respect to the amine concentration[40]. Theoretical analyses indicate that while the 1,4-addition path (forming an enol) may show lower initial barriers, 1,2-addition is often kinetically dominant because the subsequent amine-assisted keto-enol tautomerization requires significantly higher activation energies[41]. The mechanisms have been reported in the following Fig.14.

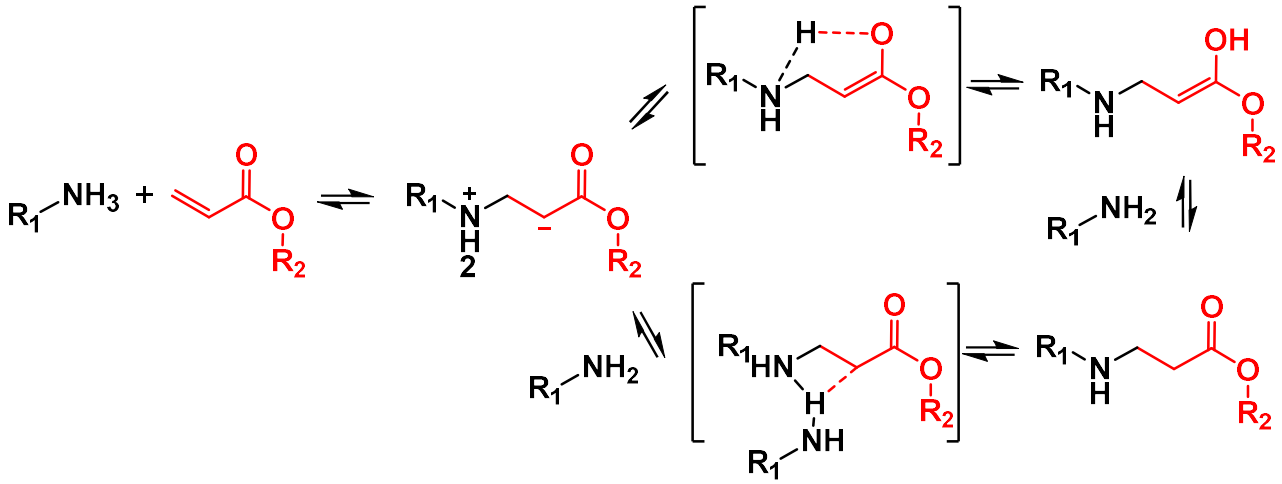

Figure 14. *Primary mechanisms for uncatalyzed aza-Micheal in an aprotic solvent.*

Within Covalent Adaptable Networks (CANs), the resulting β-amino ester linkages introduce intrinsic dynamic behavior that allows the material to behave as both a robust thermoset and a moldable plastic[1]. These systems exhibit the coexistence of two independent exchange pathways: a dissociative exchange mediated by the retro aza-Michael reaction, which typically activates above 140–150 °C causing a temporary reduction in crosslink density, and an associative exchange through transesterification[42–44]. A primary advantage of these networks is endogenous autocatalysis; tertiary amines generated *in situ* during crosslinking serve as internal basic catalysts, promoting network rearrangement without the need for external additives that could migrate or degrade[42–44]. The efficiency of this dynamic is drastically enhanced by Neighboring Group Participation (NGP)[42,43]. For instance, the deliberate introduction of β-hydroxyl groups into the polymer backbone activates the ester carbonyl through hydrogen bonding as shown in Fig.15B, accelerating stress relaxation by 16 to 50 times compared to non-hydroxylated counterparts in which the dynamicity of the system is provided by the only retro-aza Michael process[35,45]. This enables rapid recycling (e.g., 30 minutes at 150 °C) while maintaining excellent mechanical properties[42,43]. The exploration of these dynamic networks began with the pioneering work of Du Prez and co-workers in 2021, who developed the very first dissociative and dual-mode CANs based on poly(β-amino esters) (PBAEs)[3,35]. In these initial systems, crosslinked networks were synthesized through a

straightforward, catalyst-free aza-Michael addition between multifunctional acrylates, specifically trimethylolpropane triacrylate (TMPTA) and 1,4-butanediol diacrylate (BDDA), and primary amines, such as furfurylamine (FA) or alkyl amines, as schematically represented in Fig.15A. From a thermomechanical standpoint, these foundational networks exhibited glassy storage moduli (E') in the range of 2.0 to 3.0 GPa and a glass transition temperature (T_g) easily tunable between –20 °C and 55 °C depending on the crosslinking density and monomer rigidity[3,35]. Building upon these initial benchmarks, recent advancements by the same research group have significantly shifted the focus toward high-performance formulations by incorporating highly rigid or higher-functionality precursors[35,45]. Specifically, the utilization of pentaerythritol triacrylate (PETA) and aromatic bisphenol A core structures, such as those derived from bisphenol A dianhydride (BPADA) functionalization, has been extensively investigated in combination with structurally diverse primary and secondary amines, as schematically represented in Fig.15B. This strategy successfully addresses the inherent thermal limitations of early PBAE networks; the structural rigidity of the aromatic rings in BPADA and the high crosslinking density provided by PETA networks allow for a dramatic increase in the glass transition temperature (T_g far exceeding 80–100 °C) and enhanced dimensional stability[35,45,46], while fully preserving the fast, catalyst-free aza-Michael and transesterification intrinsic recyclability.

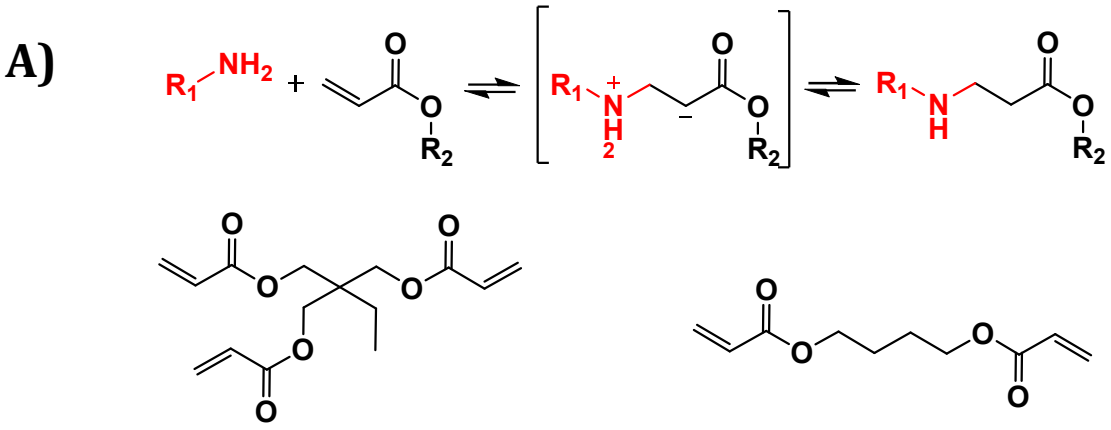

trimethylolpropane triacrylate (TMPTA)

1,4-butanediol diacrylate (BDA)

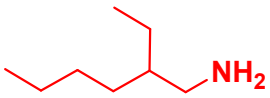

or

or

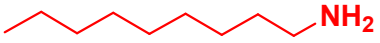

or

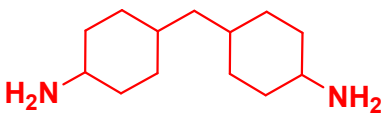

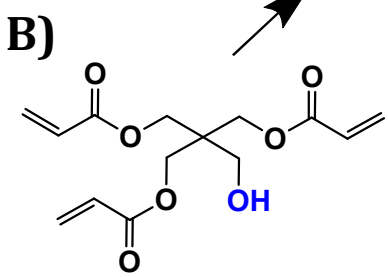

pentaerythritol triacrylate (PETA)

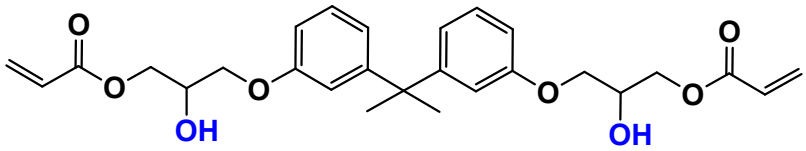

bisphenol A ethoxylate diacrylate (BPADA)

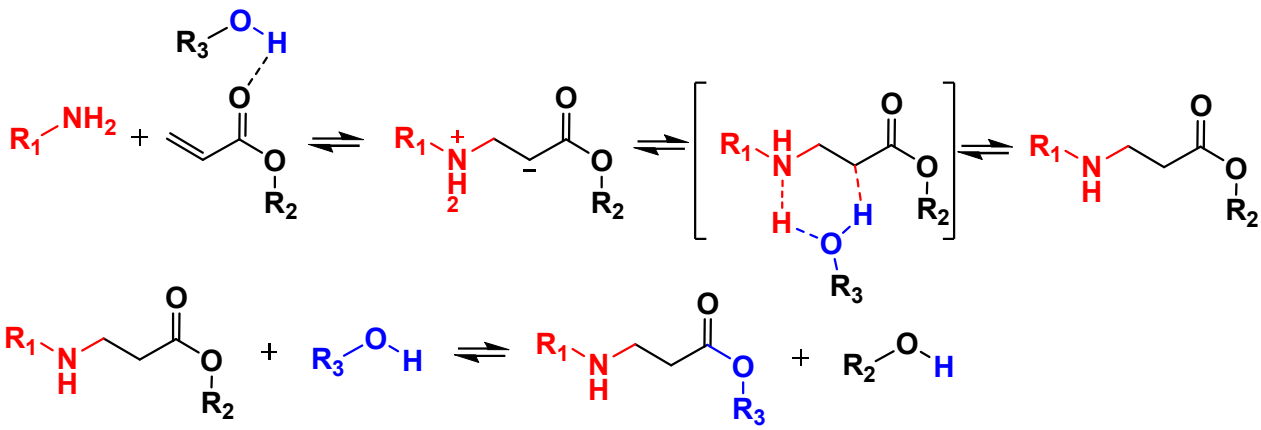

Figure 15. *Mechanism for synthetic pathways and dynamic exchange mechanisms of poly(β-amino ester) (PBAE) covalent adaptable networks (CANs) developed by Du Prez and co-workers. (A) Single-mode dissociative networks: Catalyst-free aza-Michael addition involving conventional aliphatic acrylates, specifically trimethylolpropane triacrylate (TMPTA) and 1,4-butanediol diacrylate (BDA), and various primary or secondary amines. Because these precursors lack pendant hydroxyl functions, the resulting networks reorganize their topology exclusively via a dissociative retro-aza-Michael pathway at elevated temperatures. (B) Dual-mode associative/dissociative networks: Implementation of hydroxyl-bearing acrylate monomers, such as pentaerythritol triacrylate (PETA) and bisphenol A ethoxylate diacrylate (BPADA), which explicitly introduce free -OH groups (highlighted in blue) into the polymer backbone. This spatial arrangement enables a dual-mode dynamic behavior where the dissociative retro-aza-Michael reaction coexists with an associative transesterification exchange. The latter is inherently accelerated by endogenous tertiary amine autocatalysis and Neighboring Group Participation (NGP) via hydrogen bonding, drastically optimizing the stress relaxation and reprocessing efficiency of the matrix.*

Beyond autocatalysis, reactivity can be modulated using various exogenous catalysts. Protic solvents**,** such as ethanol and water, accelerate the aza-Michael addition by stabilizing the transition state and increasing the electrophilicity of the acceptor's carbonyl; ethanol can halve the gelation time in bio-based systems[36,47]. Lewis acids, such as aluminum chloride ($AlCl_3$), and Brønsted acids, like p-toluenesulfonic acid (PTSa)**,** perform a similar role by coordinating with the carbonyl group[36]. A recent frontier is the use of ionic liquids (ILs) as green and recyclable catalysts: choline-proline ([Cho][Pro]) salts allow for complete reactions within minutes at room temperature due to the molecular rigidity of proline which organizes the reagents, while DABCO-based ionic liquids deprotonate the amine to increase its nucleophilicity through strong alkalinity[39,47], the probable mechanism have been reported in the following Fig.16.

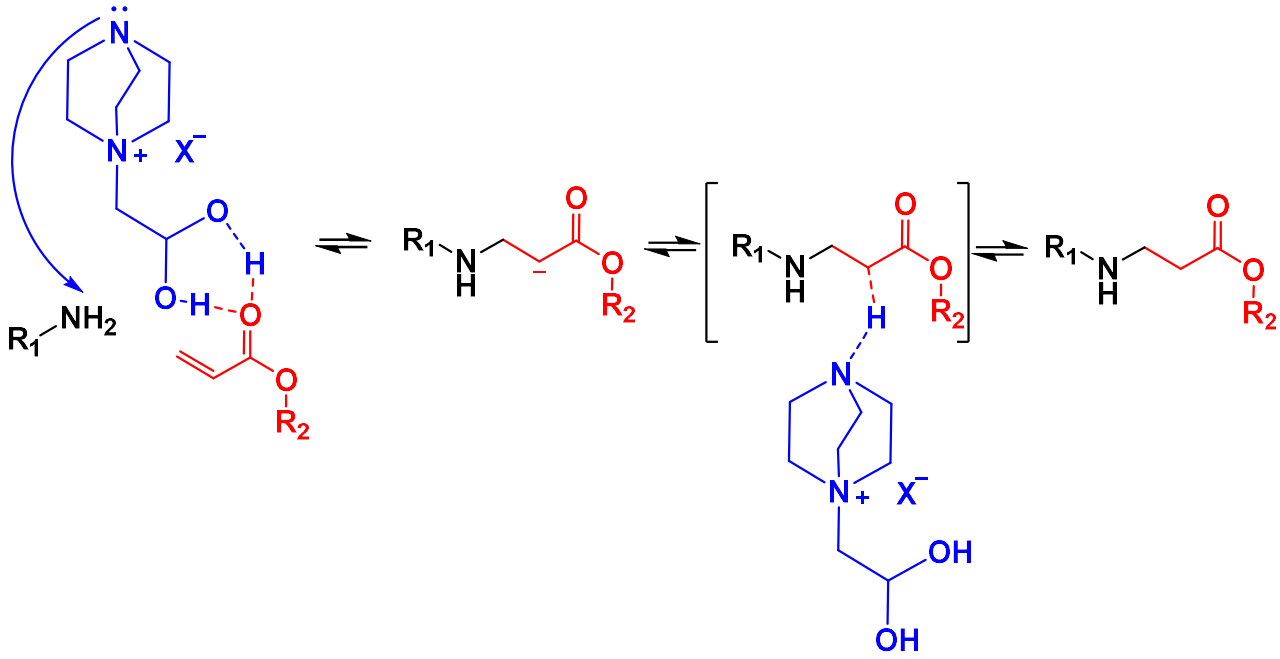

Figure 16. *Plausible mechanism for the aza-Michael addition of amines with α,β-unsatuated ester catalyzed by DABCO-based ionic liquids.*

Furthermore, the versatility of aza-Michael chemistry is extended by metal complexes, particularly those based on copper (CuCl) and phosphine ligands like DPEPhos, which enable the addition of weak nucleophiles such as aromatic amines (anilines) with yields exceeding 90% under mild conditions[38]. These innovations find practical application in critical sectors like the production of wind turbine blades, where low-viscosity aza-Michael matrices allow for the creation of glass fiber-reinforced composites that can be thermally reshaped or chemically recycled via selective degradation in mild acidic solutions (pH≤5.3), facilitating fiber recovery at the end of life[48].

2. Aim of the thesis

The primary objective of this thesis work is the synthesis and characterization of high-performance Covalent Adaptable Networks (CANs), specifically designed for use in the electrical cable coating sector. This project arises from the need to overcome the traditional dualism between thermoplastic and thermosetting materials, combining the robustness and stability of the latter with the reprocessability of the former. The development of the project is conducted in close collaboration with ELANTAS, a leading company in the electrical insulating materials sector. The intent is to respond to a concrete industrial challenge: the creation of coating systems that are not only high-performing during use but also manageable within a circular economy framework, thereby reducing the environmental impact associated with the disposal of traditional cross-linked polymers.

The core of the research focuses on the use of aza-Michael chemistry for the formation of dynamic β-amino ester linkages. This chemical platform was selected for several competitive advantages: a 100% atom economy, as the addition reaction between amine donors and acrylic acceptors occurs without the formation of byproducts; the absence of exogenous catalysts, as by leveraging the autocatalysis provided by the tertiary amines generated in situ during cross-linking, it is possible to design "catalyst-free" dynamic networks, avoiding issues of leaching or degradation of external catalysts over time; and dual dynamicity, where the objective is to balance associative (transesterification) and dissociative (retro aza-Michael) exchange mechanisms to ensure rapid reprocessability at elevated temperatures and high creep resistance at operating temperatures.

A fundamental pillar of this thesis, and a strategic objective of the collaboration with ELANTAS, is the development of a homogeneous and shelf-stable mixture. Unlike traditional aza-Michael systems, which often exhibit excessive reactivity leading to immediate gelation, this research aims to formulate a pre-polymerized resin or a latent system capable of maintaining a low viscosity for prolonged periods. This aspect is crucial for

the established business model: the company intends to sell this "ready-to-use" mixture to other industrial entities, which can then apply it in situ using standard coating techniques. The stability of the mixture ensures that the material can be stored and transported without losing its flow properties, allowing the activation of the final cross-linking only during the application phase.

The final goal of this research path is not limited to scientific validation in the laboratory but aims for the protection of intellectual property through a patent. Successfully synthesizing a CANs that combines high performance (stiffness and thermal resistance), ease of industrial application (resin stability and low viscosity), and chemical recyclability (via selective hydrolysis under mild conditions) represents a high-value innovation for the insulating polymers market. In summary, the thesis aims to validate a pathway ranging from molecular design to industrial formulation, offering a sustainable and technically superior solution for the next generation of high-performance electrical cables.

In parallel with the development of the cable-coating CANs, a second Covalent Adaptable Network has been designed, formulated, and fully characterized within the framework of the SMIP project, with the purpose of serving as a support material for microelectronics applications. This alternative CANs system was engineered to exhibit elastomeric-like mechanical behavior, providing flexibility, resilience, and dimensional stability under the thermo-mechanical stresses typical of microelectronic devices, while simultaneously preserving the hallmark features of a covalent adaptable network: recyclability and reprocessability akin to those of a thermoplastic. Through careful tuning of the network architecture and dynamic bond density, it was possible to achieve a material that bridges the gap between the soft, deformable nature of elastomers and the robust, repairable, and circular character of thermoplastic-like CANs. This approach offers a promising route toward next-generation encapsulation and support coatings in microelectronics, where the combination of mechanical compliance, chemical stability, and end-of-life recyclability is

essential for both performance and sustainability. The primary objectives and the overall developmental framework of this research work are schematically illustrated in Fig.17.

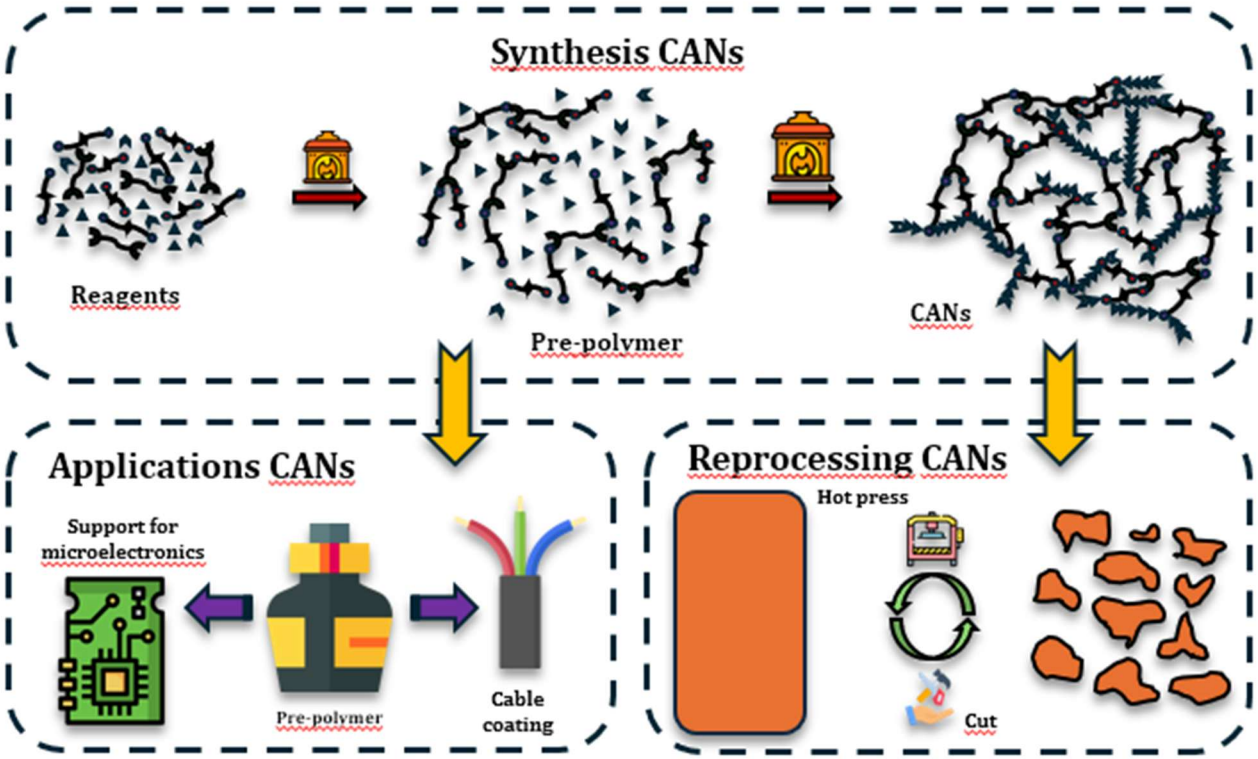

Figure 17. *Symbolic image of the research process addressed in the thesis.*

3. Experimental part

3.1 Materials

All chemicals were purchased from Sigma-Aldrich and used as received, unless otherwise specified in the methods section. The monomers employed for the syntheses include 2-hydroxyethyl methacrylate (HEMA), methyl methacrylate (MMA), 1,4-butanediol diacrylate (BDA), bisphenol A ethoxylate diacrylate (BPADA) and pentaerythritol triacrylate (PETA) and generic rigid (RA) and flexible (FA) bifunctional acrylates for the tricomponent formulation. The amine chosen for the aza-Michael addition was 4,4′-methylenebis(cyclohexylamine) (MCBA) and a different amine for the tricomponent formulation, indicated as AA. Free-radical polymerizations and crosslinking were initiated using radical initiator, indicated as I which was purchased from Sigma Aldrich and used as received. All reagents are shown in Fig.18.

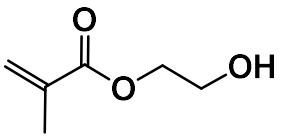

2-hydroxyethyl methacrylate (HEMA)

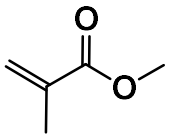

methyl methacrylate (MMA)

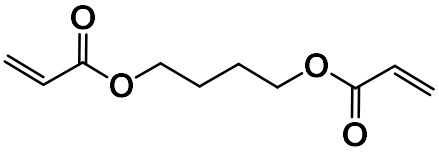

1,4-butanediol diacrylate (BDA)

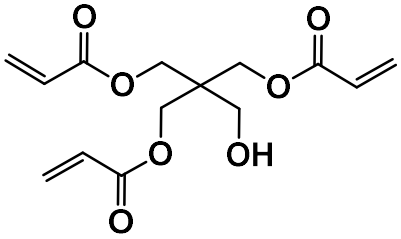

pentaerythritol triacrylate (PETA)

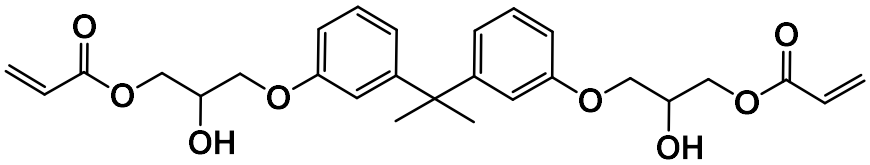

bisphenol A ethoxylate diacrylate (BPADA)

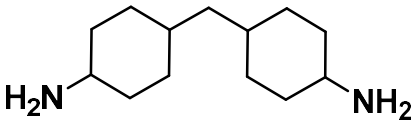

4,4'-methylenebis(cyhexylamine)(MCBA)

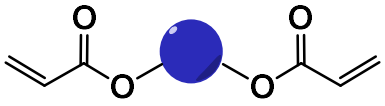

flexible diacrylate (FA)

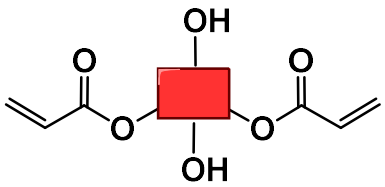

rigid diacrylate (RA)

amine (AA)

Figure 18. *All reagents used.*

3.2 Synthesis of amine-acrylic CANs bicomponent

Initially, a Covalent Adaptable Network (CAN) was synthesized via an aza-Michael reaction using only two components: MCBA and BDA. The two precursors were mixed at a molar ratio of $\frac{n_{BDA}}{n_{MCBA}} = 2$ using a FlackTek SpeedMixer DAC 330-100 PRO for 2 minutes at 2500 rpm. Subsequently, the mixture was allowed to react in a Binder FD 23 oven for 96 hours at 80 °C in air. The specific quantities of the reagents employed in the reaction are summarized in Tab.1.

Table 1. *Formulation of the synthesis: masses of the substances used in the reaction.*

Sample name	**Acrylic component**	**Amine**
	BDA (g)	**MBCA (g)**
VIT.BDA.MBCA.2.0	5.30	10.00

3.2.1 Differential scanning calorimetry (DSC) analysis of amine-acrylic CANs bicomponent

Differential Scanning Calorimetry (DSC) analyses were performed using a Mettler Toledo DSC 1 instrument equipped with standard 40 µL aluminum crucibles. The applied thermal program consisted of three consecutive ramps: a first heating scan from -60 °C to 180 °C at a heating rate of 20 °C/min, a subsequent cooling scan from 180 °C to -60 °C at a cooling rate of 10 °C/min, and a final second heating scan from -60 °C to 180 °C at 20 °C/min. To ensure a strictly inert atmosphere throughout the entire test, all measurements were carried out under a constant nitrogen purge flow of 80 mL/min.

Furthermore, Differential Scanning Calorimetry was also employed to determine the specific heat capacity (C_s) of the material using the standard sapphire method. This methodology involves a reference measurement using a 40 µL aluminum crucible containing a known amount of sapphire, which is subsequently compared with the scan of the sample housed in an identical 40 µL aluminum crucible. Unlike the previously described three-ramp program, a single heating ramp from 25 °C to 150 °C was set for the specific heat evaluation, with a constant scan rate of 10 °C/min. The final C_s

value assigned to the material was determined by calculating the average of the values obtained across the entire temperature range from 25 °C to 150 °C.

3.2.2 Compression and Dynamic Mechanical analysis

Uniaxial compression tests were performed on the vitrimer samples to evaluate their mechanical performance in the solid state. The characterization was carried out at room temperature using a ZwickRoell Universal Testing Machine (UTM) managed via testXpert software. To ensure statistical reliability and verify synthesis reproducibility, the analysis was conducted in duplicate on two distinct specimens. The samples were compressed along their primary axis at a constant crosshead displacement rate until reaching a maximum deformation of approximately 40%, corresponding to the ultimate structural failure or yielding of the network. The compressive stress (σ, expressed in MPa) was calculated by dividing the instantaneous axial force by the initial cross-sectional area of the specimen, while the compressive strain (ε, dimensionless) was determined from the platen displacement relative to the initial sample height. The compression modulus (E_c) was extracted as a chord modulus from the slope of the strictly linear elastic region of the stress-strain curve, selectively bounded between 15% and 30% of compressive strain. This specific window was chosen to exclude the initial contact and sample-platen alignment artifacts (toe region) occurring below 10% strain. The calculation was performed according to the following Eq.6:

$$E_c = \frac{\sigma_2 - \sigma_1}{\varepsilon_2 - \varepsilon_1} \qquad \text{[Eq.6]}$$

where σ_2 and σ_1 represent the compressive stress values recorded at the upper strain limit (ε_2=0.30) and lower strain limit (ε_1= 0.15) of the linear elastic range, respectively.

Dynamic Mechanical Analysis (DMA) was performed using an Anton Paar MCR 702e rheometer equipped with a three-point bending (TPB) geometry. The temperature scans were carried out over a range from -100 °C to 300 °C at a constant heating rate of 4 °C/min under controlled nitrogen

atmosphere. Regarding the loading and kinematic parameters, an initial static preload of 0.1 MPa was applied, and an oscillatory strain amplitude of 0.1% was set at a constant frequency of 1 Hz. To ensure continuous and proper contact between the geometry and the specimen throughout the thermal scan, the static force was automatically adjusted in force-tracking mode, maintaining it at 150% of the generated oscillating stress, with the dynamic force range constrained between a minimum of 10 mN and a maximum of 15 N.

3.2.3 Solubility, swelling tests and chemical recyclability

Solubility and chemical recyclability tests were performed by placing approximately 0.5 g of the polymer sample in 10 mL of solvent. The systems were maintained under stirring in an oil bath at a constant temperature of 100 °C for a duration ranging from a minimum of 18 hours to a maximum of 48 hours. Four different solvents were tested, which were carefully categorized based on the specific objective of the evaluation. Specifically, ethanol, butanol, and a 25% v/v acetic acid aqueous solution were employed to assess the chemical recyclability potential of the network via solvolysis; conversely, tetrahydrofuran (THF) was used exclusively for solubility tests aimed at verifying the chemical resistance and the eventual presence of a crosslinked gel fraction.

Following the tests, the soluble fraction (SF%) and the swelling degree (SD%) were gravimetrically determined according to the following Eq.7-8:

$$SF\% = \frac{w_i - w_d}{w_i} \cdot 100 \qquad \text{[Eq.7]}$$

$$SD\% = \frac{w_s - w_d}{w_d} \cdot 100 \qquad \text{[Eq.8]}$$

where w_i represents the initial weight of the pristine sample, w_s is the weight of the swollen sample recorded immediately after removal from the solvent, and w_d corresponds to the final weight of the dried sample.

Upon observing complete dissolution of the specimens within the three recyclability-targeted solvents (ethanol, butanol, and acetic acid), a subsequent chemical recycling step was undertaken to reform the pristine

solid material. This recovery process was specifically carried out on the butanol solution, which was treated at 100 °C under vacuum for 72 hours using a Binder FD 23 oven, successfully achieving full solvent evaporation and network reconstruction.

3.2.4 Density determination

The experimental density of the synthesized materials was evaluated using the hydrostatic weighing method, which is based on Archimedes' principle, stating that a body immersed in a fluid experiences an upward vertical buoyant force equal to the weight of the displaced fluid volume. For the execution of the measurements, a high-precision analytical balance equipped with a dedicated density determination kit was employed. This instrumental configuration involves the use of a glass vessel (a 250 mL Pyrex beaker) filled with an auxiliary reference liquid (distilled water), a thermometer for in situ temperature monitoring, and a suspended support equipped with a double basket to measure the mass both in air and when fully immersed. Since fluid density varies significantly with temperature, the test was conducted by constantly monitoring the water temperature, which was found to be 22 °C. In accordance with the reference tables at this specific temperature ($T_{H_2O} = 22°C$), the density values of distilled water ($\rho_{H_2O} = 0.99756\ \frac{g}{mL}$) and air ($\rho_{air} = 0.0012\ \frac{g}{mL}$) were set. The experimental protocol involved determining the mass of the solid specimen in air ($w_{sample\ in\ air}$) and, subsequently, the mass of the same specimen immersed in the auxiliary liquid ($w_{sample\ in\ H_2O}$). The final density of the material (ρ_{sample}) was calculated by applying the following Eq.9, which accounts for the buoyant force correction of the surrounding air:

$$\rho_{sample} = \frac{w_{sample\ in\ air}}{w_{sample\ in\ air} - w_{sample\ in\ H_2O}} \cdot \left(\rho_{H_2O} - \rho_{air}\right) + \rho_{air} \qquad [Eq.9]$$

3.3 Synthesis of amine-acrylics CANs tricomponent

To modulate the mechanical properties of the material and reduce curing times, a three-component formulation was developed by introducing a mixture of RA and FA second acrylic monomer. For this synthesis, the overall stoichiometric ratio between the acrylic and amine groups was kept constant at the value of 2.

Practically, due to its high viscosity, the RA was slightly pre-heated in an oven to facilitate dispensing and pouring. It was then pre-mixed with the FA using a FlackTek SpeedMixer DAC 330-100 PRO for 2 minutes at 2500 rpm. Subsequently, the amine was added to this blend, and the system underwent a second mixing cycle in the SpeedMixer DAC 330-100 PRO at the same condition. Finally, the resulting resin was cured in a Binder FD 23 oven at 70 °C for 48 hours. The specific quantities of the reagents employed in the reaction are summarized in Tab.2.

Table 2. *Formulation of the synthesis: masses of the substances used in the reaction.*

Sample name	**Acrylic components**	**Amine**
	RA + FA (g)	**AA (g)**
VIT.RA.FA.AA	15.0	4.665

3.3.1 Differential Scanning Calorimetry (DSC) analysis of amine-acrylics CANs tricomponent

Differential Scanning Calorimetry (DSC) analyses were performed using a Mettler Toledo DSC 1 instrument equipped with standard 40 µL aluminum crucibles. The applied thermal program consisted of three consecutive ramps: a first heating scan from -60 °C to 180 °C at a heating rate of 20 °C/min, a subsequent cooling scan from 180 °C to -60 °C at a cooling rate of 10 °C/min, and a final second heating scan from -60 °C to 180 °C at 20 °C/min. To ensure a strictly inert atmosphere throughout the entire test, all measurements were carried out under a constant nitrogen purge flow of 80 mL/min.

3.4 Synthesis of amine-acrylics CANs tricomponent + MMA

To further modulate the mechanical properties of the material and the curing times, the formulation was expanded by introducing the methacrylic monomer MMA and the thermal initiator (I). Prior to use, to remove the inhibitor (MEHQ) present in the commercial product, the MMA was purified by eluting it through a column packed with inhibitor remover replacement packing (Sigma-Aldrich, Cat.No 311332).

In this study, the impact of MMA was evaluated by testing two different concentrations, namely 50 wt% and 30 wt% based on the total mass of the system, whereas the initiator was introduced at 0.5 wt% calculated exclusively on the mass of the MMA. Furthermore, various stoichiometric ratios between the acrylic groups and the amine were investigated: in addition to the reference ratio of 2:1, ratios of 1.8:1 and 1.5:1 were also studied.

From an operational standpoint, due to its high viscosity, the RA was gently pre-heated in an oven to facilitate dispensing. In parallel, a solution was prepared by mixing the FA, the previously purified MMA, and the initiator. The pre-heated RA was then added to this liquid solution and homogenized using a SpeedMixer DAC 330-100 PRO for 2 minutes at 2500 rpm. Subsequently, the amine was added to the system, followed by a second mixing cycle in the SpeedMixer DAC 330-100 PRO in the same conditions. Finally, the resulting resin was cured in a Binder FD 23 oven at 30 °C for 3 hours and 45 minutes and after 72 hours at 90°C. Finally, the sample was heated at 135 °C for 1 h to complete the curing. The specific quantities of the reagents employed in the reaction are summarized in Tab.3.

Table 3. *Formulation of the synthesis: masses of the substances used in the reaction.*

Sample name	Acrylic components	Amine	Methacrylate	Initiator
	RA + FA (g)	AA (g)	MMA (g)	I (g)
VIT.MMA.70.30.1.5	10.0	3.74	5.88	0.029
VIT.MMA.70.30.1.8	10.0	3.12	5.62	0.028
VIT.MMA.70.30.2.0	10.0	2.79	5.48	0.027
VIT.MMA.50.50.1.5	10.0	3.74	13.74	0.069
VIT.MMA.50.50.1.8	10.0	3.12	13.12	0.066
VIT.MMA.50.50.2.0	10.0	2.79	12.79	0.064

3.4.1 Differential scanning calorimetry (DSC) analysis of amine-acrylics CANs tricomponent + MMA

Differential Scanning Calorimetry (DSC) analyses were performed using a Mettler Toledo DSC 1 instrument equipped with standard 40 µL aluminum crucibles. The applied thermal program consisted of three consecutive ramps: a first heating scan from -60 °C to 180 °C at a heating rate of 20 °C/min, a subsequent cooling scan from 180 °C to -60 °C at a cooling rate of 10 °C/min, and a final second heating scan from -60 °C to 180 °C at 20 °C/min. To ensure a strictly inert atmosphere throughout the entire test, all measurements were carried out under a constant nitrogen purge flow of 80 mL/min.

3.5 Synthesis of amine-acrylics CANs tricomponent + HEMA

The formulation was changed by introducing the methacrylic monomer HEMA but with the same thermal initiator (I). Prior to use, to remove the inhibitor (MEHQ) present in the commercial product, the HEMA was purified by eluting it through a column packed with inhibitor remover replacement packing (Sigma-Aldrich, Cat.No 311332).

In this study, the impact of HEMA was evaluated by testing differents concentrations, namely 90 wt%, 70wt%, 60 wt%, 50 wt% and 30 wt% based on the total mass of the system, whereas the AIBN initiator was introduced at 1 wt% calculated exclusively on the mass of the HEMA. Furthermore, various stoichiometric ratios between the acrylic groups and the amine were investigated: in addition to the reference ratio of 2:1, ratios of 1.8:1 and 1.5:1 were also studied.

From an operational standpoint, due to its high viscosity, the RA was gently pre-heated in an oven to facilitate dispensing. In parallel, a solution was prepared by mixing the FA, the previously purified HEMA, and the initiator. The pre-heated RA was then added to this liquid solution and homogenized using a SpeedMixer. Subsequently, the amine was added to the system, followed by a second mixing cycle in the SpeedMixer. Finally, the resulting resin was cured in a Binder FD 23 oven at 30 °C for 3 hours and 45 minutes and after 72 hours at 90°C. Finally, the sample was heated at 135 °C for 1 h to complete the curing. The specific quantities of the reagents employed in the reaction are summarized in Tab.4.

Table 4. *Formulation of the synthesis: masses of the substances used in the reaction.*

Sample name	Acrylic components	Amine	Methacrylate	Initiator
	RA + FA (g)	AA (g)	HEMA (g)	I (g)
VIT.HEMA.70.30.1.5	10.0	3.74	5.88	0.059
VIT.HEMA.70.30.1.8	10.0	3.12	5.62	0.056
VIT.HEMA.70.30.2.0	10.0	2.79	5.48	0.055
VIT.HEMA.50.50.1.5	10.0	3.74	13.74	0.137
VIT.HEMA.50.50.1.8	10.0	3.12	13.12	0.131
VIT.HEMA.50.50.2.0	10.0	2.79	12.79	0.128
VIT.HEMA.40.60.1.5	10.0	3.74	20.61	0.206
VIT.HEMA.40.60.1.8	10.0	3.12	19.68	0.199
VIT.HEMA.40.60.2.0	10.0	2.79	19.19	0.192
VIT.HEMA.30.70.1.5	10.0	3.74	32.06	0.321
VIT.HEMA.30.70.1.8	10.0	3.12	30.61	0.306
VIT.HEMA.30.70.2.0	10.0	2.79	29.84	0.298
VIT.HEMA.10.90.1.5	10.0	3.74	123.66	1.237
VIT.HEMA.10.90.1.8	10.0	3.12	118.08	1.181
VIT.HEMA.10.90.2.0	10.0	2.79	115.11	1.151

3.5.1 Solubility and swelling tests of amine-acrylics CANs tricomponent + HEMA

Solubility tests were performed by placing approximately 0.5 g of the polymer sample in 10 mL of ethanol (EtOH). The systems were maintained under stirring at room temperature for 24 hours to evaluate the chemical resistance of the network and verify the presence of a crosslinked gel fraction. Following the tests, the soluble fraction (SF%) and the swelling degree (SD%) were gravimetrically determined in accordance with the equations already described in Section 3.2.3, Eq.7-8. To ensure the complete evaporation of the absorbed EtOH and obtain an accurate dry weight, the recovered specimens were subsequently dried at 100 °C under vacuum for 72 hours using a Binder FD 23 oven.

3.5.2 Differential scanning calorimetry (DSC) analysis of amine-acrylics CANs tricomponent + HEMA

Differential Scanning Calorimetry (DSC) analyses were performed using a Mettler Toledo DSC 1 instrument equipped with standard 40 µL aluminum crucibles. The applied thermal program consisted of three consecutive ramps: a first heating scan from -60 °C to 180 °C at a heating rate of 20 °C/min, a subsequent cooling scan from 180 °C to -60 °C at a cooling rate of 10 °C/min, and a final second heating scan from -60 °C to 300 °C at 20 °C/min. To ensure a strictly inert atmosphere throughout the entire test, all measurements were carried out under a constant nitrogen purge flow of 80 mL/min.

Furthermore, utilizing the same analysis conditions, DSC was employed to investigate the reaction kinetics of the second step, specifically monitoring the free-radical polymerization and conversion of HEMA over time. The progress of the reaction and the degree of conversion (conversion%) were determined from the integration of the exothermic reaction peaks according to the following Eq.10-11:

$$x = \frac{\Delta H_t}{\Delta H_{t_0}} \qquad \text{[Eq.10]}$$

$$\text{Conversion\%} = (1 - x) \cdot 100 \qquad \text{[Eq.11]}$$

Where ΔH_t is the partial heat generated up to a specific time (t), ΔH_{t_0} is the total exothermic heat of the polymerization reaction, and x represents the ratio of the signal at time zero to the signal at time t.

3.5.3 Stress relaxation analysis

Stress relaxation analyses were performed using an Anton Paar MCR 702e rheometer equipped with a 25 mm diameter parallel-plate geometry. The tests were conducted by applying a constant strain of 1% under isothermal conditions at two different temperatures, specifically at 180 °C and 190 °C under controlled nitrogen atmosphere, to monitor the stress relaxation behavior of the network over time. The characteristic relaxation time (**τ**) was determined by fitting the experimental data with the Maxwell model, expressed according to the following Eq.12:

$$\frac{G(t)}{G_0} = e^{-\frac{t}{\tau}} \qquad \text{[Eq.12]}$$

where G(t) is the relaxation modulus at time t and G_0 is the initial modulus. Consequently, the relaxation time τ was systematically evaluated for all formulations as the time required for the normalized modulus to decay to a value of $\frac{G(t)}{G_0} = \frac{1}{e} \approx 0.36787$ (approximately 0.37).

3.5.4 Dynamic mechanical analysis (DMA)

Dynamic Mechanical Analysis (DMA) was performed using an Anton Paar MCR 702e rheometer equipped with a three-point bending (TPB) geometry. The temperature scans were carried out over a range from -100 °C to 300 °C at a constant heating rate of 4 °C/min under controlled nitrogen atmosphere. Regarding the loading and kinematic parameters, an initial static preload of 0.1 MPa was applied, and an oscillatory strain amplitude of 0.1% was set at a constant frequency of 1 Hz. To ensure continuous and proper contact between the geometry and the specimen throughout the thermal scan, the static force was automatically adjusted in force-tracking mode, maintaining it at 150% of the generated oscillating stress, with the dynamic force range constrained between a minimum of 10 mN and a maximum of 15 N.

3.5.5 Shear rate sweep analysis

In order to monitor the kinetic evolution of the first reactive stage and evaluate the shelf-stability of the pre-polymer, rheological analyses were performed on aliquots sampled at different time intervals during the reaction (carried out at 30 °C). Each collected sample was individually characterized through rotational tests to determine the flow curve (or shear rate sweep) using an Anton Paar MCR 702e rheometer equipped with a 50 mm diameter cone-plate geometry.

The tests on each aliquot were conducted under isothermal conditions at a constant temperature of 30 °C, varying the shear rate from 0.01 s^{-1} to 10 s^{-1} via a logarithmic ramp, in air to avoid the nitrogen flow stripping the HEMA monomer. This experimental approach enabled the tracking of the system's viscous behavior as a function of reaction time. The primary objective was to verify that, at the target time of 3 hours and 45 minutes (marking the end of the first step, as introduced in Chapter 3.5), the viscosity profiles reached a plateau and exhibited no further increases in subsequent samplings. This rheological stability confirms the successful formation of a kinetically dead and stable pre-polymer, which is an essential prerequisite to ensure the shelf-life and consistency of the premix prior to the second radical crosslinking step.

3.5.6 Nuclear magnetic resonance (NMR) analysis

Proton Nuclear Magnetic Resonance (^{1}H-NMR) analyses were performed using a Bruker spectrometer operating at a frequency of 500 MHz. This spectroscopic technique served as a key analytical tool to monitor the chemical progress of the system, allowing for the quantitative evaluation of the conversion degree of the acrylic double bonds and the progressive consumption of the amine groups involved in the initial aza-Michael addition step. For the measurements, the collected samples were dissolved in deuterated chloroform ($CDCl_3$). The reaction conversion was determined by tracking the evolution of the signal areas, specifically monitoring the progressive decrease in the intensity of the peaks associated with the olefinic protons of the acrylic groups relative to the group of peaks corresponding to protons which do not participate in the reaction and serve as a reliable internal structural reference. The conversion was evaluated using the following Eq.13-14.

$$x = \frac{I_t}{I_{t_0}} \qquad \text{[Eq.13]}$$

$$\text{Conversion}\% = (1 - x) \cdot 100 \qquad \text{[Eq.14]}$$

Where I_t is the average intensity (or integral area) of the three peaks corresponding to the reactive acrylic protons evaluated at a specific reaction time t, I_{t_0} is the total intensity of the acrylics peaks at the time zero and x represents the ratio of the signal at time zero to the signal at time t. Crucially, both values are strictly normalized against the area of the fixed internal reference signal which do not participate in the reaction.

3.6 Synthesis of amine-acrylics CANs four-component

Following the preliminary screening of various hybrid aza-Michael/free-radical systems, it was decided to focus the study on a non-hybrid, multi-component Covalent Adaptable Network (CAN) system. To systematically modulate the mechanical properties and evaluate the influence of monomer functionality on the final network architecture, a trifunctional acrylic monomer, pentaerythritol triacrylate (PETA), was introduced alongside the bifunctional components consisting of BDA, BPADA, and the MBCA amine. Ideally, the incorporation of this trifunctional crosslinker is expected to increase the crosslinking density, thereby leading to a distinct increment in the system's structural rigidity. For all formulated systems, the ideal stoichiometric ratio between the total moles of acrylic functional groups and amine functional groups was strictly kept constant at 2:1. From a practical standpoint, due to its high viscosity, the BPADA was slightly pre-heated in an oven to facilitate dispensing and pouring, and it was then pre-mixed with BDA using a FlackTek SpeedMixer DAC 330-100 PRO for 2 minutes at 2500 rpm. Subsequently, the trifunctional monomer PETA was added to this initial acrylic blend before introducing the amine (MBCA). The entire system then underwent a second mixing cycle in the SpeedMixer under the same conditions, and the resulting homogeneous resin was finally cast and cured in a Binder FD 23 oven at 80 °C for 48 hours and at 100°C 24 hours. The complete set of investigated compositions is summarized in Tab.5. As indicated, the matrix of samples includes the newly developed four-component series at varying ratios, alongside a specific three-component analog system. This three-component formulation serves as a direct benchmark where BPADA has been entirely replaced by PETA, consisting solely of BDA, PETA, and MBCA.

Table 5. *Formulation of the synthesis: masses of the substances used in the reaction.*

Sample name	Acrylic components			Amine
	PETA (g)	BPADA (g)	BDA (g)	MBCA (g)
VIT.PETA.2.1.80.20	8.00	0	2.00	7.06
VIT.PETA.2.1.75.20.5	7.50	0.50	2.00	6.79
VIT.PETA.2.1.70.20.10	7.00	1.00	2.00	6.53
VIT.PETA.2.1.60.20.20	6.00	2.00	2.00	5.99
VIT.PETA.2.1.40.20.40	4.00	4.00	2.00	4.93
VIT.PETA.2.1.20.20.60	2.00	6.00	2.00	3.86
VIT.PETA.2.1.10.20.70	1.00	7.00	2.00	3.33
VIT.PETA.2.1.5.20.75	0.50	7.50	2.00	3.06

3.6.1 Solubility and swelling tests of amine-acrylics CANs four-component

Solubility tests were performed by placing approximately 0.5 g of the polymer sample in 10 mL of tetrahydrofuran (THF). The systems were maintained under stirring at room temperature for 24 hours to evaluate the chemical resistance of the network and verify the presence of a crosslinked gel fraction. Following the tests, the soluble fraction (SF%) and the swelling degree (SD%) were gravimetrically determined in accordance with the equations already described in Section 3.2.3, Eq.7-8. To ensure the complete evaporation of the absorbed THF and obtain an accurate dry weight, the recovered specimens were subsequently dried at 100 °C under vacuum for 72 hours using a Binder FD 23 oven.

3.6.2 Differential Scanning Calorimetry (DSC) analysis of amine-acrylics CANs four-component

Differential Scanning Calorimetry (DSC) analyses were performed using a Mettler Toledo DSC 1 instrument equipped with standard 40 µL aluminum crucibles. The applied thermal program consisted of three consecutive ramps: a first heating scan from -60 °C to 180 °C at a heating rate of 20 °C/min, a subsequent cooling scan from 180 °C to -60 °C at a cooling rate of

10 °C/min, and a final second heating scan from -60 °C to 300 °C at 20 °C/min. To ensure a strictly inert atmosphere throughout the entire test, all measurements were carried out under a constant nitrogen purge flow of 80 mL/min.

3.6.3 Stress relaxation analysis

Stress relaxation analyses were performed using an Anton Paar MCR 702e rheometer equipped with a 25 mm diameter parallel-plate geometry. The tests were conducted by applying a constant strain of 1% under isothermal conditions at three different temperatures, specifically at 150 °C, 165 °C and 180 °C under controlled nitrogen atmosphere, to monitor the stress relaxation behavior of the network over time. The characteristic relaxation time (τ) was systematically evaluated using Eq.12, as described in detail in Section 3.5.3. This value corresponds to the time required for the normalized modulus to decay to $\frac{G(t)}{G_0} = \frac{1}{e} \approx 0.36787$.

Furthermore, the characteristic relaxation times (τ) obtained at each temperature were utilized to construct an Arrhenius plot. By employing the linearized form of the Arrhenius equation (Eq. 15):

$$\ln(\tau) = \ln(\tau_0) + \frac{E_a}{RT} \qquad \text{[Eq.15]}$$

and plotting $\ln(\tau)$ as a function of the reciprocal of the absolute temperature ($\frac{1}{T}$), it was possible to calculate the activation energies (E_a). Specifically, E_a was directly determined from the slope (m) of the resulting linear regression line according to Eq.16:

$$E_a = m \cdot R \qquad \text{[Eq.16]}$$

where m is the slope of the linear fit, R represents the universal gas constant ($8.314 \frac{J}{K \cdot mol}$), and τ_0 is the pre-exponential frequency factor representing the theoretical relaxation time at infinite temperature.

3.6.4 Dynamic mechanical analysis (DMA)

Dynamic Mechanical Analysis (DMA) was performed using an Anton Paar MCR 702e rheometer equipped with a three-point bending (TPB) geometry. The temperature scans were carried out over a range from -100 °C to 250 °C at a constant heating rate of 4 °C/min under controlled nitrogen atmosphere. Regarding the loading and kinematic parameters, an initial static preload of 0.1 MPa was applied, and an oscillatory strain amplitude of 0.05% was set at a constant frequency of 1 Hz. To ensure continuous and proper contact between the geometry and the specimen throughout the thermal scan, the static force was automatically adjusted in force-tracking mode, maintaining it at 150% of the generated oscillating stress, with the dynamic force range constrained between a minimum of 10 mN and a maximum of 15 N.

3.7 Reprocessing test of all the synthesized CANs

The reprocessability of the synthesized materials was evaluated through hot-pressing tests (reprocessing), carried out using a Vogt hot press (model Handhebelpresse P150 H K). For each test, a constant load of approximately 4.5 tons was applied. The operational parameters of temperature and time were optimized and tailored according to the specific nature of the analyzed polymer system; specifically, temperatures of either 150 °C or 180 °C and processing residence times ranging from 30 minutes to 1 hour and 30 minutes were set, the details of which will be systematically discussed in the subsequent Chapter 4.

4. Result and discussion

4.1 Synthesis and characterization of amine-acrylic CANs bicomponent

4.1.1 Synthesis, solubility and swelling tests

Within the framework of the SMIP project, a specific class of Covalent Adaptable Networks (CANs) was synthesized and systematically characterized. The network architecture is based on the catalyst-free aza-Michael addition between the acrylic monomer 1,4-butanediol diacrylate (BDA) and the amine monomer MCBA, leading to the formation of a cross-linked poly(β-amino ester) system. The synthesis was performed by establishing a precise stoichiometric control, with a molar ratio of reactive acrylic groups to amine groups equal to 2.0. To ensure complete conversion and the proper development of the network topology, the curing reaction was carried out in an oven at 80 °C for 96 hours. For clarity and consistency throughout this study, the synthesized sample was designated as VIT.BDA.MCBA.2.0. The comprehensive synthetic pathway of the network, and its corresponding recycling mechanism are schematically illustrated in Fig.19.

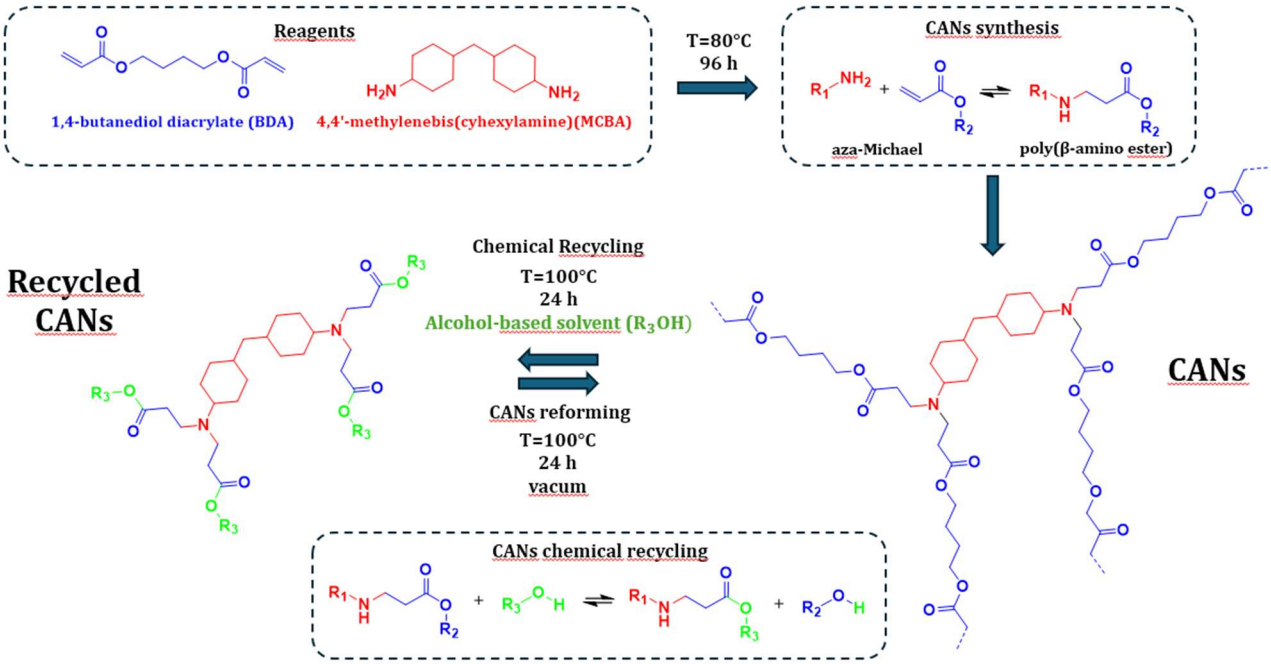

Figure 19. *Comprehensive schematic overview of the reagents, polymerization chemistry, and chemical recycling/reforming loop of the VIT.BDA.MCBA.2.0 covalent adaptable networks (CANs).*

The initial phase of the characterization aimed to confirm the cross-linked nature of the Covalent Adaptable Networks (CANs) synthesized for the SMIP project by demonstrating their insolubility in strong organic solvents. To this end, the samples were subjected to immersion tests in tetrahydrofuran (THF) at 100 °C for 24 hours. In order to quantify any potential material loss and the solvent absorption capacity, the soluble fraction (SF%) and the swelling degree (SD%) were calculated using the equations described in chapter 3.2.3 and the results obtained are reported in the Tab.6:

Table 6. *Masses and results of soluble fraction (SF%) and swelling degree (SD%), where w_i represents the initial weight of the pristine sample, w_s is the weight of the swollen sample recorded immediately after removal from the solvent, w_d corresponds to the final weight of the dried sample, w_{as} represents the mass of the adsorbed solvent and w_l indicates the lost sample mass.*

Sample name and results %	$\mathbf{w_i}$ **(g)**	$\mathbf{w_s}$ **(g)**	$\mathbf{w_{as}}$ **(g)**	$\mathbf{w_d}$ **(g)**	$\mathbf{w_l}$ **(g)**
VIT.BDA.MBCA.2.0	0.3647	0.677	0.3679	0.3091	0.0556
SF%	15%				
SD%	119%				

As evidenced by the results reported in the table, the material exhibits a relatively high soluble fraction compared to the ideal zero value expected for a perfectly cross-linked polymer. In contrast, the swelling ratio is entirely consistent with the data reported in the literature[42,43].

4.1.2 Recyclability test

Following the evaluation of chemical resistance, the study proceeded with recyclability tests. For this purpose, the samples were immersed at 100 °C in three different reactive media: butanol, ethanol, and a 25% v/v acetic acid solution. The objective of the test was to induce the breakdown of the network through the transesterification reactions between the CANs and the solvent molecules catalysed by the amine groups in β-position, achieving the complete solubilization of the material. As shown in Fig. 20, all three systems yielded excellent results, although exhibiting different reaction efficiencies and kinetics. Specifically, the transesterification process led to complete solubilization in 48 h in ethanol, 24 h in butanol, and only 18 h when using the 25% v/v acetic acid.

Subsequently, the recovery of the material previously solubilized in butanol was carried out. For this purpose, the solution was subjected to a thermal treatment in a Binder FD 23 oven at 100 °C for 72 h under vacuum. The removal of the excess butanol by evaporation allows the chemical equilibrium to shift towards the reverse transesterification reaction: under these conditions, the butanediol formed as a byproduct during the previous solubilization phase reacts again, recreating the cross-links. This process leads to the reformation of the initial polymer network, ensuring and demonstrating the effective recyclability of the product, as shown in Fig.21. As further confirmation of the recycling process efficacy, the following chapter will demonstrate that the glass transition temperature (T_g) of the material remains unaltered after the treatment.

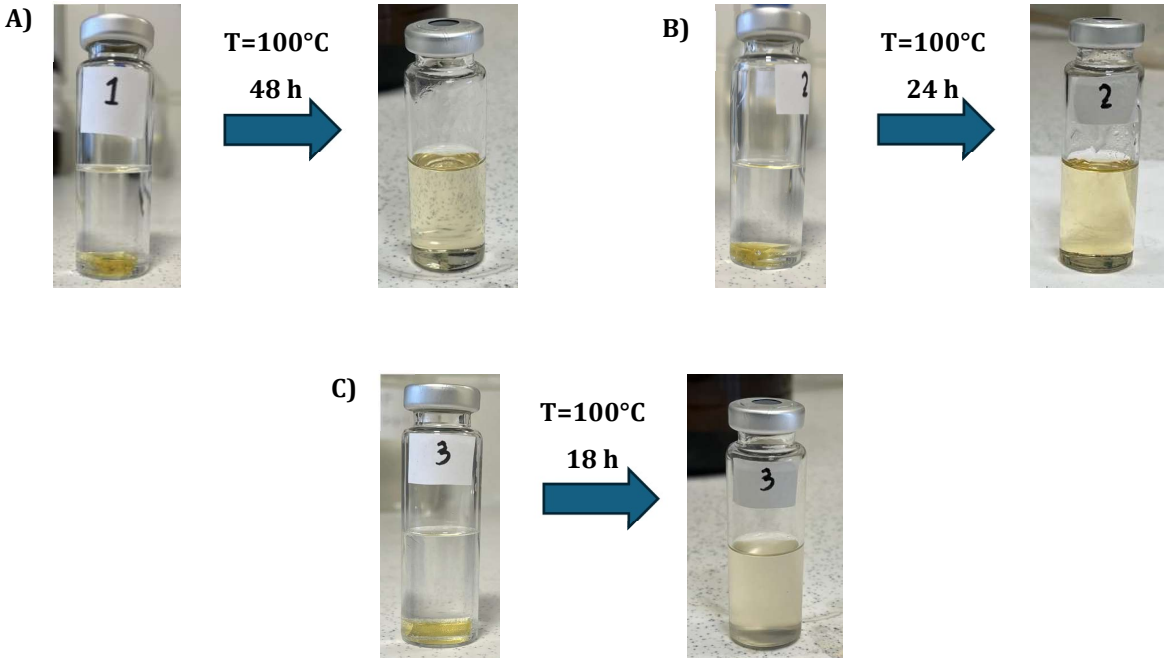

Figure 20. *Solubilization of CANs by transesterification in three differents solvets A) Ethanol, B) Butanol and C) Acetic acid 25% v/v.*

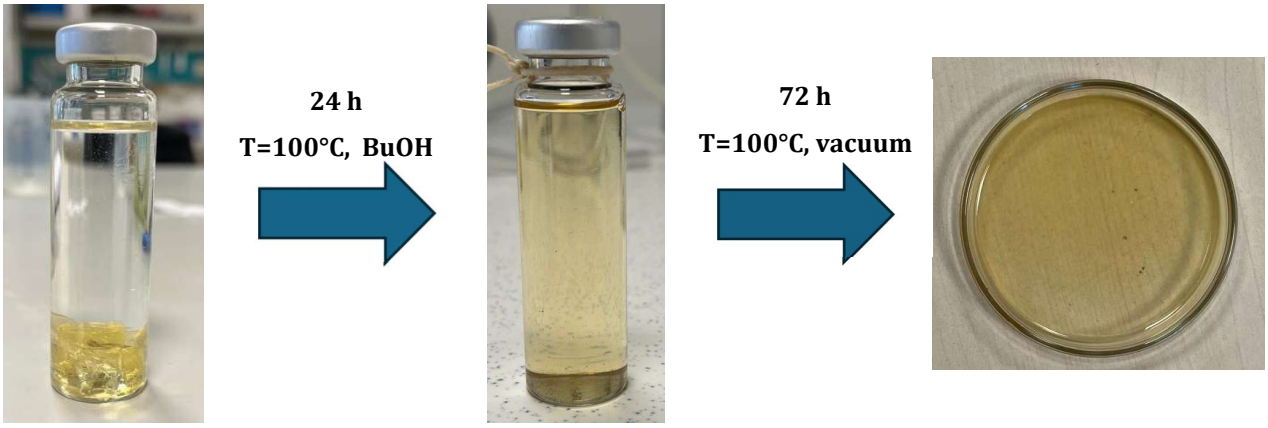

Figure 21. *Solubilization of CANs by transesterification in three differents solvets A) Ethanol, B) Butanol and C) Acetic acid 25% v/v.*

4.1.3 Thermal characterization of amine-acrylic CANs bicomponent

Differential Scanning Calorimetry (DSC) was employed, according to the methodology detailed in Chapter 3, to determine the glass transition temperature (T_g) before and after recycling, thereby evaluating the structural reinstatement of the network. Additionally, the sapphire method was utilized to measure the specific heat capacity (C_s) of the pristine starting material. As summarized in Tab.7, the consistent sub-zero T_g values of both the pristine and reprocessed samples (-20.44 °C and -17.36 °C, respectively), together with the $C_s$value of 2.05 ± 0.12 $\frac{J}{g \cdot °C}$ recorded for the initial matrix, are typical for elastomeric systems and in perfect agreement with literature data, confirming the intrinsic rubbery nature of the network. Remarkably, as shown in Fig.22, the T_g of the recycled sample is very similar to the one of the pristine material, thus confirming the chemical recyclability of the material,

Table 7. *DSC thermal analysis results for the VIT.BDA.MBCA.2.0 formulation, showing the glass transition temperature variations for the pristine (T_g) and recycled ($T_{g,recycled}$) networks, alongside the specific heat capacity (C_s).*

Sample name		
VIT.BDA.MBCA.2.0		
T_g (h)	**$T_{g,recycled}$ (h)**	**$C_s(\frac{J}{g \cdot °C})$**
-20.44	-17.36	2.05±0.12

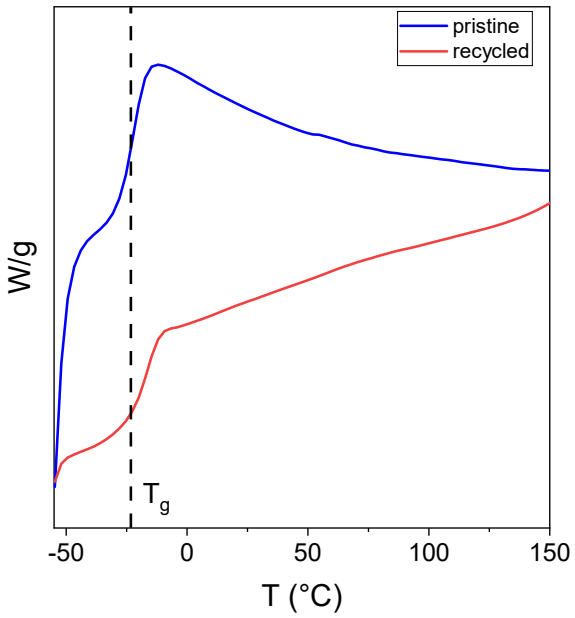

Figura 22. *DSC curves (range from -60 °C to +180 °C) of the VIT.BDA.MCBA.2.0 sample comparing pristine and recycled states. The dashed line indicates the glass transition temperature (T_g).*

This perfect overlap underscores that the dynamic network completely reconstructs its original cross-linking density and macromolecular mobility during the reforming stage.

4.1.4 Density measurement

The density of the material was determined according to the procedure detailed in experimental Section 3.2.4. The results shown in the following Tab.8.

Table 8. *Experimental weights and density values determined via Archimedes' principle for the VIT.BDA.MBCA.2.0 formulation, including sample weights in air ($w_{sample\ in\ air}$) and water ($w_{sample\ in\ H_2O}$), alongside air, water, and final specimen densities ($\rho_{air_{(T=22°C)}}, \rho_{H_2O_{(T=22°C)}}, \rho_{sample}$) measured at 22 °C.*

Sample name				
VIT.BDA.MBCA.2.0				
$\mathbf{w_{sample\ in\ air}(g)}$	$\mathbf{w_{sample\ in\ H_2O}(g)}$	$\mathbf{\rho_{air_{(T=22°C)}}(\frac{g}{mL})}$	$\mathbf{\rho_{H_2O_{(T=22°C)}}(\frac{g}{mL})}$	$\mathbf{\rho_{sample}(\frac{g}{mL})}$
0.682	0.075	0.0012	0.9976	1.120

The experimental density value of 1.120 $\frac{g}{mL}$ is in perfect agreement with standard literature data for crosslinked acrylic polymer networks, which typically range between 1.0 and 1.4 $\frac{g}{mL}$[49].

4.1.5 Compression and Dynamic Mechanical analysis

The uniaxial compression behavior of the VIT.BDA.MCBA vitrimer sample was evaluated following the protocol detailed in Section 3.7.4. As illustrated in Fig.23, an excellent overlapping and reproducibility can be observed between the two tested replicates, demonstrating the high homogeneity of the synthesized networks. The compression modulus (E_c), extracted from the linear elastic region bounded between 15% and 30% strain as described in the experimental section, was found to be approximately 8.0 MPa. This value is in optimal agreement with literature data reported for crosslinked acrylic networks and advanced elastomeric vitrimers with high structural cohesion. Furthermore, the curves exhibit a characteristic yield/ultimate compressive strength of approximately 3.0 - 3.1 MPa at a deformation of 35%–40%, just before the onset of structural failure. These maximum stress values are fully consistent with reference values in scientific literature for high-performance elastomeric systems, confirming that the incorporation

of the BDA/MCBA crosslinking architecture successfully imparts robust solid-state mechanical integrity to the vitrimer matrix[15,50].

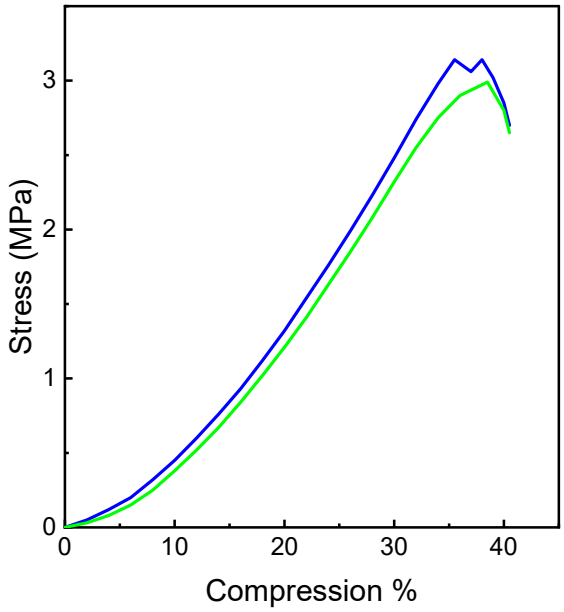

Figure 23. *Uniaxial compression behavior of VIT.BDA.MCBA vitrimer at room temperature. The curves show the characteristic engineering stress (MPa) plotted against the compressive strain (%) up to the point of network failure (≈40%). The plot displays two distinct replicates (blue and green curves).*

Subsequently, Dynamic Mechanical Analysis (DMA) was performed on the VIT.BDA.MCBA.2.0 sample in a temperature range from -100 °C to 150 °C. As displayed in Fig.24, the T_g value was determined from the peak of the tan(δ) curve, showing a perfect agreement with the previously discussed DSC data. Furthermore, the storage modulus (E') in the rubbery plateau above T_g was found to be approximately 5 MPa, which is in excellent accordance with the elastic modulus value obtained from the uniaxial compression tests, confirming the consistency between the dynamic and static mechanical behavior of the network, as can be observed in the following Fig.24, which displays the plots of the storage modulus (E'), loss modulus (E''), and damping factor (tan(δ)).

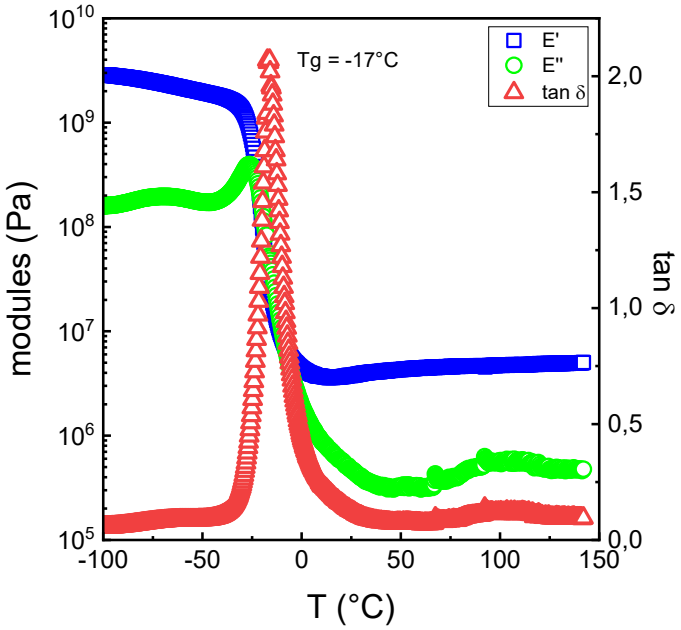

Figure 24. *DMA curves (storage modulus E', loss modulus E'' and tan(δ) vs temperature from -100 °C to +150 °C) for the VIT.BDA.MCBA.2.0 network. The T_g corresponding to the maximum of the tan(δ) peak.*

4.2 Synthesis and characterization of amine-acrylic CANs tricomponent

4.2.1 Synthesis and thermal characterization of amine-acrylic CANs tricomponent

Having concluded the characterization phase of the materials intended for the SMIP project, this chapter illustrates the results obtained within the framework of the project developed for ELANTAS. From a formulation perspective, the study involved a transition from a two-component to a three-component system. The introduction of a third reagent was designed to tune the network rigidity, thereby achieving higher glass transition temperatures (T_g). The primary objective of this research is the development of a hybrid, two-step curing system that combines a vitrimer oligomer component with a radical monomer intended for subsequent polymerization. The utility of this approach lies in the formulation of a processable, two-step reaction sequence designed to yield a commercially viable pre-polymer. In the first stage, the vitrimer oligomers are synthesized to establish a processable framework; subsequently, the system can undergo a second radical curing step to achieve the final, fully cross-linked network. This architecture provides dual advantages, offering the scalability and handling characteristics of traditional commercial resins alongside the advanced recyclability and reprocessability typical of vitrimeric materials. However, before evaluating the formulation as a whole, it is crucial to fully understand the behavior of the dynamic matrix. Therefore, this chapter describes a series of preliminary studies focused exclusively on the vitrimeric component. The synthesis was carried out using RA, FA, and AA, monomers previously identified as optimal candidates, by conducting the reaction at 70 °C for 48 h with an acrylate-to-amine functional group ratio equal to 2 (acrylate/amine = 2). The sample was named VIT.RA.FA.AA. The comprehensive synthetic pathway of the network, and its corresponding reprocessing mechanism are schematically illustrated in Fig.25.

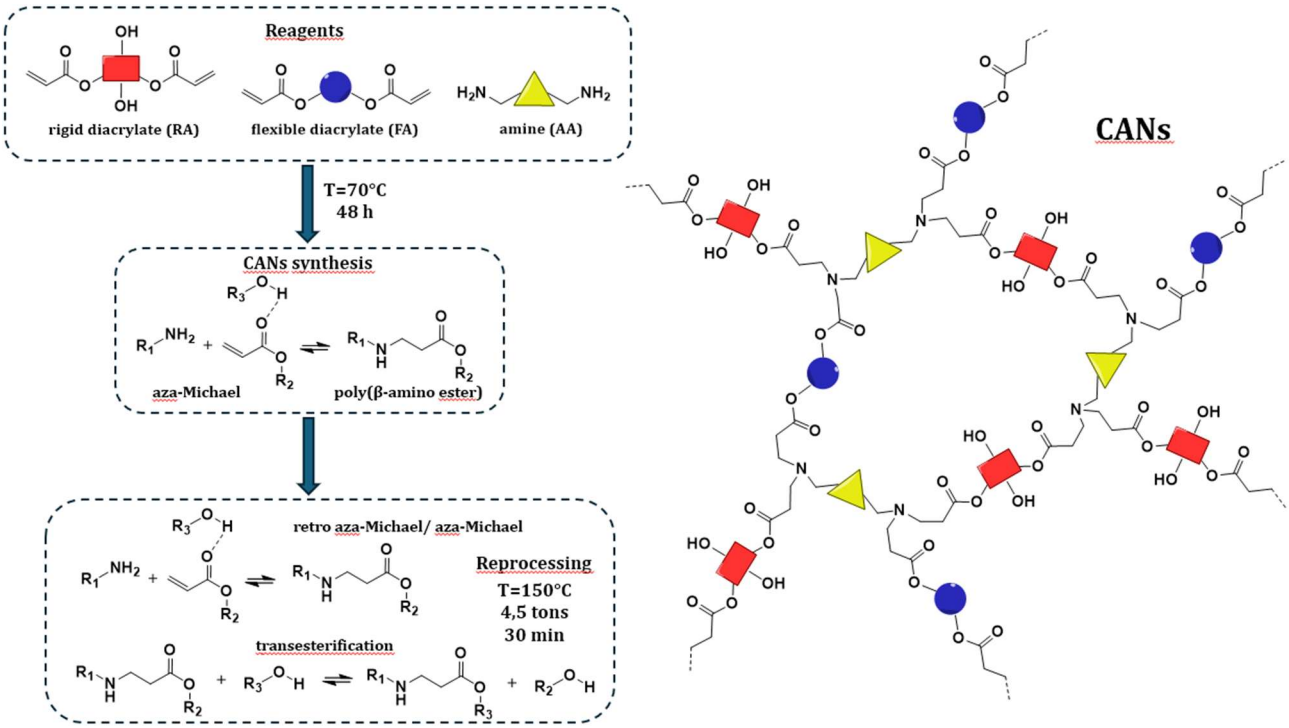

***Figura 25**. Comprehensive schematic overview of the reagents, polymerization chemistry, and reforming loop of the VIT.RA.FA.AA covalent adaptable networks (CANs).*

The characterization of this new class of materials relied primarily on thermo-mechanical testing. First, to verify the effective increase in T_g, Differential Scanning Calorimetry (DSC) analyses were performed using a Mettler Toledo DSC 1 instrument. The resulting thermograms and the corresponding analysis parameters are reported in Fig.26. Specifically, the T_g evaluated from the ISO midpoint during the first heating scan was approximately 61 °C, representing a substantial increase compared to the value of roughly -20 °C observed for the two-component CANs discussed in the previous chapter**.** The T_g was measured during the first heating scan. This choice is justified because, in the first heating, the heat flow curve shows a steep slope immediately after T_g that could be mistaken for an endothermic peak arising from retro-aza-Michael reactions. Indeed, in the second heating scan the observed T_g is lower, likely because not all network points opened by retro-aza-Michael reactions during the first heating fully reclosed on cooling. This incomplete reformation increases network mobility and consequently reduces the measured T_g.

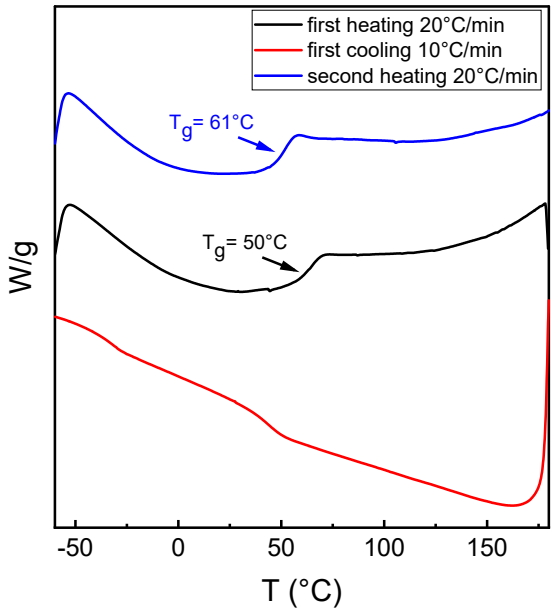

Figure 26. *DSC thermogram of the three-component CANs. The thermal cycle consists of a first heating scan from -60 °C to 180 °C at 20 °C/min (black curve), a cooling scan from 180 °C to -60 °C at 10 °C/min, and a second heating scan from -60 °C to 180 °C at 20 °C/min, all ramps were perfomed with a nitrogen flow of 80 mL/min.*

4.2.2 Reprocessing and self-healing tests

Following the thermal analysis, which confirmed the increased rigidity of the network, reprocessing tests were conducted. The purpose of these tests was to assess whether the enhanced structural rigidity of the system still allowed for proper material reprocessing. The results were highly positive, demonstrating excellent reprocessability: the material was successfully reprocessed by subjecting it to a temperature of 150 °C under an applied load of 4.5 tons for 30 minutes, Fig.27.

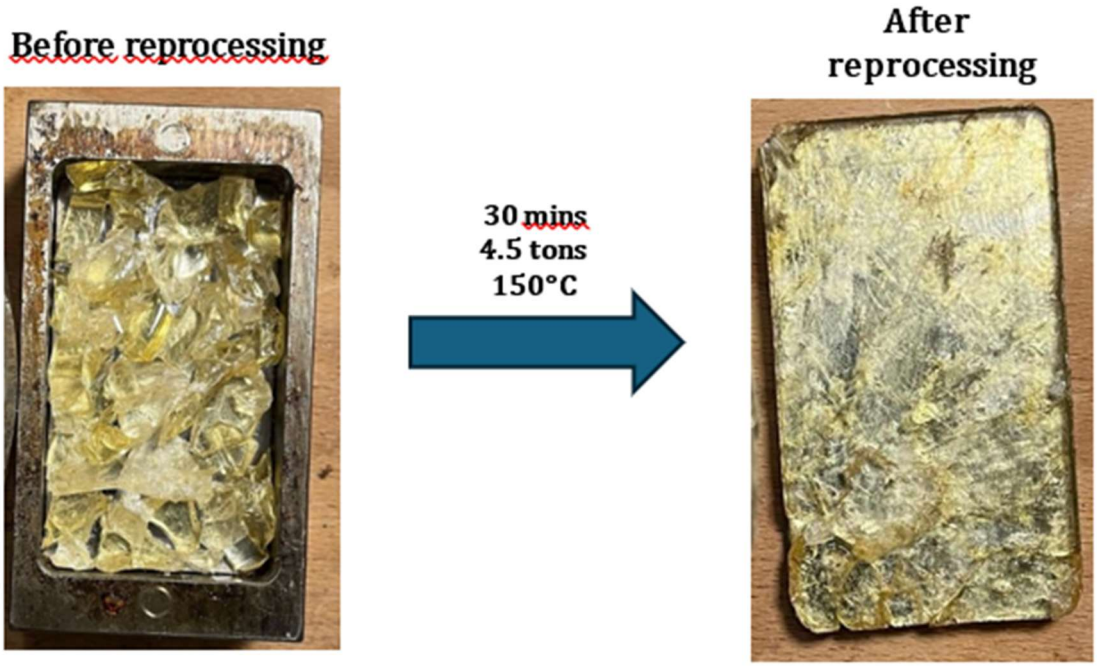

Figure 27. *Reprocessing of the three-component CANs.*

Finally, a series of tests was carried out to evaluate the self-healing properties of the polymer. These tests, however, yielded poor results, as can be observed in Fig.28. This outcome was largely expected: the increase in the structural rigidity of the network, aimed at raising the T_g, inevitably restricts the mobility of the polymer chains, thereby hindering the diffusion mechanisms required for effective self-healing.

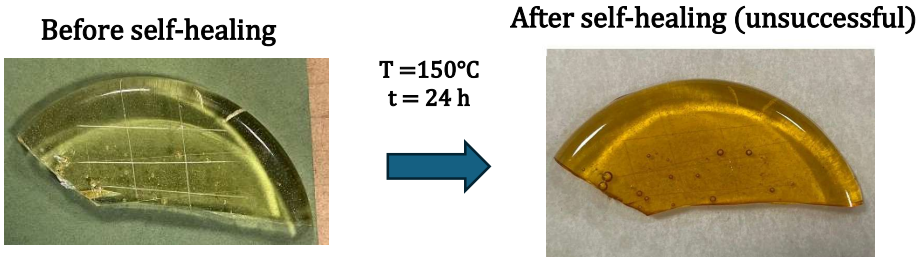

Figure 28. *Test self-healing of the three-component CANs. The test was performed for 24 h at a temperature of 150 °C in Binder FD 23 oven.*

4.3 Synthesis and characterization of amine-acrylic CANs tricomponent + MMA

4.3.1 Synthesis and reprocessing test

In continuity with the findings of the previous chapter, the research activity proceeded by testing the introduction of a methacrylic monomer, namely methyl methacrylate (MMA). The specific objective was to further increase the glass transition temperature (T_g) of the material while simultaneously preserving its reprocessability. At this stage, the investigation of self-healing properties was excluded a priori, as efforts were deliberately focused on optimizing the thermo-mechanical performance. To achieve this, the synthesis protocol involves two main reaction steps: an initial aza-Michael addition carried out at 30 °C for 3 hours and 45 minutes to allow the formation of oligomeric segments, followed by a second radical polymerization step in the presence of a thermal initiator (I) at 90 °C for 72 hours, and concluded with a post-curing stage at 135 °C for 1 hour. The comprehensive synthetic pathway of the network, and its corresponding reprocessing mechanism are schematically illustrated in Fig.29.

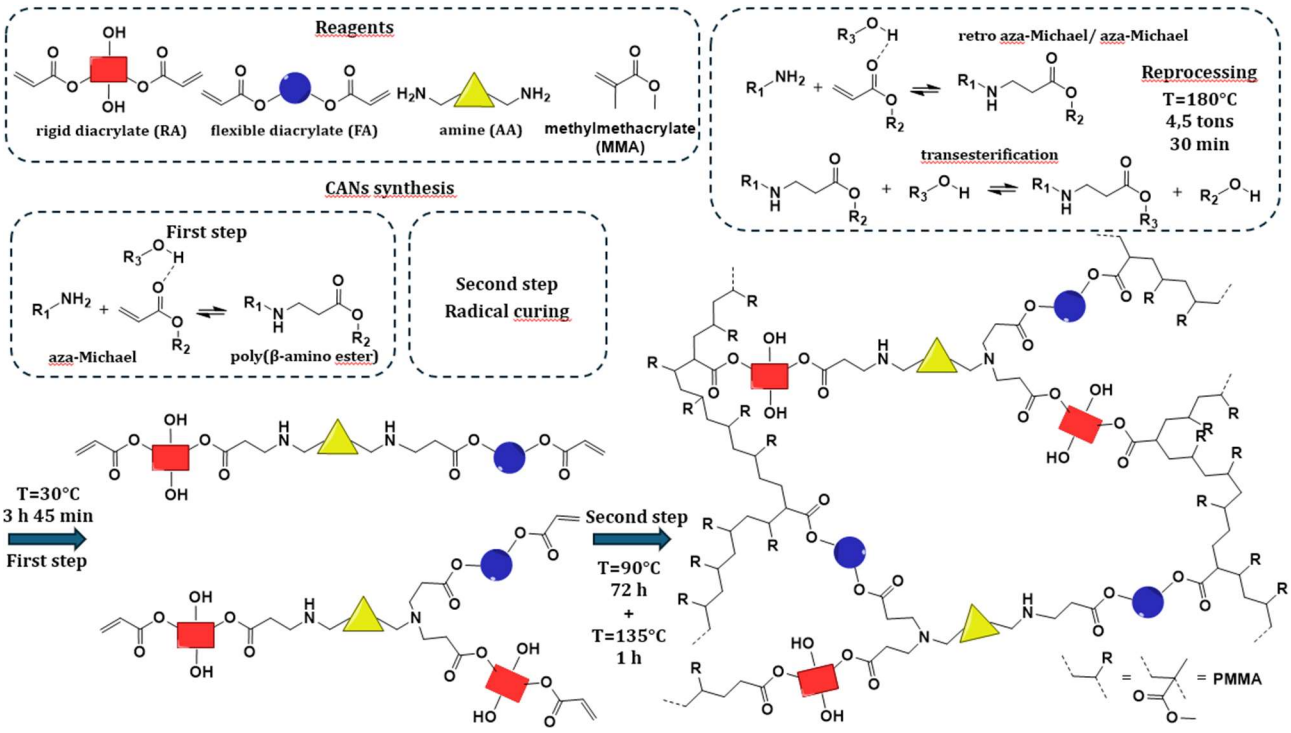

Figure 29. *Comprehensive schematic overview of the reagents, polymerization chemistry, and reforming loop of the VIT.MMA.X.Y.Z covalent adaptable networks (CANs).*

To systematically investigate the network architecture, three different initial molar ratios between the acrylic and amine groups were tested, precisely 2, 1.8, and 1.5. Concurrently, the mass percentage between the vitrimeric component and the radical matrix was varied, evaluating formulations with 50 wt% vitrimer / 50 wt% MMA and 70 wt% vitrimer / 30 wt% MMA. Accordingly, the samples were designated using the systematic nomenclature VIT.MMA.X.Y.Z, where X is the weight percentage of the vitrimer component, Y is the weight percentage of MMA, and Z represents the initial molar ratio between the acrylic and amine functional groups. Concurrently, as introduced in Chapter 2, the design of a shelf-stable premix was undertaken, grounded in a precise chemical rationale. During the prepolymerization phase, the aza-Michael addition is highly selective toward acrylic double bonds. Indeed, the choice to employ MMA as a latent monomer is based on well-established kinetic considerations in the literature[51]: methacrylic monomers are extremely poor Michael acceptors due to the methyl group in the alpha (α) position. This substituent hinders the nucleophilic attack of the amine through two synergistic effects: on one hand, it generates significant steric hindrance; on the other hand, it exerts an electron-donating inductive effect that substantially reduces the electrophilicity of the double bond. Ideally, this behavior allows MMA to remain unreacted during this primary reaction, thereby yielding a partially reacted and stable system. The task of completing the crosslinking in second step is thus left to the end user, who can trigger the radical polymerization of the latent MMA via a thermal initiator.

Since reprocessability represents the binding prerequisite of the entire study without which the practical applicability of the synthesized materials is voided the experimental investigation commenced precisely with the verification of this property. As illustrated in Fig.30 (which displays a representative selection of the performed tests), in all cases the reprocessing results were unsatisfactory, exhibiting extremely slow kinetics and only partial shape recovery. The low reprocessability of the system can be tentatively associated with the dilution of the dynamic bonds in a MMA matrix.

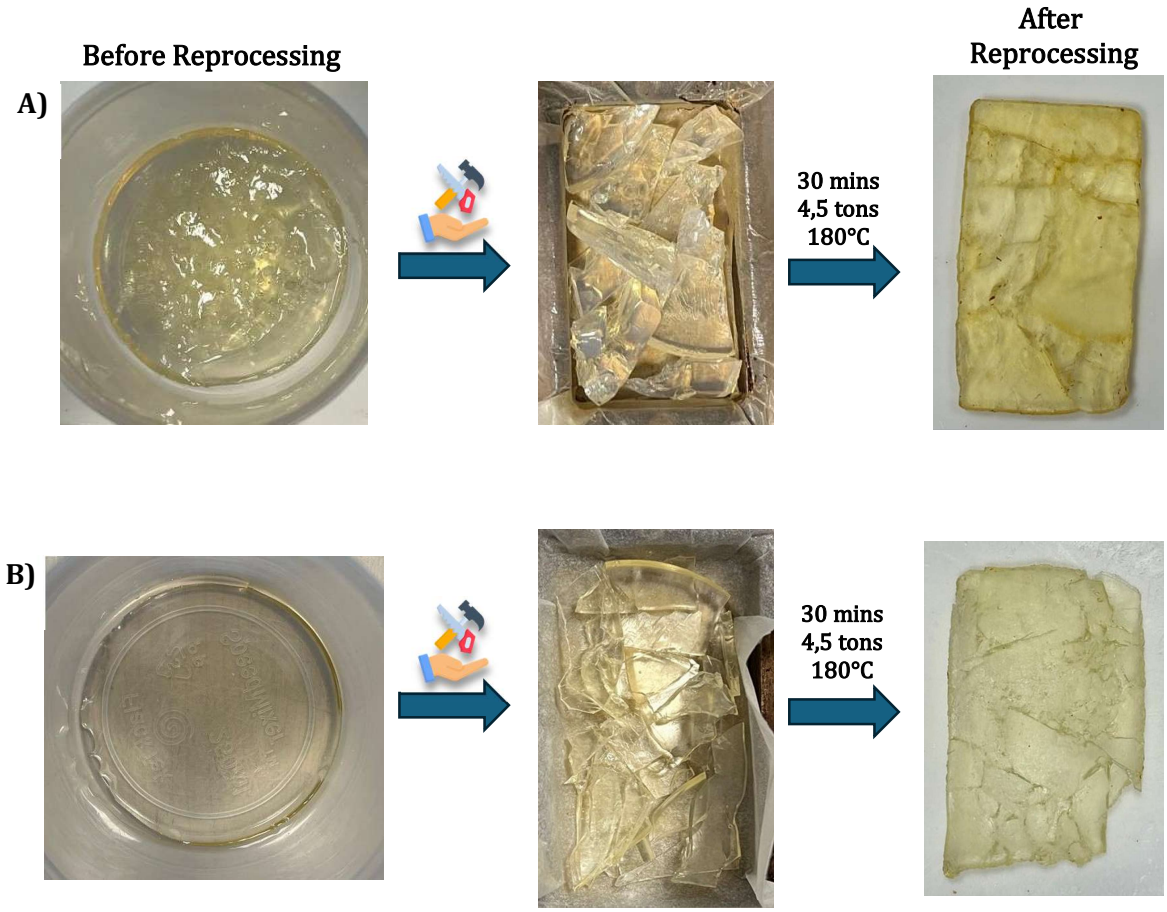

Figure 30. *Reprocessing of the three-component CANs + MMA. A) Reprocessing of VIT.MMA.50.50.1.5; B) Reprocessing of VIT.MMA.70.30.2.0.*

4.3.2 Thermal characterization of amine-acrylic CANs tricomponent + MMA

Nevertheless, to provide a comprehensive analytical overview, the various samples were also characterized via Differential Scanning Calorimetry (DSC). The experimental parameters are detailed in the reference thermogram, while Tab.9 and Fig.31 comprehensively report the complex data relative to all the analyzed systems.

Table 9. *Glass transition temperatures (T_g) of the different formulations determined by DSC analysis.*

Sample name	T_g(°C)
VIT.MMA.70.30.1.5	62.1
VIT.MMA.70.30.1.8	60.5
VIT.MMA.70.30.2.0	74.0
VIT.MMA.50.50.1.5	26.6
VIT.MMA.50.50.1.8	47.0
VIT.MMA.50.50.2.0	58.0

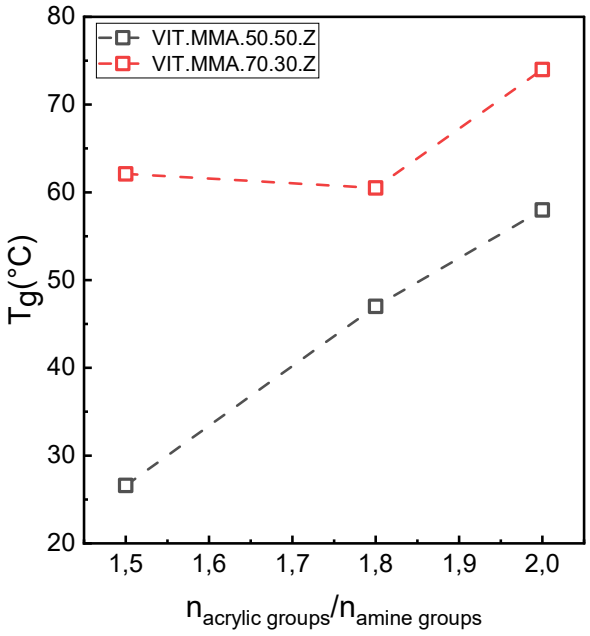

Figure 31. *Glass transition temperature (T_g) as a function of the acrylic-to-amine group molar ratio ($\frac{n_{acrylic\ groups}}{n_{amine\ groups}} = Z$) for the two analyzed sample series.*

As a general trend, an increase in the $\frac{n_{\text{acrylic groups}}}{n_{\text{amine groups}}}$ ratio from 1.5 to 2.0 leads to a progressive shift of T_g toward higher temperatures for both series. From a macromolecular standpoint, this behavior is directly related to the stoichiometry of the aza-Michael addition reaction. A ratio approaching the ideal value of 2.0 ensures that each primary amine group can potentially react with two acrylic functionalities, acting as a fully effective branching point and promoting the formation of tertiary amines. Consequently, this maximizes the overall crosslink density of the Covalent Adaptable Network (CAN). The restriction of segmental mobility of the polymer chains, induced by a highly interconnected tridimensional network, inherently requires higher thermal energy to trigger the cooperative movements associated with the glass transition, thus increasing T_g. It is worth noting that for the VIT.MMA.70.30 series (red curve), the sample at a ratio of 1.8 exhibits a slight deviation from the expected linear trend, showing a plateau before rising sharply at 2.0. When comparing the two formulations, the VIT.MMA.70.30 series (characterized by a higher content of the dynamic vitrimer phase) consistently displays significantly higher T_g values than the VIT.MMA.50.50 counterpart across the entire stoichiometric range. This outcome is unexpected since pure polymethyl methacrylate has a T_g of approximately 100°C abd was attributed to the presence of unreacted MMA monomers that play the role of plasticizing agent.

4.4 Synthesis and characterization of amine-acrylic CANs tricomponent + HEMA

4.4.1 Synthesis and reprocessing test

In light of the unsatisfactory results obtained with methyl methacrylate (MMA) concerning reprocessability, this chapter which constitutes the core of the entire experimental characterization illustrates the transition to a novel methacrylic monomer: hydroxyethyl methacrylate (HEMA). The replacement of MMA with HEMA was guided by a precise formulation rationale aimed at resolving the critical issues of the previous system. Specifically, the incorporation of HEMA introduces a significant concentration of pendant hydroxyl (-OH) groups into the network, which act positively and synergistically across multiple physico-chemical fronts. First, the hydroxyl groups present in the ester portion of HEMA act as nucleophiles, enabling transesterification reactions with other ester groups within the polymer network. The activation of this dynamic covalent exchange mechanism represents the key element to drastically enhance the material's reprocessability at high temperatures. Second, as discussed in the introductory chapter regarding reaction kinetics, the -OH groups exert a pronounced catalytic effect on the aza-Michael addition; their presence facilitates the nucleophilic attack of the amine, thereby optimizing the prepolymerization phase of the system. Finally, the massive presence of these groups generates a dense network of hydrogen-bonding interactions. This leads to a twofold advantage: on one hand, the increase in physical interactions further raises the structural rigidity and, consequently, the glass transition temperature (T_g); on the other hand, the thermally reversible nature of these physical bonds cooperates with the transesterification reactions to facilitate reprocessing.

To systematically evaluate this strategy, the exact same experimental matrix and two-step synthesis protocol detailed in the previous chapter were replicated, simply substituting MMA with HEMA. The formulations maintained the identical reaction conditions, an initial aza-Michael step carried out at 30 °C for 3 hours and 45 minutes to allow the formation of oligomeric segments, followed by a second radical polymerization step in

the presence of a thermal initiator (I) at 90 °C for 72 hours, and a post-curing stage at 135 °C for 1 hour. The comprehensive synthetic pathway of the network, and its corresponding reprocessing mechanism are schematically illustrated in Fig.32.

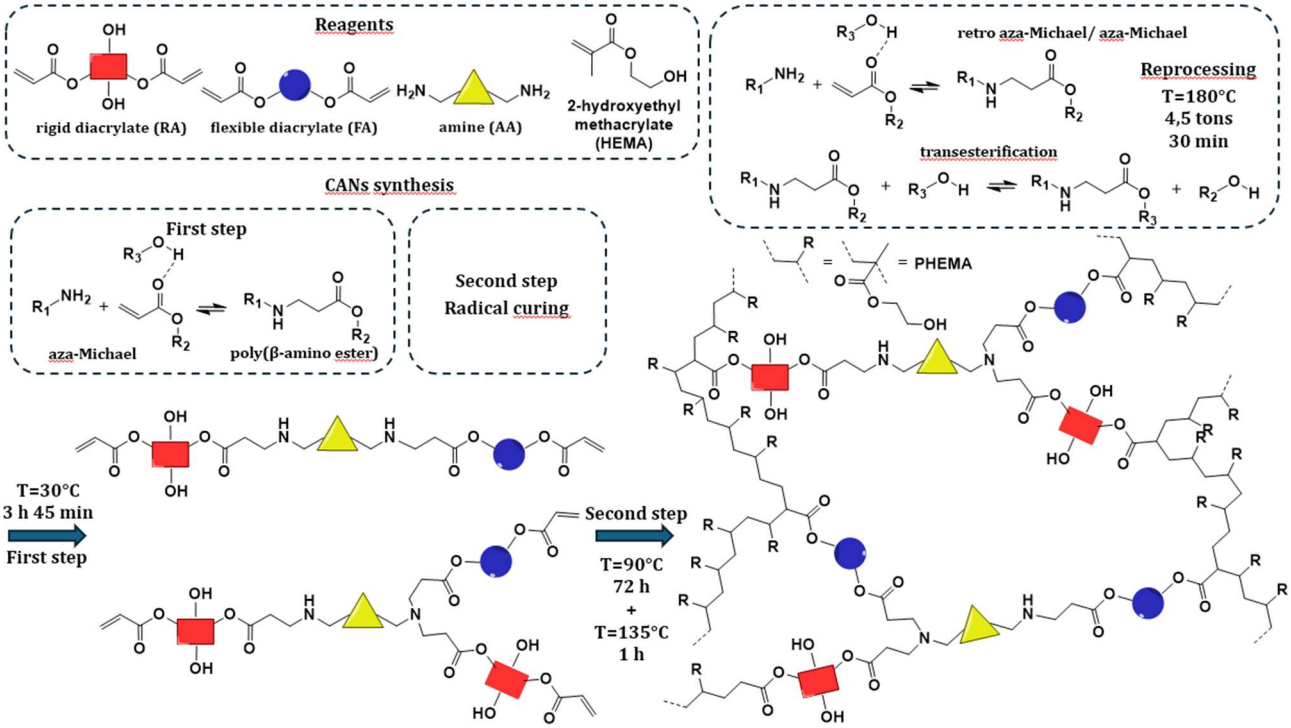

Figura 32. *Comprehensive schematic overview of the reagents, polymerization chemistry, and reforming loop of the VIT.HEMA.X.Y.Z covalent adaptable networks (CANs).*

Furthermore, the same initial molar ratios between the acrylic and amine groups (2, 1.8, and 1.5) were evaluated, while the mass percentages ranged from 70 wt% vitrimer / 30 wt% HEMA down to 10 wt% vitrimer / 90 wt% HEMA. Accordingly, these new hybrid networks were designated using the systematic nomenclature VIT.HEMA.X.Y.Z, where X is the weight percentage of the vitrimer component, Y is the weight percentage of HEMA, and Z represents the initial molar ratio between the acrylic and amine functional groups

Strictly following the methodological approach adopted in the previous chapter, the absolute priority of this study phase was assigned to the evaluation of reprocessability. Given that this is the binding condition for the applicability of the developed Covalent Adaptable Networks (CANs), the experimental workflow commenced precisely with the validation of this property. Consistent with the formulation premises, the study of self-

healing properties was excluded a priori. The marked increase in structural rigidity, actively sought to elevate the T_g, inevitably restricts the mobility of the polymer chains, thus hindering the macromolecular interdiffusion mechanisms required for effective self healing. Therefore, attention was exclusively focused on finding the perfect balance between high thermo-mechanical performance and a rapid, complete reprocessing cycle. As shown in Fig.33, the reprocessing tests yielded outstanding results, demonstrating a significant improvement compared to the previous MMA-based formulations. As anticipated, the strategic replacement of MMA with HEMA successfully enhanced the recycling efficiency of the system. This confirms that the introduction of HEMA optimizes the network architecture, facilitating a more effective topological rearrangement during the hot-pressing process.

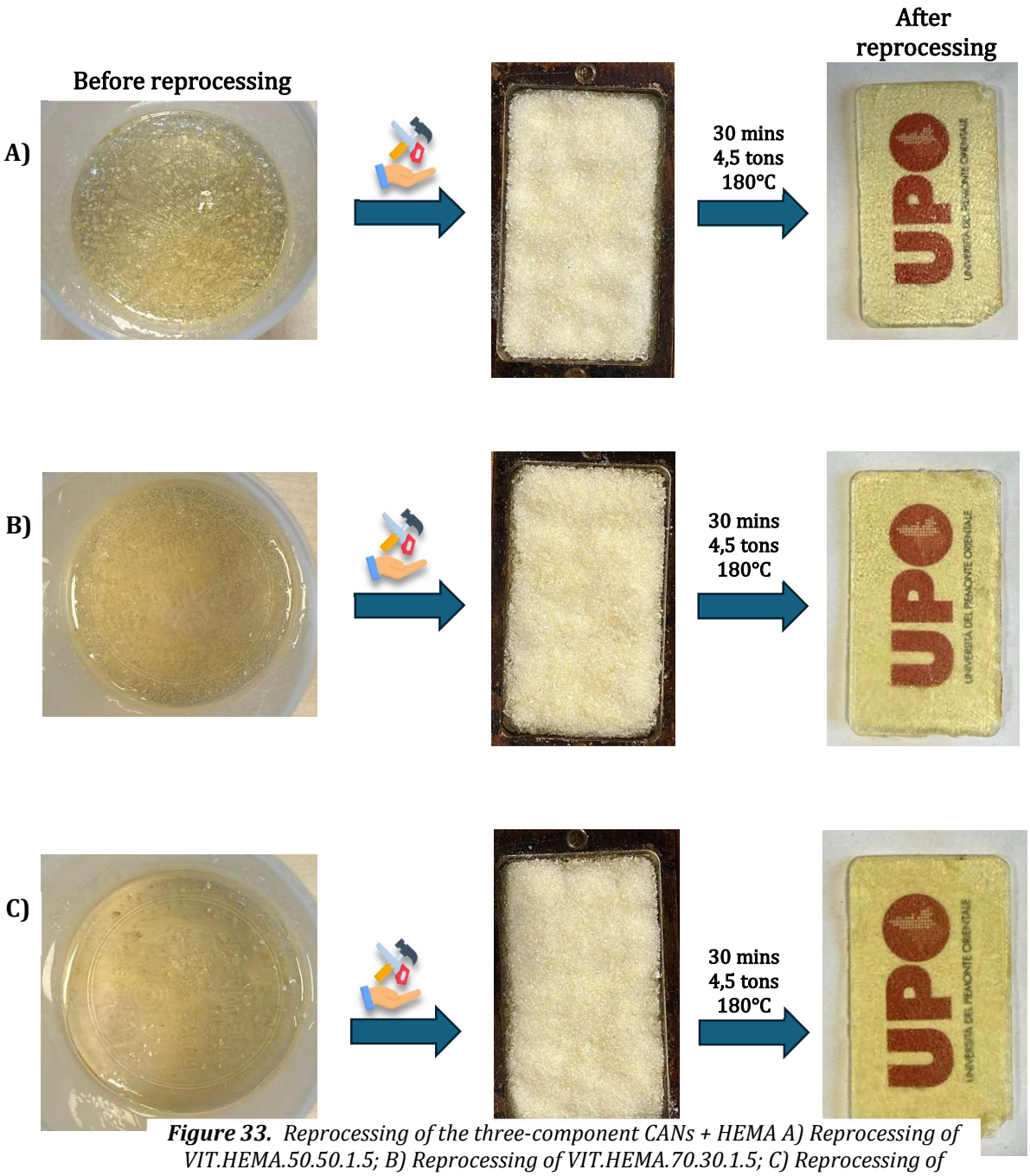

Figure 33. *Reprocessing of the three-component CANs + HEMA A) Reprocessing of VIT.HEMA.50.50.1.5; B) Reprocessing of VIT.HEMA.70.30.1.5; C) Reprocessing of VIT.HEMA.70.30.1.8*

To conclude this chapter, it is highlighted that all synthesized materials were subjected to at least three consecutive reprocessing cycles to confirm their recyclability. However, the time required for a complete reprocess of the material progressively begin to lengthen after multiple cycles. This phenomenon is closely linked to repeated thermo-mechanical stress, which causes partial and irreversible mechanical degradation of a fraction of the polymer network. Another interesting experimental observation, which deserves further future investigation, concerns the influence of the ground

polymer particle size on the reprocessing kinetics. Smaller fragments, owing to their higher specific surface area, significantly accelerate the thermal compaction process; nonetheless, this extensive fragmentation induces a greater number of irreversible fractures within the network, limiting the total number of achievable recycling cycles before a decay in properties occurs. Conversely, the use of coarser pieces slows down the reprocessing kinetics due to the smaller initial contact area, but better preserves the structural integrity of the network, potentially enabling a higher number of total recycling cycles.

4.4.2 Solubility and swelling tests

This section presents the results of the solubility and swelling tests conducted in ethanol, which were performed to confirm the effective crosslinking of the network and to evaluate its swelling degree (as thoroughly detailed in the experimental section). The quantitative data and the corresponding graphic trends are summarized and illustrated in the following Tab.10 and Fig.34-35.

Table 10. *Results of solubility (SF%) and swelling tests (SD%) before and post reprocessing, for the two analyzed sample series.*

Sample name	SF%	SD%	SF% (post reprocessing)	SD% (post reprocessing)
VIT.HEMA.70.30.1.5	6.36	46.60	15.59	68.24
VIT.HEMA.70.30.1.8	6.17	27.70	11.82	67.20
VIT.HEMA.70.30.2.0	4.81	33.70	6.90	39.40
VIT.HEMA.50.50.1.5	2.90	34.90	0.33	41.2
VIT.HEMA.50.50.1.8	1.98	27.50	1.63	44.45
VIT.HEMA.50.50.2.0	1.31	26.70	1.84	38.90
VIT.HEMA.40.60.1.5	7.30	/	/	/
VIT.HEMA.40.60.1.8	6.40	/	/	/
VIT.HEMA.40.60.2.0	9.30	/	/	/
VIT.HEMA.30.70.1.5	11.40	/	/	/
VIT.HEMA.30.70.1.8	10.70	/	/	/
VIT.HEMA.30.70.2.0	6.20	/	/	/
VIT.HEMA.10.90.1.5	25.70	/	/	/
VIT.HEMA.10.90.1.8	25.00	/	/	/
VIT.HEMA.10.90.2.0	14.10	/	/	/

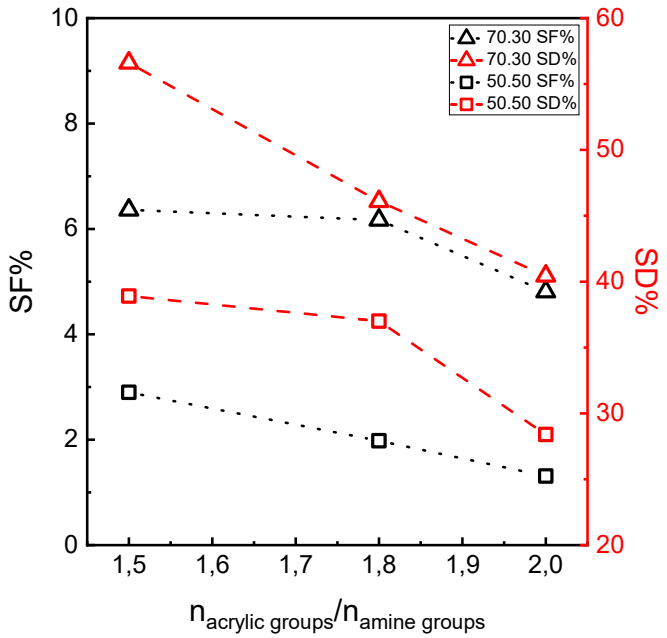

Figure 34. *Soluble fraction (SF%, left axis) and swelling degree (SD%, right axis) as a function of the acrylic-to-amine group molar ratio ($\frac{n_{acrylic\ groups}}{n_{amine\ groups}}$) for the two analyzed sample series before reprocessing .*

As illustrated in the dual-Y plot in Fig.34, the trends of the soluble fraction (SF%, left axis) and swelling degree (SD%, right axis) in ethanol are analyzed as a function of the molar ratio between acrylic and amine groups ($\frac{n_{acrylic\ groups}}{n_{amine\ groups}}$) for both the 50.50 and 70.30 material series. The 40.60, 30.70, and 10.90 series (characterized by a higher HEMA content) were excluded from subsequent characterization tests. These formulations exhibited significantly high soluble fractions, indicating that the material synthesis was incomplete and probably a substantial portion of the HEMA monomer was not effectively integrated into the polymer network and remains free in the material.

A fully consistent trend is observed for both sample series: as the functional ratio increases from 1.5 to 2.0, both the soluble fraction and the swelling degree exhibit a progressive decrease. This behavior is a direct consequence of the increased crosslink density of the system at the end of the reaction. As the ratio approaches the ideal stoichiometric value of 2.0, the aza-Michael addition reaction achieves its maximum structural

efficiency. This drastically reduces the presence of unreacted molecules or dangling chains thereby lowering the SF% and generates a highly dense three-dimensional network. In accordance with classical polymer physics models, such a highly interconnected structure exerts significant elastic resistance against the penetration of solvent molecules, limiting the volumetric expansion of the network and consequently reducing the SD% values. A direct comparison between the two formulations reveals that the 70.30 series (characterized by a higher fraction of CANs, component) systematically exhibits higher SF% and SD% values than its 50.50 counterpart at any given functional ratio.

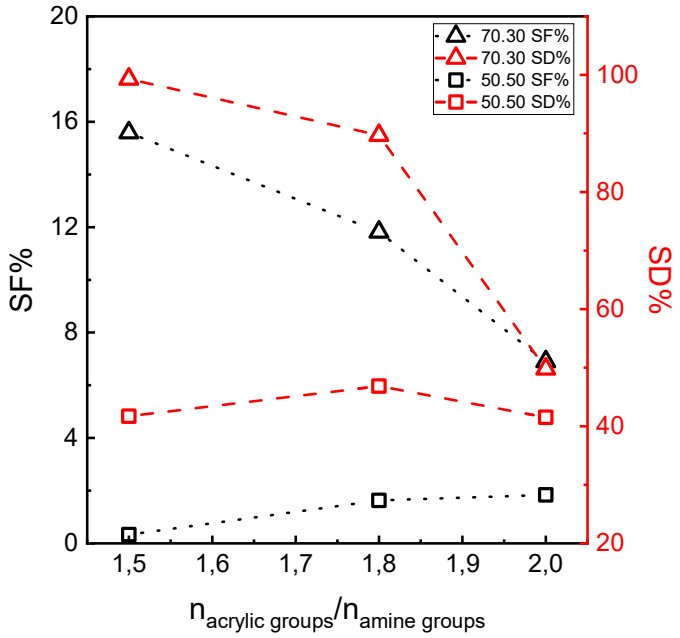

Figure 35. *Soluble fraction (SF%, left axis) and swelling degree (SD%, right axis) as a function of the acrylic-to-amine group molar ratio ($\frac{n_{acrylic\ groups}}{n_{amine\ groups}}$) for the two analyzed sample series post reprocessing.*

The same solubility and swelling tests were subsequently performed on the reprocessed materials to evaluate the structural integrity of the networks after recycling. As shown in Fig.35, even after the reprocessing cycle, the 70.30 series consistently exhibits higher SF% and SD% values compared to the 50.50 series across all functional ratios, mirroring the behavior observed in the pristine samples. For the 70.30 series, the characteristic decreasing trend as a function of the functional ratio is successfully

preserved post-reprocessing. However, a noticeable increase in the absolute values of both SF% and SD% is observed compared to the pre-reprocessing state. This behavior can be attributed to the mechanical steps involved in the recycling protocol: the initial grinding of the bulk material inevitably induces local micro-fractures and mechanical stress within the polymer matrix. These structural disruptions can lead to irreversible damage or create additional topological defects (such as cleaved chains or isolated fragments) that are not fully healed by the dynamic exchange reactions during the subsequent hot-pressing step, ultimately resulting in a slightly weakened network with higher solvent permeability and extractable content. In contrast, the 50.50 series demonstrates a distinct behavior, where the original stoichiometric trend tends to flatten or slightly invert compared to the pristine state. Nevertheless, the absolute variations in SF% and SD% for this series remain remarkably small. This structural stability suggests that the higher content of the free-radical polymerized HEMA matrix provides superior resistance against mechanical grinding, effectively safeguarding the overall network density and minimizing the impact of the reprocessing cycle on the material's final properties.

4.4.3 Thermal characterization of amine-acrylic CANs tricomponent + HEMA

This section discusses the thermal and dynamic mechanical properties of the synthesized materials, focusing on the determination of their glass transition temperatures (T_g) via Differential Scanning Calorimetry (DSC) and Dynamic Mechanical Analysis (DMA). In accordance with the protocols thoroughly detailed in the experimental section, both characterizations were systematically performed on the various samples across the investigated series. The compiled quantitative data and the corresponding experimental profiles are summarized, illustrated, and compared in the following Tab.11 and Fig.32-34.

Table 11. *Glass transition temperatures (T_g) of the analyzed samples determined via DSC (before and post-reprocessing) and DMA. For the DMA analysis, the T_g was evaluated at the maximum peak of the loss factor ($tan\ (\delta)$).*

Sample name	T_g(°C) DSC (before reprocessing)	T_g(°C) DSC (post reprocessing)	T_g(°C) DMA (max tan(δ)peak)
VIT.HEMA.70.30.1.5	58.3	46.4	72.8
VIT.HEMA.70.30.1.8	53.2	43.5	64.2
VIT.HEMA.70.30.2.0	60.2	47.0	70.5
VIT.HEMA.50.50.1.5	60.9	55.5	82.0
VIT.HEMA.50.50.1.8	63.4	54.5	85.6
VIT.HEMA.50.50.2.0	68.8	47.3	81.4

It is important to specify that the $T_g$values reported in the table were determined exclusively from the first heating scan of the three-ramp thermal cycle detailed in the experimental section. This choice is fundamentally dictated by the thermal behavior and dynamic nature of the network. As observed in the DSC thermograms (Fig. 36), which are reported as a representative example for the VIT.HEMA.70.30.2.0 sample, heating the material up to 180 °C triggers the activation of the retro-aza-Michael reaction, which causes the thermal cleavage of the crosslinking points. In the first scan, this phenomenon is visible through the onset of an endothermic signal that appears truncated due to the upper temperature

limit of the run (180 °C). When the sample is subjected to the second heating scan which extends up to 300 °C the complete endothermic peak corresponding to the retro-aza-Michael cleavage is fully resolved. Because these cleaved network points do not completely reform during the intermediate cooling step, the overall crosslink density of the network is altered, resulting in a significant decrease in the T_g value recorded during the second heating. Therefore, the first heating scan represents the only reliable measurement to evaluate the glass transition temperature of the pristine, fully crosslinked material.

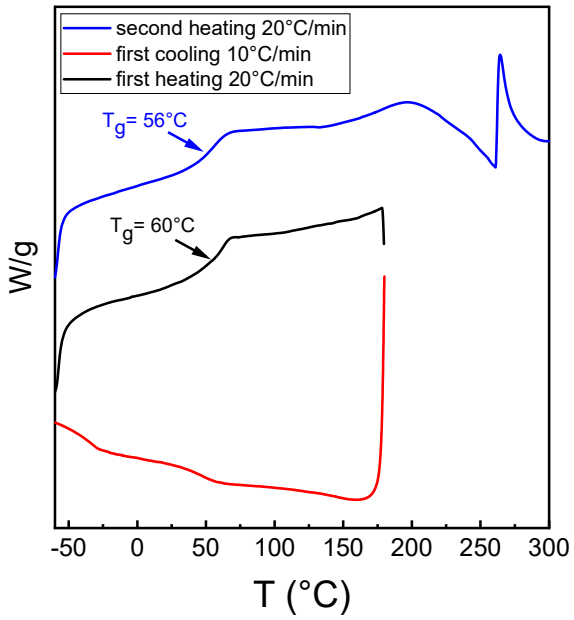

Figure 36. *Example DSC thermogram of VIT.HEMA.70.30.2.0. The thermal cycle consists of a first heating scan from -60 °C to 180 °C at 20 °C/min (black curve), a cooling scan from 180 °C to -60 °C at 10 °C/min, and a second heating scan from -60 °C to 300 °C at 20 °C/min, all ramps were perfomed with a nitrogen flow of 80 mL/min.*

Concurrently, Fig.37 reports the DMA thermogram for the same VIT.HEMA.70.30.2.0 sample as a representative example. The plot illustrates a sharp decrease in the storage modulus (E') of several orders of magnitude upon reaching the glass transition, which is mirrored by a well-resolved peak in the damping factor (tan(δ)) representing the T_g. Above this transition, the material exhibits a stable rubbery plateau region, confirming the structural integrity and effective crosslinking of the hybrid network architecture.

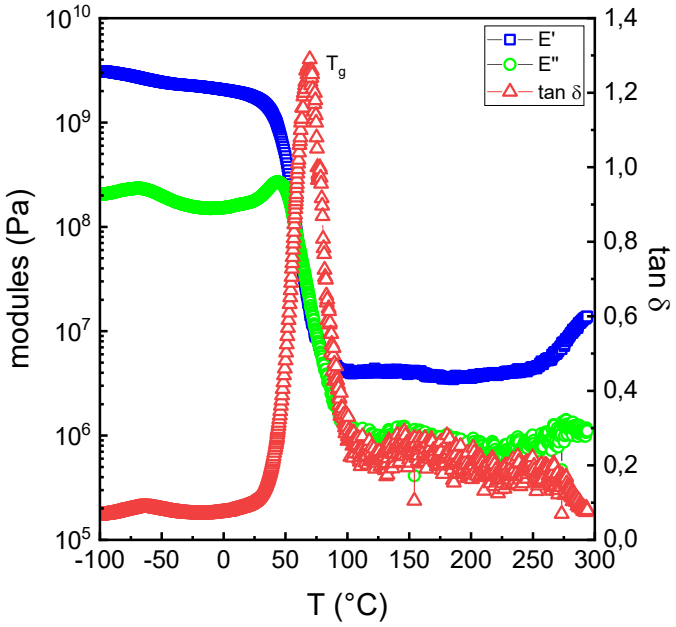

Figura 37. *Example DMA thermogram for the VIT.70.30.2.0 vitrimer sample measured from -100 °C to 300 °C in three-point bending mode, displaying the temperature dependence of the storage modulus (E', blue squares), loss modulus (E'', green circles), and loss factor (tan(δ), red triangles).*

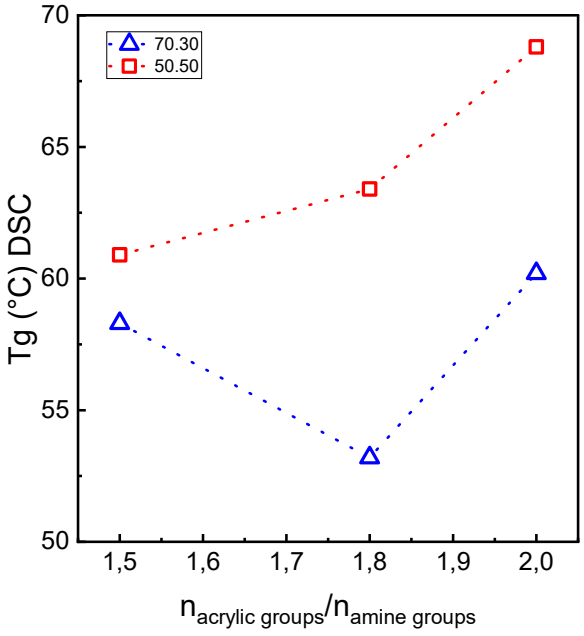

Figure 38. *Glass transition temperature (T_g) as a function of the acrylic-to-amine group molar ratio ($\frac{n_{acrylic\ groups}}{n_{amine\ groups}}$) for the two analyzed sample series before reprocessing. Left Y-*

axis: T_g values evaluated via DSC analysis; Right Y-axis: T_g values evaluated via DMA analysis.

The Fig.38 illustrates the evolution of the glass transition temperature (T_g) for the pristine materials as a function of the acrylic-to-amine molar ratio, comparing the 50.50 and 70.30 series. A direct comparison between the two series reveals that the 50.50 formulation (containing 50% HEMA and 50% CANs) consistently displays higher T_g values at equivalent functional ratios than the 70.30 counterpart. The higher concentration of HEMA introduces a greater density of hydroxyl (-OH) groups, which promotes strong intermolecular hydrogen bonding interactions that further restrict macromolecular chain mobility. Regarding the individual trends, the 50.50 series exhibits a steady, monotonic increase in T_g as the functional ratio rises, which aligns with the progressive increase in crosslink density. In contrast, the 70.30 series displays a distinct, non-linear "J-shaped" profile; here, the second data point deviates from the expected upward trajectory, acting as a local minimum between the other two points.

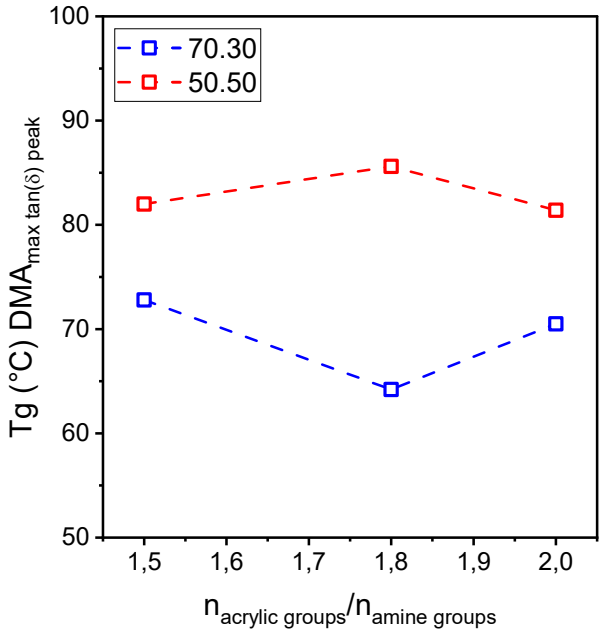

Figure 39. *Glass transition temperature (T_g) as a function of the acrylic-to-amine group molar ratio ($\frac{n_{acrylic\ groups}}{n_{amine\ groups}}$) for the two analyzed sample series after reprocessing. T_g values evaluated via DMA analysis.*

The Fig.39 compares the glass transition temperatures (T_g) obtained from DMA for the two analyzed sample series, VIT.HEMA.70.30.Z and VIT.HEMA.50.50.Z. Consistent with the behavior observed in the pristine state, a cross-series comparison reveals that the 50.50 series maintains higher T_g values than the 70.30 counterpart across all functional ratios. This trend is clearly corroborated by both the DSC and DMA analytical techniques. When evaluating the individual series profiles post-reprocessing, the 70.30 formulation preserves its characteristic trend. Conversely, the 50.50 series demonstrates a distinct response: the T_g values derived from DSC exhibit an inversion of the original stoichiometric trend observed in the pristine samples. Meanwhile, the corresponding T_g values obtained via DMA show minimal overall variation across the investigated range, with the intermediate functional ratio acting as a local maximum.

The final Fig.40 explicitly illustrates the comparative trends between the pre- and post-reprocessing states, highlighting a universal decrease in T_g for all synthesized samples following the recycling cycle. As indicated by the vertical dotted lines, a distinct behavior in the thermal gap ($\Delta T_g = T_{g,\text{before reprocessing}} - T_{g,\text{post reprocessing}}$) can be observed between the two series. For the 50.50 series, the ΔT_g noticeably widens as the functional ratio increases, expanding from approximately 5 °C at the lowest ratio to nearly 20 °C at the highest. Conversely, the 70.30 series exhibits a much more stable trend, with a nearly constant ΔT_g of approximately 12 °C across the entire range of investigated functional ratios.

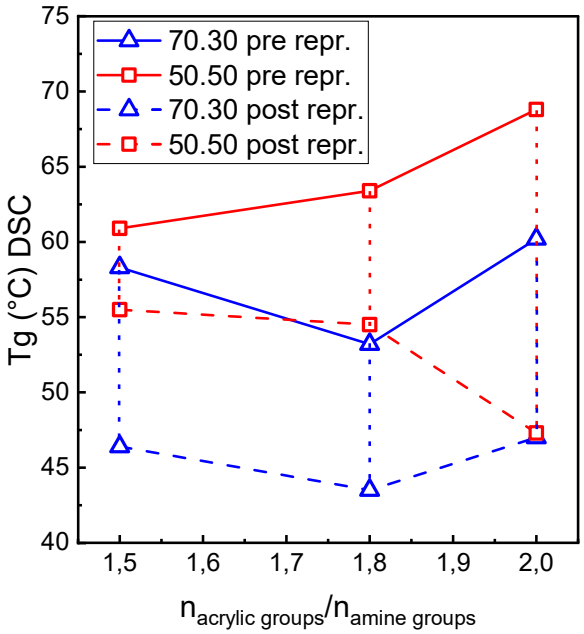

Figure 40. *Comparison between the glass transition temperature (T_g) before and after reprocessing, as a function of the acrylic-to-amine group molar ratio ($\frac{n_{acrylic\ groups}}{n_{amine\ groups}}$) for the two analyzed sample series.*

4.4.4 Dynamic mechanical analysis (DMA)

In addition to determining the glass transition temperature (T_g) as discussed in Section 4.4.3, Dynamic Mechanical Analysis (DMA) was instrumental in comparing the storage modulus (E') of the synthesized materials both below and above the glass transition region, specifically evaluated at 0 °C. The trends of these moduli are summarized and compared in the following Tab.12 and dual-Y plot (Fig.41). Furthermore, a representative DMA thermogram for sample VIT.HEMA.50.50.1.5 is provided to illustrate the characteristic viscoelastic behavior of the network. All parameters regarding the analysis have been accurately described in chapter 3.5.4.

Table 12. *Storage modulus (E') values evaluated at 0 °C ($E'_{0°C}$) and 150°C ($E'_{150°C}$) for the two investigated series of synthesized vitrimer formulations, determined via DMA analysis in three-point bending mode.*

Sample name	$\mathbf{E'_{0°C}(Pa)}$	$\mathbf{E'_{150°C}(Pa)}$
VIT.HEMA.70.30.1.5	$2.74 \cdot 10^9$	$3.17 \cdot 10^6$
VIT.HEMA.70.30.1.8	$2.87 \cdot 10^9$	$4.18 \cdot 10^6$
VIT.HEMA.70.30.2.0	$2.14 \cdot 10^9$	$3.93 \cdot 10^6$
VIT.HEMA.50.50.1.5	$3.47 \cdot 10^9$	$5.21 \cdot 10^6$
VIT.HEMA.50.50.1.8	$2.44 \cdot 10^9$	$4.18 \cdot 10^6$
VIT.HEMA.50.50.2.0	$2.95 \cdot 10^9$	$5.20 \cdot 10^6$

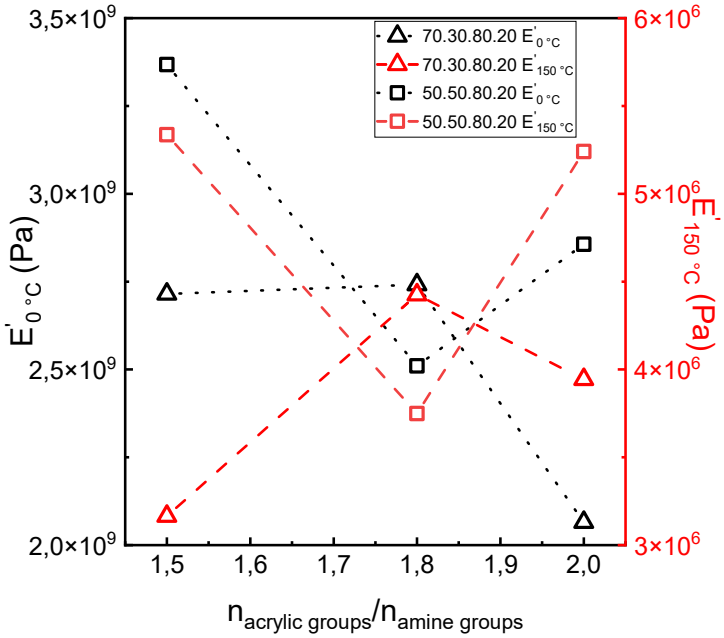

Figura 41. *Storage modulus values evaluated at 0 °C ($E'_{0°C}$, black curves, left axis) and 150 °C ($E'_{0°C}$, red curves, right axis) as a function of the acrylic-to-amine functional group ratio ($\frac{n_{acrylic\ groups}}{n_{amine\ groups}}$) for the two investigated vitrimer series, determined via DMA analysis in three-point bending mode.*

As shown in the dual-Y plot in Fig.41 and the compiled data in Tab.20, the storage modulus (E') values were evaluated both below the glass transition temperature (at 0 °C, left Y-axis) and within the rubbery plateau region (at 150 °C, right Y-axis) as a function of the acrylic-to-amine group molar ratio.

The 50.50 series exhibits a distinct "V-shaped" trend, where the sample prepared at the intermediate functional ratio of 1.8 acts as a clear local minimum. This non-monotonic profile remains remarkably consistent in both the glassy state at 0 °C and the rubbery state at 150 °C. Conversely, the 70.30 series demonstrates approximately the opposite behavior, showing an inverted V-shaped trend. Although less pronounced in the glassy state, the intermediate 1.8 ratio clearly constitutes a local maximum for both analyzed temperatures.

When comparing the two formulations, a highly consistent relationship between the series is maintained both above and below T_g. At the outer functional ratios of 1.5 and 2.0, the 50.50 series displays a significantly

higher storage modulus than the 70.30 counterpart, indicating a stiffer and more rigid network structure. However, at the intermediate ratio of 1.8, a complete inversion of this trend is observed, with the 70.30 formulation exhibiting higher mechanical stiffness than the 50.50 system. Nonetheless, the storage modulus values for all samples both below and above T_g do not show major discrepancies and remain strictly within the same order of magnitude. This suggests that the observed fluctuations might simply arise from experimental error or minor testing variability rather than a distinct structural phenomenon. Finally, it should be noted that the DMA thermogram reported in the following Fig.42 serves as a representative example of the behavior observed across all the investigated systems, specifically illustrating the viscoelastic profile of the VIT.HEMA.50.50.1.5 sample.

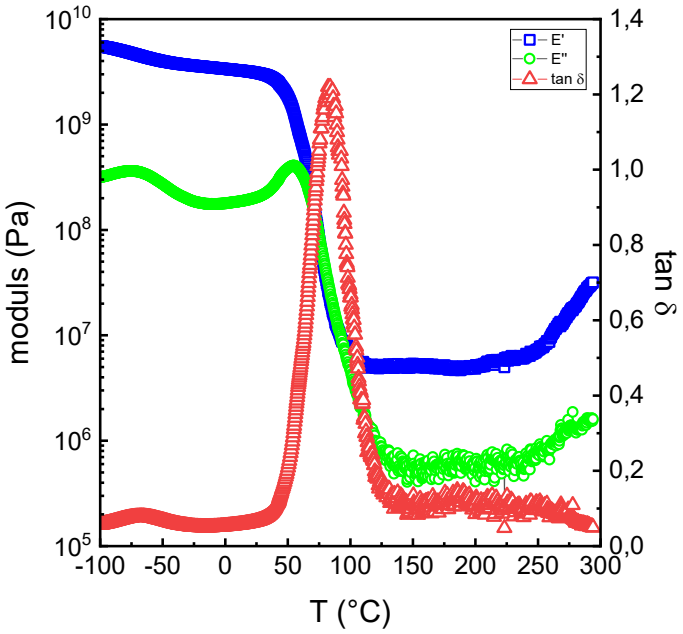

Figure 42. *Example DMA thermogram for the VIT.HEMA.50.50.1.5 vitrimer sample measured from -100 °C to 300 °C in three-point bending mode, displaying the temperature dependence of the storage modulus (E', blue squares), loss modulus (E'', green circles), and loss factor (tan(δ), red triangles).*

The representative DMA thermogram illustrates the characteristic viscoelastic behavior of the synthesized Covalent Adaptable Network (CAN). Below 50 °C, the material resides in a rigid glassy state, exhibiting a

high storage modulus (E') of approximately $5 \cdot 10^9$ Pa. Upon further heating, a sharp glass transition takes place between 50 °C and 110 °C, characterized by a drop of nearly three orders of magnitude in E' and a single, symmetric tan(δ) peak centered at around 80 °C, which reflects excellent network homogeneity. Above 110 °C, the modulus stabilizes into a well-defined rubbery plateau ($5 \cdot 10^6$ Pa) that confirms the thermal and structural stability of the crosslinked matrix, before showing a slight upturn above 220 °C due to minor secondary thermal phenomena such as post-curing.

4.4.5 Stress relaxation analysis

Stress relaxation analyses were performed to determine the characteristic relaxation times of the different formulations. The specific testing parameters, along with the methodology and criteria adopted to evaluate the relaxation behavior, are thoroughly detailed in experimental Section 3.5.3. The experimental outcomes of this characterization are summarized and illustrated in the subsequent Tab.13 and Fig.43-44.

Table 13. *Characteristic relaxation times (τ) at 180 °C and 190 °C for the two investigated sample series, determined from isothermal stress relaxation analyses.*

Sample name	$\tau_{180°C}$	$\tau_{190°C}$
VIT.HEMA.70.30.1.5	70	828
VIT.HEMA.70.30.1.8	67	585
VIT.HEMA.70.30.2.0	115	867
VIT.HEMA.50.50.1.5	144	1382
VIT.HEMA.50.50.1.8	183	/
VIT.HEMA.50.50.2.0	320	/

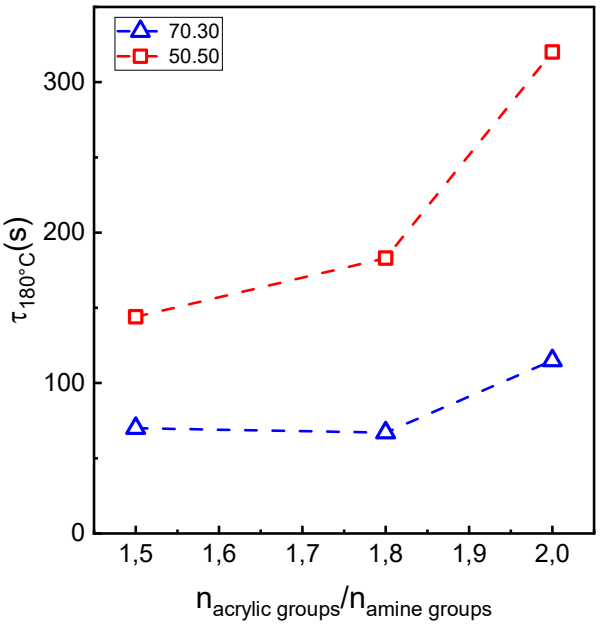

Figure 43. *Characteristic relaxation times (τ) at 180 °C as function of ratio between acrylic groups and amine groups for the two investigated sample series, determined from isothermal stress relaxation analyses.*

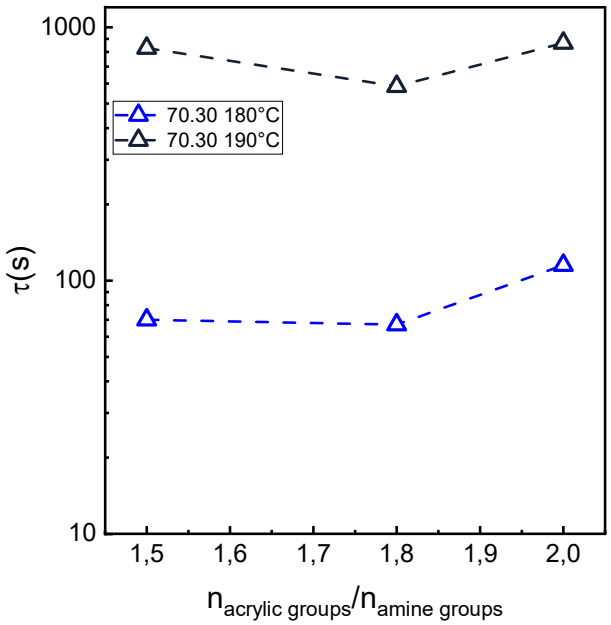

Figure 44. *Characteristic relaxation times (τ) at 180 °C and 190°C as function of ratio between acrylic groups and amine groups for the sample serie 70.30, determined from isothermal stress relaxation analyses.*

As observed in Tab.19, some experimental data points are missing. This omission is elucidated by the trends illustrated in Fig.44, which displays the relaxation times on a logarithmic scale. The prolonged thermal treatment at 180 °C for approximately 3 hours, conducted prior to the 190 °C measurements, induced irreversible degradation within a portion of the polymer matrix. This thermal damage severely impaired the adaptable properties of the Covalent Adaptable Network (CAN), triggering an anomalous and counterintuitive shift where the relaxation times increased rather than decreased upon raising the temperature.

Conversely, Fig.43 compares the two investigated series by plotting the relaxation times as a function of the stoichiometric ratio between the acrylic and amine functional groups. At any given ratio, the 50:50 series consistently exhibits longer relaxation times compared to the 70:30 series, a behavior that aligns perfectly with the discussions in the previous chapters regarding the effects of increasing the HEMA content. Furthermore, for both series, the maximum relaxation time is achieved at the ideal 2:1 ratio, providing definitive confirmation that an increase in this

functional ratio directly enhances the structural rigidity of the system. A representative example of the obtained stress relaxation curves of the sample VIT.HEMA.70.30.2.0 is illustrated in Fig.45.

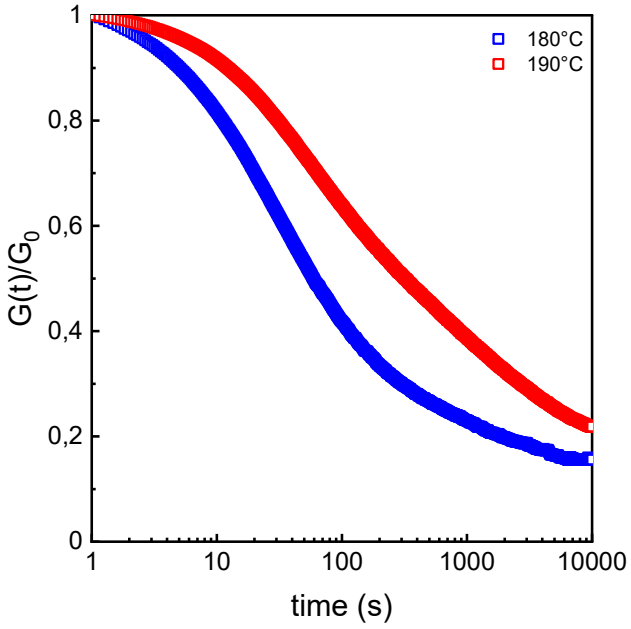

Figure 45. *Normalized relaxation modulus ($\frac{G(t)}{G_0}$) as a function of time (on a logarithmic scale) at 180 °C and 190 °C for the VIT.HEMA.70.30.2.0 formulation, highlighting the anomalous shift toward longer relaxation times at the higher temperature.*

4.4.6 Cinetic of first reaction step of amine-acrylic CANs tricomponent + HEMA

To have more information on the two reaction steps that make up the overall synthesis, they were analyzed in details separately using the sample VIT.HEMA.50.50.1.5 as typical example.

In details, the kinetic study of the first reaction stage, focusing on the formation of oligomers via aza-Michael addition and the monitoring of acrylate group conversion, was conducted using 1H-NMR spectroscopy according to the methodology detailed in Section 3.2.1. Concurrently, viscosity change of the solution occurring during this initial step was monitored using a rotational rheometer via shear rate sweep analysis, as described in Section 3.5.4. The quantitative conversion data and the time evolution of the corresponding 1H-NMR spectra are reported and discussed in Tab.14 and Fig.46, whereas the rheological data illustrating the evolution of the system's flow properties are presented separately in Tab.15 and Fig.47.

Table 14. *Reaction kinetics of first step for the VIT.HEMA.50.50.1.5 formulation, monitoring the acrylate double bond conversion percentage (%) as a function of reaction time (h), using 1H-NMR.*

Sample name	
VIT.HEMA.50.50.1.5	
Reaction time (h)	**Conversion %**
0	0
0.08	78.2
0.25	79.4
0.50	80.5
1	81.6
2	82.4
4	81.3
96	95.4

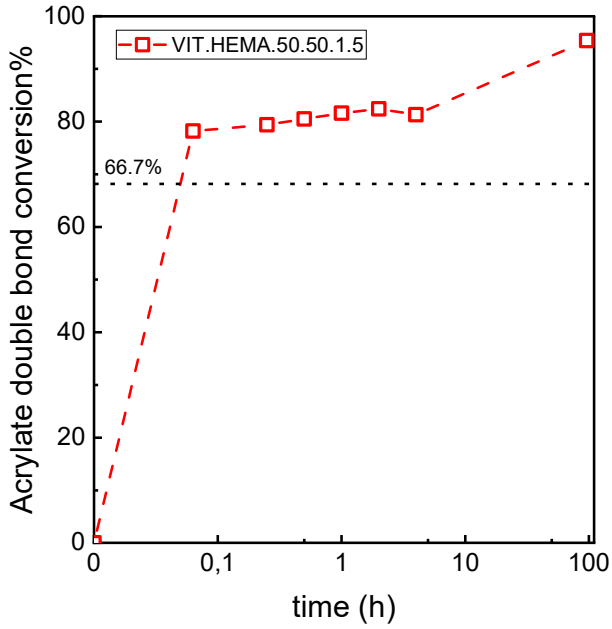

Figure 46. *Reaction kinetics of the first step for the VIT.HEMA.50.50.1.5 formulation, monitoring the acrylate double bond conversion percentage (%) as a function of reaction time (h). The horizontal black dotted line represents the threshold beyond which the amines have already converted into tertiary amines.*

The kinetic profile analysis reveals that the reaction is extremely rapid during the very initial experimental stages, reaching a conversion higher than 78% within just 5 minutes from the start of the process. In this context, exceeding the critical threshold of 66.7% indicates that a fraction of secondary amines has already begun to react further to form tertiary amines. This phenomenon triggers a significant structural evolution, shifting the system from a linear configuration toward the formation of branched CANs oligomers that bear more than two acrylic functional groups. Following this sharp initial surge, the mixture enters a medium-term stabilization phase extending up to approximately 6 hours, a period characterized by only a slight and gradual increase in conversion. Nevertheless, prolonged tracking reveals that the oligomeric mixture lacks long-term stability. At extended reaction times, such as 96 hours, the degree of conversion continues to progress upward. This behavior demonstrates the persistence of an active residual reactivity within the system even at 30

°C, preventing the definitive stabilization of the oligomeric formulation over time.

Table 15. *Reaction kinetics of the first step and time stability for the VIT.HEMA.50.50.1.5 formulation, monitoring the viscosity as a function of time (h), using rheometer.*

Sample name	
VIT.HEMA.50.50.1.5	
time (h)	**Viscosity(Pa· s)**
0	3.38
0.25	7.34
0.5	11.28
1	11.60
2	11.60
3	13.61
3.75	13.92
6	14.80
18	11.03
24	9.65
96	4.95
168	3.88
360	2.26
432	2.46

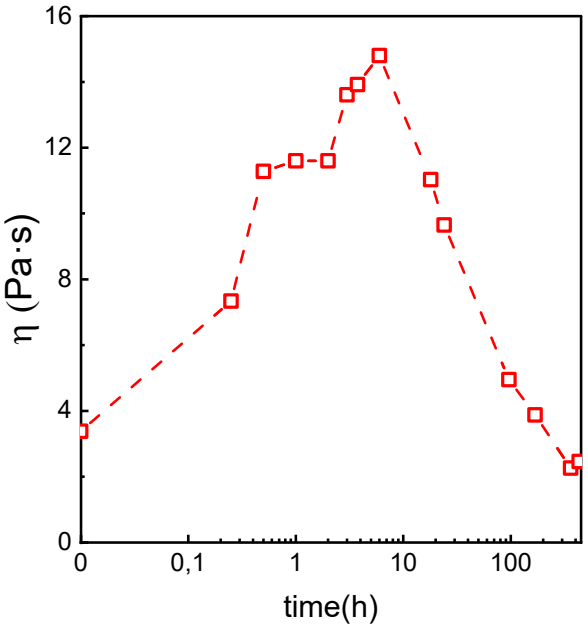

Figura 47. *Reaction kinetics of the first step and time stability for the VIT.HEMA.50.50.1.5 formulation, monitoring the viscosity (η) as a function of time (h), using rheometer.*

As illustrated in Fig.47 ("Viscosity analysis of the mixture"), the rheological profile displays a peculiar dynamic: the viscosity progressively increases during the initial hours, reaching a maximum of approximately 14 Pa·s at 6 hours, followed by a gradual decrease over longer reaction times. This behavior can be attributed to the continuous reactivity between amines and acrylates that persists throughout the reaction, in perfect agreement with the findings highlighted by the 1H-NMR analysis. As the process advances, the molecular weight of the oligomers increases while their overall concentration simultaneously decreases, because the growing chains tend to react and merge with one another. Consequently, at short reaction times, the viscometric trend is predominantly governed by the increase in macromolecular mass, which drives the initial rise in viscosity. Conversely, at extended times, the drastic drop in the concentration of the species in solution becomes the dominant factor, accounting for the subsequent decrease in viscosity. This unique rheological trend further substantiates the conclusion that the oligomeric mixture lacks long-term stability, confirming the presence of a persistent residual reactivity.

In conclusion, the study of the first reaction stage highlights that the formation of the vitrimer oligomers occurs extremely rapidly, on the order of a few minutes. Nonetheless, the chemical process continues to progress over time, gradually altering the molecular composition of the mixture and precluding the possibility of storing the formulation at room temperature for extended periods. In light of this evidence, the previously selected condition, specifically, a treatment of 4 hours at 30 °C, is confirmed as an excellent kinetic and rheological compromise. This time window allows the system to reach sufficiently high conversions while simultaneously ensuring a temporary stabilization of the viscosity, capturing an ideal plateau before the value starts decreasing due to the drop in oligomer concentration. Finally, although the rapid initial surge in conversion might suggest the opportunity to shorten the duration of this first step below 30 minutes, such a choice would be disadvantageous for practical applications. Within that narrow time frame, the properties of the system change too abruptly, as demonstrated by the initial spike in viscosity. Such an accelerated dynamic would introduce significant kinetic variability, complicating the practical handling of the material and hindering the subsequent standardization of the manufacturing process.

4.4.7 Cinetic of second reaction step of amine-acrylic CANs tricomponents + HEMA

Concurrently, the kinetic study of the second reaction step concerning the formation of the final network via the free-radical polymerization of HEMA and the oligomers synthesized during the first stage was monitored via Differential Scanning Calorimetry (DSC), following the protocol described in Section 3.5.1. The polymerization progress was evaluated by tracking the progressive decrease of the characteristic exothermic reaction peak. The compiled kinetic data and the corresponding thermograms are presented in the following Tab.16 and Fig.48.

Table 16. *Reaction kinetics of the second step for the VIT.HEMA.50.50.1.5 formulation, detailing the reaction enthalpy (ΔH) and the corresponding HEMA conversion percentage as a function of reaction time.*

Sample name		
VIT.HEMA.50.50.1.5		
Reaction time (h)	**ΔH ($\frac{J}{g}$)**	**HEMA conversion %**
0	-226.76	0
1	-2.44	98.94
2	-1.67	99.27
24	-0.85	99.63
96	0	100

According to the results summarized in the table and presented in the following figure, the polymerization reaction proceeds at a remarkably rapid rate, achieving a conversion of approximately 100% after just 1 hour. This fast kinetic behavior is further substantiated by the DSC thermograms shown in Fig.49, which illustrate the characteristic exothermic peak and its progressive decrease in area over time, directly reflecting the rapid consumption of the reactive functional groups.

However, despite this seemingly complete initial conversion, at longer curing times the residual exothermic peak becomes broad and ill-defined, making it extremely difficult to pinpoint the exact threshold for absolute

completion. For this reason, a prolonged curing profile consisting of 72 hours at 90 °C, supplemented by a final hour at 135 °C, was reasonably established. This specific temperature sequence is strictly dictated by a fundamental chemical constraint: the majority of the curing process must be confined to temperatures below 100 °C. If the system is heated above 100 °C before the radical polymerization is nearly completed, the retro-aza-Michael reaction is prematurely activated. This thermal cleavage gradually releases free acrylate groups that undergo irreversible radical polymerization, ultimately depleting the dynamic bonds responsible for the vitrimeric behavior of the network. Therefore, the extended treatment at 90 °C is necessary to safely maximize conversion, while the brief post-curing at 135 °C ensures a fully crosslinked network without sacrificing its essential dynamic properties.

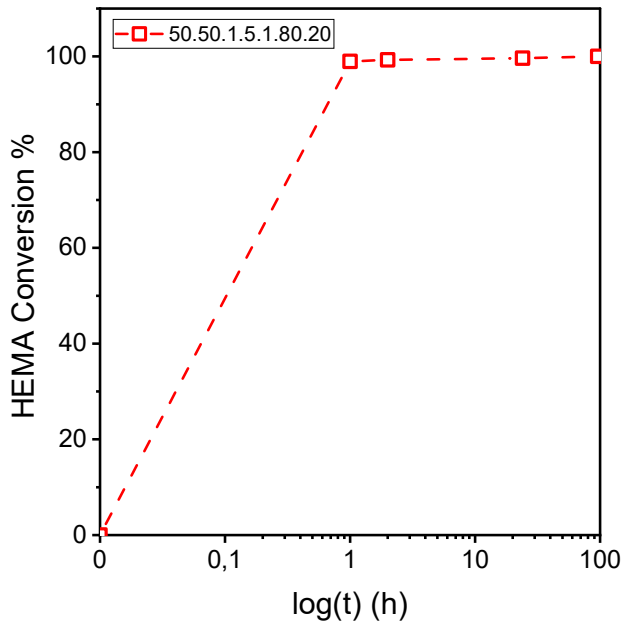

Figure 48. *HEMA monomer conversion (second reaction step) monitored over time with DSC.*

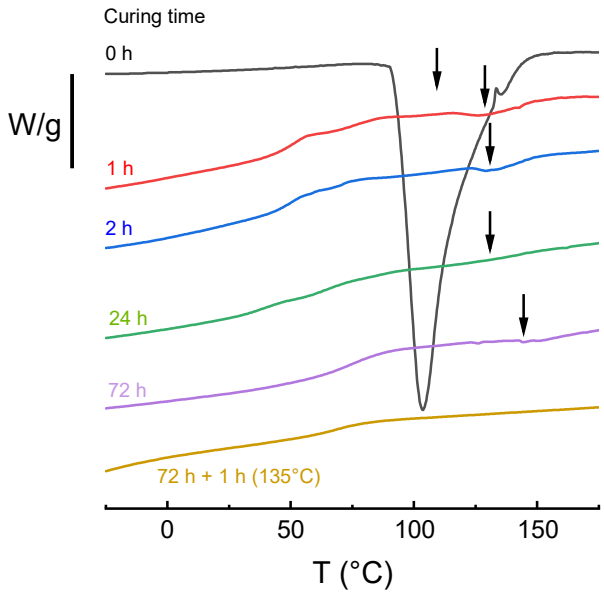

Figura 49. *DSC curves of the VIT.HEMA.50.50.1.5 sample treated at 30 °C for 4 h and then cured at 90 °C for different times.*

4.5 Synthesis and characterization of amine-acrylic CANs four-component

4.5.1 Synthesis and reprocessing test

This section focuses on the systematic investigation of a multi-component covalent adaptable network (CAN) system based on the combination of three distinct acrylic monomers and a single amine crosslinker, a study developed with the primary objective of modulating the thermal and mechanical characteristics of aza-Michael vitrimers by strategically tailoring the network formulation. The design rationale relies on blending two difunctional acrylates, namely BDA and BPADA, with a trifunctional acrylate, PETA, which are subsequently crosslinked using the amine monomer MCBA. The chemical structures of these four building blocks, along with the generalized reaction pathways, are schematically illustrated in Fig.50, providing a comprehensive overview of the components involved in the network architecture.

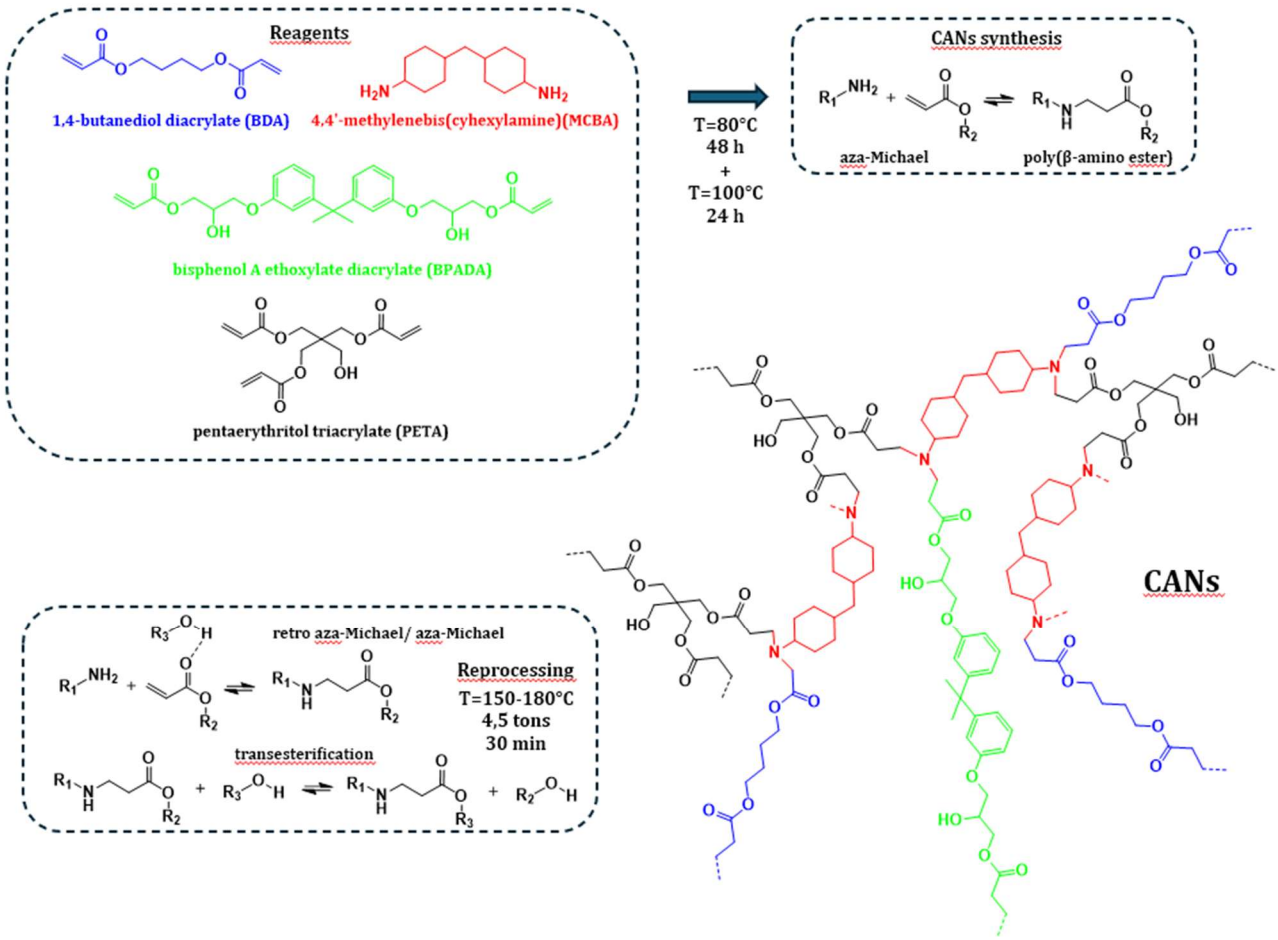

Figura 50. *Comprehensive schematic overview of the reagents, polymerization chemistry, and reforming loop of the VIT.PETA.X.Y.Z covalent adaptable networks (CANs).*

To evaluate how compositional changes influence the macroscopic behavior of the material, several formulations were prepared by maintaining a constant stoichiometric balance, characterized by an initial molar ratio between the total acrylic groups and amine functional groups equal to 2. Within this structural framework, the mass percentages of the acrylic components were systematically adjusted by varying the concentration of the trifunctional PETA from 5 wt% to 80 wt% and modifying the concentration of the rigid BPADA spacer accordingly from 0 wt% to 75 wt%, while the weight fraction of BDA was strictly maintained at a fixed baseline of 20 wt% across all mixtures. The synthesis protocol was conducted through a controlled thermal cycle to ensure full network conversion via the aza-Michael addition, executing the reaction at 80 °C for 48 hours, followed by a post-curing stage at 100 °C for 24 hours. To track and differentiate these hybrid networks, a systematic nomenclature was

adopted whereby the samples were designated as VIT.PETA.X.Y.Z, where X represents the mass percentage of PETA, Y represents the mass percentage of BDA (which is consistently 20), and Z represents the mass percentage of BPADA.

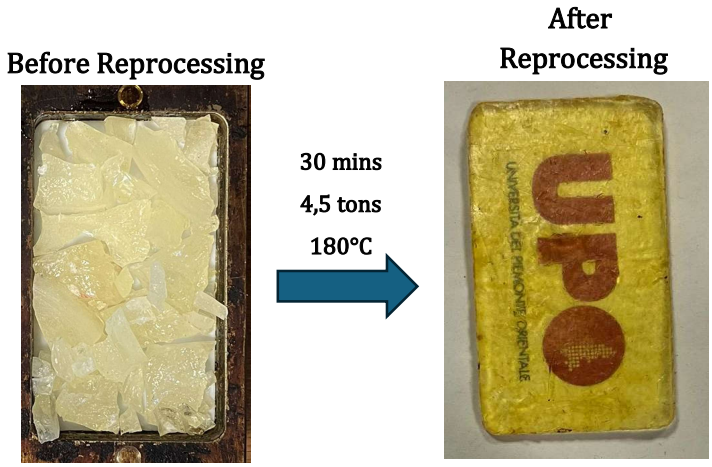

Figure 51. *Reprocessing of the four-component (VIT.PETA.75.20.5).*

All samples were reprocessed with the previously described approach and as illustrated in Fig.51, the reprocessing tests yielded outstanding results across all formulated materials, successfully confirming their inherent reprocessability. However, a closer look at Tab.17 and Fig.52, where a vertical dotted line marks the 50 wt% PETA threshold relative to the BDA and BPADA matrices, reveals a clear composition-dependent behavior. Specifically, all samples containing less than 50 wt% of PETA were efficiently reprocessed at 150 °C. In contrast, formulations exceeding this 50 wt% limit required a higher temperature of 180 °C to undergo successful reprocessing. This phenomenon indicates that increasing the percentage of the trifunctional PETA monomer significantly rigidifies the polymer network by increasing its crosslinking density. Consequently, the system demands either higher reprocessing temperatures to accelerate the dynamic bond exchange or, alternatively, extended processing times if maintained at 150 °C.

Table 17. *Reprocessing time ($t_{reprocessing}$) and temperature ($T_{reprocessing}$)conditions for the VIT.PETA.2.1 sample serie.*

Sample name	$t_{reprocessing}$(min)	$T_{reprocessing}$(°C)
VIT.PETA.2.1.80.20	30	180
VIT.PETA.2.1.75.20.5	30	180
VIT.PETA.2.1.70.20.10	30	180
VIT.PETA.2.1.60.20.20	30	180
VIT.PETA.2.1.40.20.40	30	150
VIT.PETA.2.1.20.20.60	30	150
VIT.PETA.2.1.10.20.70	30	150
VIT.PETA.2.1.5.20.75	30	150

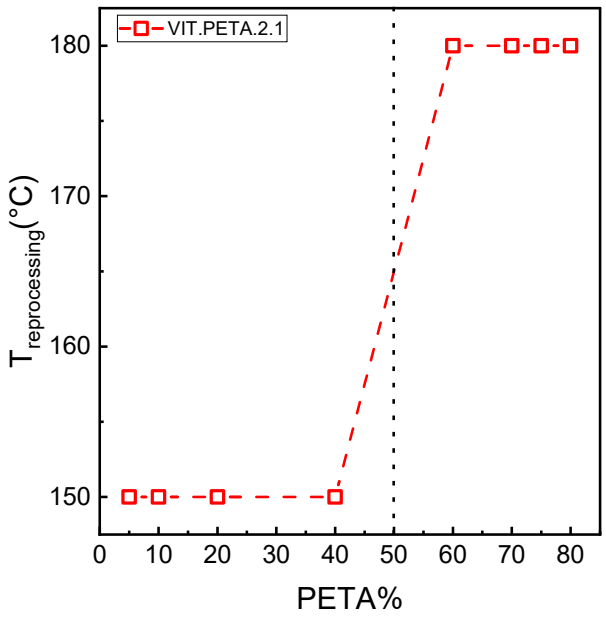

Figura 52. *Reprocessing temperature ($T_{reprocessing}$) conditions for the VIT.PETA.2.1 sample serie as a function of PETA% mass fraction relative to total acrylic monomers.*

4.5.2 Solubility and swelling tests

This section presents the results of the solubility and swelling tests conducted in THF, which were performed to confirm the effective crosslinking of the network and to evaluate its swelling degree (as thoroughly detailed in the experimental section). The quantitative data and the corresponding graphic trends are summarized and illustrated in the following Tab.18 and Fig.53.

Table 18. *Results of soluble fraction (SF%) and swelling degree (SD%), for the analyzed sample serie VIT.PETA.2.1.*

Sample name	SF%	SD%
VIT.PETA.2.1.80.20	0.59	12.49
VIT.PETA.2.1.75.20.5	0	13.62
VIT.PETA.2.1.70.20.10	0.30	31.62
VIT.PETA.2.1.60.20.20	0.37	16.95
VIT.PETA.2.1.40.20.40	1.35	41.30
VIT.PETA.2.1.20.20.60	1.80	64.74
VIT.PETA.2.1.10.20.70	1.73	80.23
VIT.PETA.2.1.5.20.75	8.34	202.51

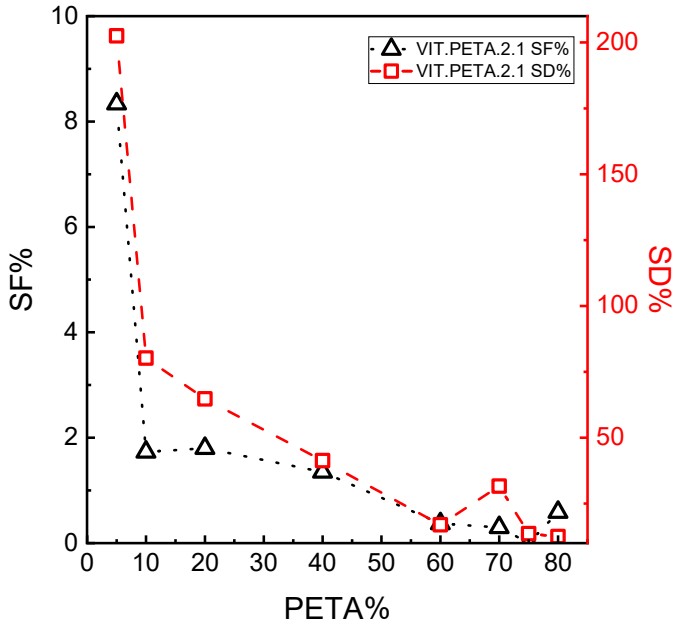

Figure 53. *Soluble fraction (SF%, left axis) and swelling degree (SD%, right axis) as a function of PETA% mass fraction relative to total acrylic monomers, for the analyzed sample serie.*

Based on the obtained results, all investigated samples with the sole exception of the 5 wt% PETA formulation, which exhibits a slightly higher soluble fraction demonstrate outstanding chemical resistance, indicating the successful formation of a well-developed polymer network. A closer inspection of the trends reveals that both the swelling degree (SD%, right y-axis) and the soluble fraction (SF%, left y-axis) systematically increase as the PETA content decreases. This behavior strongly corroborates the findings previously discussed in the reprocessing section; a higher percentage of the trifunctional PETA monomer increases the overall crosslinking density, resulting in a more rigid and dense network architecture that significantly restricts solvent penetration and limits structural expansion.

4.5.3 Thermal characterization of amine-acrylic CANs four component

This section discusses the thermal and dynamic mechanical properties of the synthesized materials, focusing on the determination of their glass transition temperatures (T_g) via Differential Scanning Calorimetry (DSC) and Dynamic Mechanical Analysis (DMA). In accordance with the protocols thoroughly detailed in the experimental section, both characterizations were systematically performed on the various samples across the investigated series. The compiled quantitative data and the corresponding experimental profiles are summarized, illustrated, and compared in the following Tab.19 and Fig.54.

Table 19. *Glass transition temperatures (T_g) of the analyzed samples determined via DSC (before and post-reprocessing) and DMA. For the DMA analysis, the T_g was evaluated at the maximum peak of the loss factor ($tan\ (\delta)$).*

Sample name	**T_g(°C) DSC** (**before reprocessing**)	**T_g(°C) DSC** (**post reprocessing**)	**T_g(°C) DMA** (**max tan(δ)peak**)
VIT.PETA.2.1.80.20	96.0	71.9	82.4
VIT.PETA.2.1.75.20.5	91.4	68.0	83.3
VIT.PETA.2.1.70.20.10	89.0	67.0	82.1
VIT.PETA.2.1.60.20.20	87.8	70.0	79.3
VIT.PETA.2.1.40.20.40	79.4	51.0	57.0
VIT.PETA.2.1.20.20.60	76.0	54.0	69.7
VIT.PETA.2.1.10.20.70	67.4	50.0	57.8
VIT.PETA.2.1.5.20.75	62.5	51.0	59.5

It is important to specify that the $T_g$values reported in the table were determined exclusively from the first heating scan of the three-ramp thermal cycle detailed in the experimental section. This choice is fundamentally dictated by the thermal behavior and dynamic nature of the network; as previously detailed in Section 4.4.3, exposure to elevated temperatures (above 100 °C) triggers the retro aza-Michael reaction. This thermally induced, reversible cleavage promotes a transient rearrangement of the covalent bonds, temporarily modifying the original

network architecture and enabling the topological flow required for reprocessing.

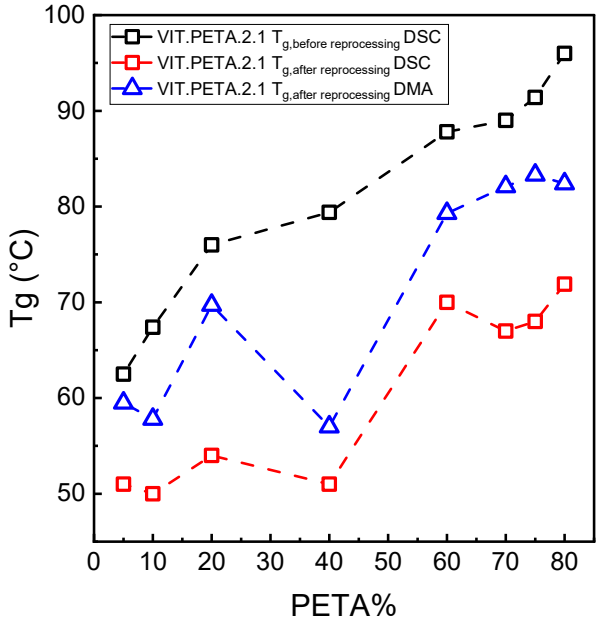

Figure 54. *Glass transition temperature (T_g) as a function of PETA% mass fraction relative to total acrylic monomers, for the analyzed sample seriebefore and after reprocessing. Squares black: DSC derived values before reprocessing, squares red: DSC derived values after reprocessing and triangles blue: DMA derived values after reprocessing.*

The characterization procedures are thoroughly detailed in the experimental section. As illustrated in Fig.54, a distinct correlation is observed between the network composition and its thermal properties; specifically, increasing the weight percentage of PETA leads to a progressive upward shift in the glass transition temperature (T_g) of the pristine material (black curve). This trend firmly corroborates the conclusions drawn in the preceding sections, confirming that a higher content of the trifunctional monomer increases the network's crosslinking density and overall structural rigidity, thereby restricting segmental chain mobility. Regarding the reprocessed samples, the curves obtained from both DSC (red curve) and DMA (blue curve) analyses exhibit a strong correlation, proving an excellent match between the two characterization techniques. Despite minor local fluctuations, most notably the deviation observed at 40 wt% PETA, both post-reprocessing profiles successfully

preserve the overall ascending trend as a function of PETA content. Nevertheless, a direct comparison between the pre- and post-reprocessing DSC curves reveals a distinct downshift in the glass transition temperature, which decreases on average by approximately 20 °C after processing. Consistent with findings observed for the other material formulations, this systematic drop can be ascribed to the intensive mechanical grinding and thermal stress required during the recycling step. These processes inevitably induce a minor degree of chain scission or permanent topological disruption within the network, resulting in an increased free volume or a slight reduction in the effective crosslinking density of the reprocessed matrix.

4.5.4 Dynamic mechanical analysis (DMA)

In addition to determining the glass transition temperature (T_g) as discussed in Section 4.6.3, Dynamic Mechanical Analysis (DMA) was instrumental in comparing the storage modulus (E') of the synthesized materials below the glass transition region, specifically evaluated at 0 °C. Due to instrumental torque limitations, the storage modulus could not be reliably evaluated above the glass transition for several formulations, as the drastic softening of the networks upon entering the rubbery state yielded force values below the minimum sensitivity threshold of the instrument. Consequently, the analysis focuses exclusively on the glassy state properties, the trends of which are summarized and compared in Tab.25 and Fig.55. All experimental parameters regarding this characterization have been accurately described in Section 3.7.4.

Table 20. *Storage modulus (E') values evaluated at 0 °C ($E'_{0°C}$) for the investigated serie of synthesized vitrimer formulations, determined via DMA analysis in three-point bending mode.*

Sample name	$\mathbf{E'_{0°C}(Pa)}$
VIT.PETA.2.1.80.20	$1.80 \cdot 10^9$
VIT.PETA.2.1.75.20.5	$7.15 \cdot 10^8$
VIT.PETA.2.1.70.20.10	$1.06 \cdot 10^9$
VIT.PETA.2.1.60.20.20	$1.27 \cdot 10^9$
VIT.PETA.2.1.40.20.40	$1.35 \cdot 10^9$
VIT.PETA.2.1.20.20.60	$1.66 \cdot 10^9$
VIT.PETA.2.1.10.20.70	$1.13 \cdot 10^9$
VIT.PETA.2.1.5.20.75	$4.60 \cdot 10^8$

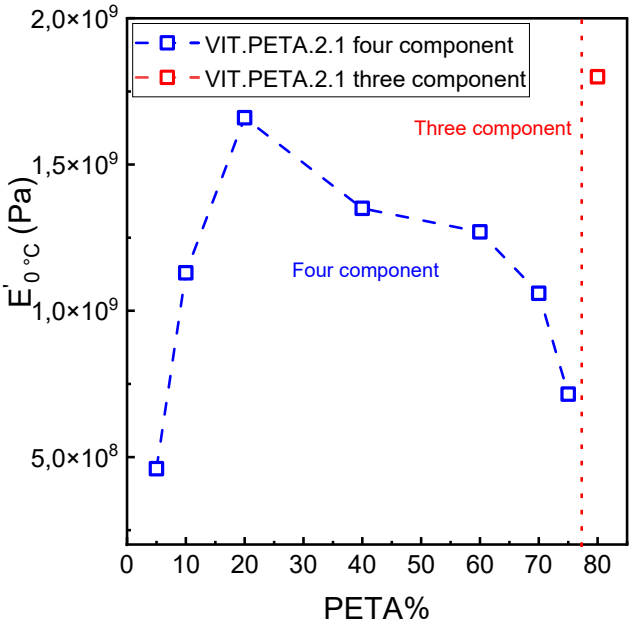

Figura 55. *Storage modulus values evaluated at 0 °C ($E'_{0°C}$, blue curves, left axis) and 150 °C ($E'_{0°C}$, red curves, right axis) as a function of the acrylic-to-amine functional group ratio ($\frac{n_{acrylic\ groups}}{n_{amine\ groups}}$) for the two investigated vitrimer series, determined via DMA analysis in three-point bending mode.*

The Fig.55 illustrates the storage modulus measured at 0 °C ($E'_{0°C}$), well below the glass transition temperature (T_g), plotted against the PETA content (PETA%) for the VIT.PETA.2.1 vitrimer series. First and foremost, it must be emphasized that the storage modulus values across the entire series are remarkably similar, all hovering around 1 GPa. Consequently, the subtle fluctuations observed among the samples are minor, meaning that the structural justifications outlined below must be treated purely as tentative, unconfirmed hypotheses rather than definitive physical phenomena. The graph clearly distinguishes between the four-component covalent adaptable networks (CANs) and the unique three-component formulation. This latter system, corresponding to the VIT.PETA.2.1.80.20 sample, is positioned in red to the right of the vertical dotted line and contains only PETA and BDA, completely omitting the BPADA monomer. It exhibits the highest glassy modulus of the entire series, approaching $1.8 \cdot 10^9$ Pa. This superior stiffness in the glassy state is directly related to its composition; by completely removing the long, bulky BPADA spacer, the

system eliminates the steric incompatibility and structural frustration that limits the curing efficiency in the four-component blends. This allows the small, highly multifunctional PETA molecules to pack tightly and react fully with the BDA crosslinker, creating an ultra-dense, homogeneous covalent skeleton with an extremely low molecular weight between crosslinks (M_c) whose sheer physical compactness easily overcomes the lower density of hydrogen-bonding hydroxyl groups compared to the BPADA-containing formulations. Conversely, the four-component CANs, represented by the blue markers, display a non-monotonic, parabolic trend with increasing PETA concentration. This distinct bell-shaped behavior can be attributed to a competitive equilibrium between two opposing structural factors: the increase in covalent crosslinking density versus the loss of secondary non-covalent interactions. In the low-concentration regime, moving from 5% PETA to the maximum peak at 20% PETA ($1.67 \cdot 10^9$ Pa), the storage modulus scales up sharply due to the dominant reinforcing effect of PETA, which successfully increases the covalent reticulation of the matrix. Beyond this 20% threshold, however, a progressive and continuous decrease in $E'_{0°C}$ is observed, reaching its lowest value at 75% PETA. This downward trend is driven by the fact that increasing the PETA content drastically reduces the relative fraction of BPADA within the formulation. Because BPADA possesses two hydroxyl groups per molecule and heavily contributes to the formation of physical hydrogen bonds and intermolecular packing interactions, its sharp dilution causes a severe drop in the overall H-bond density of the network. Below the glass transition temperature, these secondary physical interactions are crucial for restricting local cooperative chain movements; when their concentration falls too low, the material loses its glassy cohesiveness, overriding the stiffening effect of the covalent crosslinks. Therefore, the maximum at 20% PETA represents the optimal synergetic compromise where the network benefits from an enhanced covalent crosslinking density without drastically sacrificing the physical hydrogen-bonding network provided by the BPADA component.

4.5.5 Stress relaxation analysis

Stress relaxation analyses were performed to determine the characteristic relaxation times (τ) of the different formulations. The specific testing parameters, along with the experimental methodology and the criteria adopted to evaluate the relaxation behavior, are thoroughly detailed in Section 3.5.3. Furthermore, the temperature dependence of these relaxation times was exploited to determine the activation energy (E_a) of the dynamic network rearrangement. The theoretical framework for the calculation of τ and the linear regression methodology based on the Arrhenius equation are comprehensively described in Section 3.5.3 and Section 3.7.3, respectively. The comprehensive experimental outcomes of this characterization, encompassing both the relaxation times and the calculated activation energies, are summarized and illustrated in Tab.21 and Fig.56-57.

Table 21. *Characteristic relaxation times (τ) at 150 °C, 165 °C and 180°C for the investigated sample serie, determined from isothermal stress relaxation analyses.*

Sample name	$\tau_{150°C}(s)$	$\tau_{165°C}(s)$	$\tau_{180°C}(s)$	$E_a(\frac{kJ}{mol})$
VIT.PETA.2.1.80.20	402	62	22	155.9
VIT.PETA.2.1.75.20.5	387	53	23	151.2
VIT.PETA.2.1.70.20.10	293	49	24	134.2
VIT.PETA.2.1.60.20.20	226	41	25	117.0
VIT.PETA.2.1.40.20.40	91	35	6	166.1
VIT.PETA.2.1.20.20.60	81	32	6	133.8
VIT.PETA.2.1.10.20.70	80	17	5	146.4
VIT.PETA.2.1.5.20.75	80	15	4	159.4

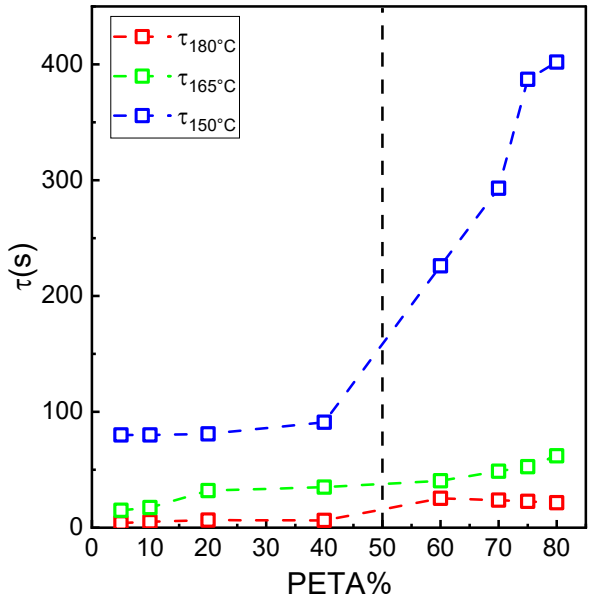

Figure 56. *Characteristic relaxation times (τ) at 150°C, 165°C and 180 °C as a function of PETA% mass fraction relative to total acrylic monomers for the investigated sample serie, determined from isothermal stress relaxation analyses.*

The Fig.56 illustrates the characteristic relaxation times (τ) of the VIT.PETA.2.1 vitrimer series plotted against the PETA content (PETA%) at three distinct isotherms (150 °C, 165 °C, and 180 °C). As expected, a conventional thermal behavior is observed across all formulations, where increasing the temperature from 150 °C (blue curve) to 180 °C (red curve) induces a significant drop in the relaxation times. This confirms a classic Arrhenius-like, thermally activated process where higher thermal energy accelerates the dynamic bond exchange kinetics.

Regarding the compositional effect, the curves display two remarkably distinct regimes across all investigated temperatures. Below 50% PETA (vertical black dot line is the 50%), the characteristic relaxation times remain virtually constant and independent of the PETA concentration, indicating that the network topology allows for sufficient cooperative chain mobility and that minor compositional adjustments do not restrict the macroscopic stress relaxation rate. Conversely, a strong positive dependence emerges above 50% PETA, where τ scales up sharply with increasing PETA content, reaching its peak value for the three-component

VIT.PETA.2.1.80.20 system. This phenomenon can be attributed to the multifunctional nature of PETA, which drastically increases the crosslinking density and induces severe steric hindrance, thereby restricting the free volume and slowing down the cooperative chain segment rearrangements necessary to complete the bond exchange. Notably, this pronounced upward trend is highly visible at 150 °C, whereas the curves become significantly flattened at 165 °C and 180 °C. This behavior suggests that at elevated temperatures, the bond exchange kinetics approach a maximum rate plateau (corresponding to a minimum threshold for τ), which drastically diminishes the network's sensitivity to both compositional changes and further temperature increases.

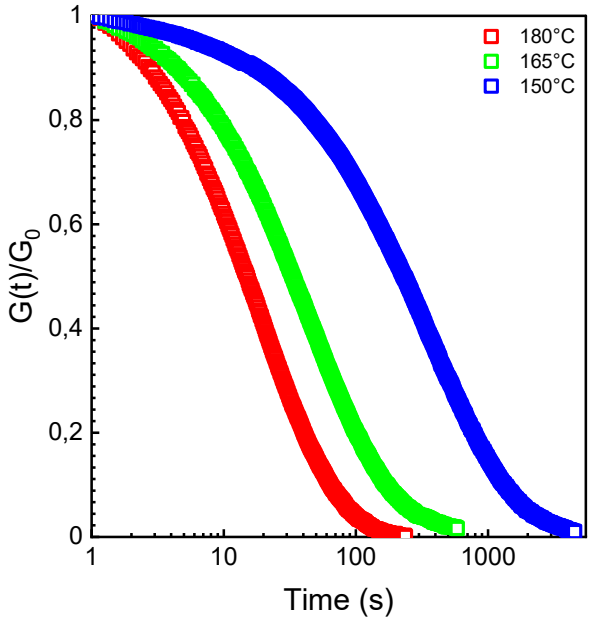

Figure 57. *Normalized relaxation modulus ($\frac{G(t)}{G_0}$) as a function of time (on a logarithmic scale) at 150 °C, 165°C and 180 °C for the VIT.PETA(2.1)(75.20.5).*

Fig.57 displays the representative stress relaxation curves ($\frac{G(t)}{G_0}$ as a function of time) for the VIT.PETA.75.20.5 sample measured at 150 °C, 165 °C, and 180 °C. The curves exhibit a well-defined and complete decay of the normalized modulus, where the progressive shift of the isotherms toward shorter timescales with increasing temperature confirms the expected clean, thermally activated kinetics of the dynamic network rearrangement.

Notably, the temperature-induced acceleration is significantly more pronounced when transitioning from 150 °C to 165 °C than from 165 °C to 180 °C.

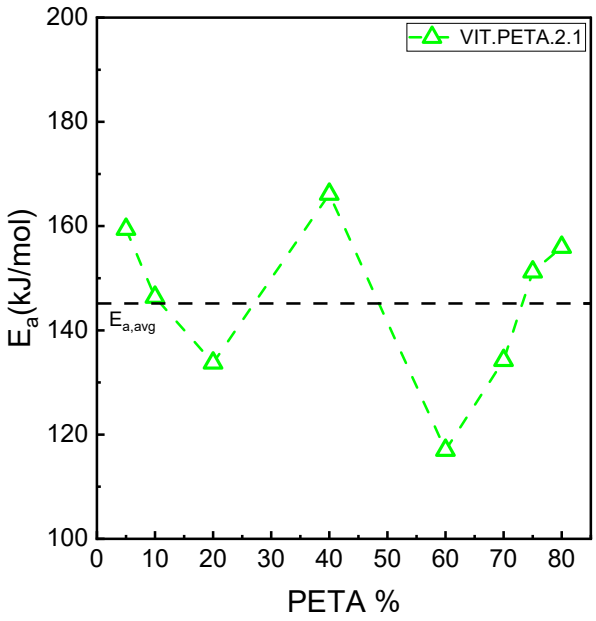

Figure 58. *Activation energy (E_a) of the VIT.PETA.2.1 series as a function of PETA% mass fraction relative to total acrylic monomers. The dashed horizontal line indicates the calculated average value ($E_{a,avg} \approx 145 \frac{kJ}{mol}$).*

The activation energy (E_a) profile of the VIT.PETA.2.1 vitrimer series plotted against the PETA content is displayed in Fig. 58, where a dashed horizontal line highlights the calculated average activation energy. From a methodological standpoint, it should be emphasized that utilizing a standard linear Arrhenius approach to extract a single E_a value is not strictly rigorous for this system, given the concurrent presence of two distinct dynamic chemistry pathways. Nevertheless, this remains the standard and widely accepted practice currently adopted in the literature.

The experimental E_a values obtained for the VIT.PETA.2.1 series exhibit an average value ($E_{a,avg} \approx 154 \frac{kJ}{mol}$) perfectly in line with data reported in the literature for similar poly(β-amino ester) networks[13,52]. Within this network, stress relaxation is governed by the coexistence of transesterification and retro-aza-Michael exchange, whose relative

contributions shift dynamically as a function of structural and compositional variations[13,37,46,53]. At lower PETA concentrations, which correspond to higher BPADA fractions, the density of hydroxyl groups (-OH) significantly increases, thereby promoting and enhancing the weight of the transesterification pathway[13]. Transesterification is likely the prevailing reaction in this regime, as it typically possesses a lower activation energy barrier compared to its retro-aza-Michael counterpart[52]. Conversely, as the PETA content increases, the system becomes highly crosslinked, leading to an elevated crosslinking density characterized by a prominent concentration of both dynamic retro-aza-Michael linkages and rigid, acrylate-derived backbones.

Crucially, the E_a profile shows only minor fluctuations around its average value across the entire investigated compositional range. This stability indicates that the intrinsic chemical energy barrier required to activate the bond exchange mechanisms remains fundamentally unaltered. Consequently, the remarkably distinct regimes and the sharp variations in macroscopic relaxation times (τ) observed as a function of PETA percentage (Fig.56) are not dictated by shifts in E_a. Instead, they can be primarily ascribed to variations in the pre-exponential frequency factor (τ_0). It is the alteration of τ_0, which directly reflects the local topological constraints, steric hindrance, and reduced free volume of the heavily crosslinked PETA network, that ultimately modulates the macroscopic rate of stress relaxation.

The detailed experimental and mathematical procedure utilized to extract these activation energy values from the stress relaxation isotherms is thoroughly described in Chapter 3.7.3.

Finally, Fig.53 displays representative Arrhenius plots (ln (τ) versus $\frac{1}{T}$) for selected samples VIT.PETA.80.20 and VIT.PETA.10.20.70 of the synthesized series, illustrating the linear regressions used to determine the activation energies (E_a).

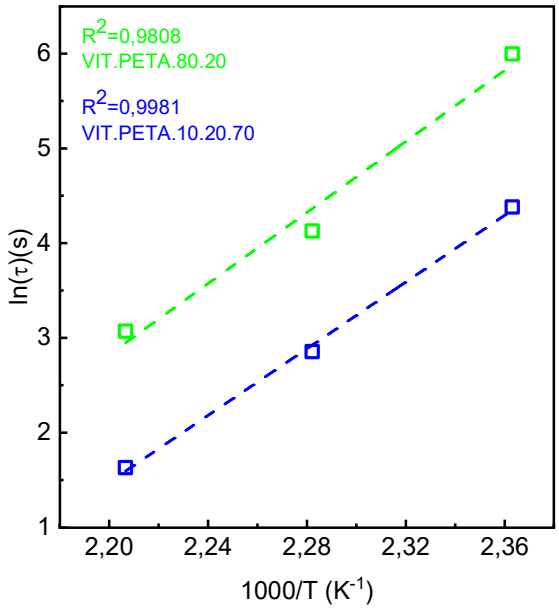

Figure 53. *Representative Arrhenius plots (ln τ versus 1000/T) and relative linear regressions for selected vitramer samples of the VIT.PETA.2.1 series, used to determine the corresponding activation energies (E_a).*

5. Conclusions

The aza-Michael reaction has proven to be an extremely effective synthetic platform for the development of adaptable polymer networks, ensuring 100% atom economy and the absence of toxic byproducts. However, the introduction of a monomer for free-radical polymerization highlighted contrasting results: while the use of methyl methacrylate (MMA) yielded unsatisfactory outcomes due to extremely slow reprocessing kinetics, the use of hydroxyethyl methacrylate (HEMA) proved to be the solution. This success is attributed to the presence of hydroxyl (-OH) groups, which exert a marked catalytic effect on the aza-Michael addition and establish a dense network of hydrogen bonds.

It was observed that increasing the HEMA content and the stoichiometric ratio between acrylic and amine groups act synergistically to raise the glass transition temperature (T_g) of the system, optimizing network stiffness while maintaining excellent reprocessing properties. Detailed kinetic investigations via NMR and rheology revealed an extremely rapid oligomer formation, reaching conversions above 78% in just five minutes. Nonetheless, a persistent residual reactivity was identified, which currently prevents long-term storage of the pre-polymer formed in the first reaction step, necessitating strict temporal management prior to final crosslinking.

A technological hurdle currently being addressed is the use of the radical initiator I, which releases nitrogen gas upon decomposition, creating undesirable macroscopic porosity within the network; research is now focused on replacing I with alternative thermal or photochemical initiators. In parallel, studies on systems without radical monomers showed that introducing a higher-functionality monomer like PETA significantly increases T_g by raising the matrix's crosslinking density. It was found, however, that increasing the PETA fraction in this series leads to longer relaxation times and higher reprocessing temperatures, particularly when the PETA content exceeds 50 wt% of the total acrylic mass, due to steric hindrance that slows dynamic bond exchange.

Finally, within the SMIP project, the material demonstrated mechanical properties and chemical recyclability via selective solvolysis that are ideal for microelectronic supports. Building on these results, current research is focusing on enhancing the network's compression properties by incorporating inorganic nanoparticles such as alumina or silica, leading to the development of advanced composite materials with even higher performance and structural stability.

6. Bibliography

(1) Scheutz, G. M.; Lessard, J. J.; Sims, M. B.; Sumerlin, B. S. Adaptable Crosslinks in Polymeric Materials: Resolving the Intersection of Thermoplastics and Thermosets. *J. Am. Chem. Soc.* **2019**, *141* (41), 16181–16196. https://doi.org/10.1021/jacs.9b07922.

(2) Van Zee, N. J.; Nicolaÿ, R. Vitrimers: Permanently Crosslinked Polymers with Dynamic Network Topology. *Progress in Polymer Science* **2020**, *104*, 101233. https://doi.org/10.1016/j.progpolymsci.2020.101233.

(3) Guerre, M.; Taplan, C.; Winne, J. M.; Du Prez, F. E. Vitrimers: Directing Chemical Reactivity to Control Material Properties. *Chem. Sci.* **2020**, *11* (19), 4855–4870. https://doi.org/10.1039/D0SC01069C.

(4) Zheng, J.; Png, Z. M.; Ng, S. H.; Tham, G. X.; Ye, E.; Goh, S. S.; Loh, X. J.; Li, Z. Vitrimers: Current Research Trends and Their Emerging Applications. *Materials Today* **2021**, *51*, 586–625. https://doi.org/10.1016/j.mattod.2021.07.003.

(5) Winne, J. M.; Leibler, L.; Du Prez, F. E. Dynamic Covalent Chemistry in Polymer Networks: A Mechanistic Perspective. *Polym. Chem.* **2019**, *10* (45), 6091–6108. https://doi.org/10.1039/C9PY01260E.

(6) Ye, G.; Wang, C.; Guo, Y.; Yang, Q.; Huo, S. Vitrimer as a Sustainable Alternative to Traditional Thermoset: Recent Progress and Future Prospective. *ACS Polym. Au* **2025**, *5* (5), 445–457. https://doi.org/10.1021/acspolymersau.5c00081.

(7) Podgórski, M.; Fairbanks, B. D.; Kirkpatrick, B. E.; McBride, M.; Martinez, A.; Dobson, A.; Bongiardina, N. J.; Bowman, C. N. Toward Stimuli-Responsive Dynamic Thermosets through Continuous Development and Improvements in Covalent Adaptable Networks (CANs). *Advanced Materials* **2020**, *32* (20), 1906876. https://doi.org/10.1002/adma.201906876.

(8) Jourdain, A.; Asbai, R.; Anaya, O.; Chehimi, M. M.; Drockenmuller, E.; Montarnal, D. Rheological Properties of Covalent Adaptable Networks with 1,2,3-Triazolium Cross-Links: The Missing Link between Vitrimers and

Dissociative Networks. *Macromolecules* **2020**, *53* (6), 1884–1900. https://doi.org/10.1021/acs.macromol.9b02204.

(9) Montarnal, D.; Capelot, M.; Tournilhac, F.; Leibler, L. Silica-Like Malleable Materials from Permanent Organic Networks. *Science* **2011**, *334* (6058), 965–968. https://doi.org/10.1126/science.1212648.

(10) Capelot, M.; Unterlass, M. M.; Tournilhac, F.; Leibler, L. Catalytic Control of the Vitrimer Glass Transition. *ACS Macro Lett.* **2012**, *1* (7), 789–792. https://doi.org/10.1021/mz300239f.

(11) Capelot, M.; Unterlass, M. M.; Tournilhac, F.; Leibler, L. Catalytic Control of the Vitrimer Glass Transition. *ACS Macro Lett.* **2012**, *1* (7), 789–792. https://doi.org/10.1021/mz300239f.

(12) Capelot, M.; Montarnal, D.; Tournilhac, F.; Leibler, L. Metal-Catalyzed Transesterification for Healing and Assembling of Thermosets. *J. Am. Chem. Soc.* **2012**, *134* (18), 7664–7667. https://doi.org/10.1021/ja302894k.

(13) Lee, G.; Song, H. Y.; Choi, S.; Kim, C. B.; Hyun, K.; Ahn, S. Harnessing β-Hydroxyl Groups in Poly(β-Amino Esters) toward Robust and Fast Reprocessing Covalent Adaptable Networks. *Macromolecules* **2022**, *55* (23), 10366–10376. https://doi.org/10.1021/acs.macromol.2c01872.

(14) Zheng, J.; Png, Z. M.; Ng, S. H.; Tham, G. X.; Ye, E.; Goh, S. S.; Loh, X. J.; Li, Z. Vitrimers: Current Research Trends and Their Emerging Applications. *Materials Today* **2021**, *51*, 586–625. https://doi.org/10.1016/j.mattod.2021.07.003.

(15) Kloxin, C. J.; Bowman, C. N. Covalent Adaptable Networks: Smart, Reconfigurable and Responsive Network Systems. *Chem. Soc. Rev.* **2013**, *42* (17), 7161–7173. https://doi.org/10.1039/C3CS60046G.

(16) Leung, W. H.; Leitao, E. M.; Verbeek, C. J. R. Polyester Transesterification through Reactive Blending and Its Applications: A Comprehensive Review. *Polymer* **2025**, *329*, 128488. https://doi.org/10.1016/j.polymer.2025.128488.

(17) H. Otsuka, Polym. J. 2013, 45, 879; b) K. Jin, L. Li, J. M. Torkelson, Adv. Mater. 2016, 28, 6746; c) Q. An, I. D. Wessely, Y. Matt, Z. Hassan, S. Bräse, M. Tsotsalas, Polym. Chem. 2019, 10, 672.

(18) J. P. Brutman, D. J. Fortman, G. X. De Hoe, W. R. Dichtel, M. A. Hillmyer, J. Phys. Chem. B 2019, 123, 1432.

(19) N. Kuhl, R. Geitner, J. Vitz, S. Bode, M. Schmitt, J. Popp, U. S. Schubert, M. D. Hager, J. Appl. Polym. Sci. 2017, 134, 44805;

(20) Collins, S.; Peace, S. K.; Richards, R. W.; MacDonald, W. A.; Mills, P.; King, S. M. Transesterification in Poly(Ethylene Terephthalate). Molecular Weight and End Group Effects. *Macromolecules* **2000**, *33* (8), 2981–2988. https://doi.org/10.1021/ma991637+.

(21) Zhou, L.; Zhao, G.; Jiang, W. Effects of Catalytic Transesterification and Composition on the Toughness of Poly(Lactic Acid)/Poly(Propylene Carbonate) Blends. *Ind. Eng. Chem. Res.* **2016**, *55* (19), 5565–5573. https://doi.org/10.1021/acs.iecr.6b00315.

(22) Kenwright, A. M.; Peace, S. K.; Richards, R. W.; Bunn, A.; MacDonald, W. A. Transesterification in Poly(Ethylene Terephthalate) and Poly(Ethylene Naphthalene 2, 6-Dicarboxylate) Blends; the Influence of Hydroxyl End Groups. *Polymer* **1999**, *40* (21), 5851–5856. https://doi.org/10.1016/S0032-3861(98)00806-4.

(23) Snyder, R. L.; Fortman, D. J.; De Hoe, G. X.; Hillmyer, M. A.; Dichtel, W. R. Reprocessable Acid-Degradable Polycarbonate Vitrimers. *Macromolecules* **2018**, *51* (2), 389–397. https://doi.org/10.1021/acs.macromol.7b02299.

(24) Alexandrova, L.; Cabrera, A.; Hernández, M. A.; Cruz, M. J.; Abadie, M. J. M.; Manero, O.; Likhatchev, D. Transesterification in Poly(Ethylene Terephthalate) and Poly(Ethylene Naphthalate 2,6-Dicarboxylate) Blends: Model Compounds Study. *Polymer* **2002**, *43* (20), 5397–5403. https://doi.org/10.1016/S0032-3861(02)00348-8.

(25) Lai, W.; Wu, G. Reactive Blending and Transesterification-Induced Degradation of Isosorbide-Based Polycarbonate Blends. *Polymer Degradation and Stability* **2019**, *162*, 201–212. https://doi.org/10.1016/j.polymdegradstab.2019.02.020.

(26) Lai, W.; Su, L.; Zhang, M.; Yan, J.; Wu, G. Tuning the Optical Clarity of Glass Fiber-reinforced Polycarbonates by Reactive Blending with Alternatives from Biorenewable Isosorbide. *J. Polym. Sci. Part A: Polym. Chem.* **2019**, *57* (15), 1670–1681. https://doi.org/10.1002/pola.29432.

(27) Yang, R.; Xu, G.; Lv, C.; Dong, B.; Zhou, L.; Wang, Q. $Zn(HMDS)_2$ as a Versatile Transesterification Catalyst for Polyesters Synthesis and Degradation toward a Circular Materials Economy Approach. *ACS Sustainable Chem. Eng.* **2020**, *8* (50), 18347–18353. https://doi.org/10.1021/acssuschemeng.0c07595.

(28) Fortunato, B.; Munari, A.; Manaresi, P.; Monari, P. Inhibiting Effect of Phosphorus Compounds on Model Transesterification and Direct Esterification Reactions Catalysed by Titanium Tetrabutylate: 2. *Polymer* **1994**, *35* (18), 4006–4010. https://doi.org/10.1016/0032-3861(94)90287-9.

(29) Román-Leshkov, Y.; Davis, M. E. Activation of Carbonyl-Containing Molecules with Solid Lewis Acids in Aqueous Media. *ACS Catal.* **2011**, *1* (11), 1566–1580. https://doi.org/10.1021/cs200411d.

(30) Fiorini, M.; Pilati, F.; Berti, C.; Toselli, M. Reactive Blending of Poly(Ethylene Terephthalate) and bisphenoI-A Polycarbonate: Effect of Various Catalysts and Mixing Time on the Extent of Exchange Reactions.

(31) Zhang, P.; Yin, P.; Yang, L.; Cui, X.; Xing, H.; Suo, X. Recent Advances and Challenges in Ionic Materials for Post-Combustion Carbon Capture. *Carbon Capture Science & Technology* **2024**, *11*, 100180. https://doi.org/10.1016/j.ccst.2023.100180.

(32) Huczynski, A.; Brzezinski, B.; Furukawa, T. 1,5,7-Triazabicyclo[4.4.0]Dec-5-Ene[1]. In *Encyclopedia of Reagents for Organic*

Synthesis; John Wiley & Sons, Ltd: Chichester, UK, 2014; pp 1–8. https://doi.org/10.1002/047084289X.rn00786.pub2.

(33) Luo, Z.-X.; Tian, G.-Q.; Chen, S.-C.; Wu, G.; Wang, Y.-Z. Solvent-Free One-Pot Recycling of Polylactide to Usable Polymers and Their Closed-Loop Recyclability. *Macromolecules* **2024**, *57* (14), 6828–6837. https://doi.org/10.1021/acs.macromol.4c01104.

(34) Self, J. L.; Dolinski, N. D.; Zayas, M. S.; Read De Alaniz, J.; Bates, C. M. Brønsted-Acid-Catalyzed Exchange in Polyester Dynamic Covalent Networks. *ACS Macro Lett.* **2018**, *7* (7), 817–821. https://doi.org/10.1021/acsmacrolett.8b00370.

(35) Taplan, C.; Guerre, M.; Du Prez, F. E. Covalent Adaptable Networks Using β-Amino Esters as Thermally Reversible Building Blocks. *J. Am. Chem. Soc.* **2021**, *143* (24), 9140–9150. https://doi.org/10.1021/jacs.1c03316.

(36) Peyrton, J.; Avérous, L. Aza-Michael Reaction as a Greener, Safer, and More Sustainable Approach to Biobased Polyurethane Thermosets. *ACS Sustainable Chem. Eng.* **2021**, *9* (13), 4872–4884. https://doi.org/10.1021/acssuschemeng.1c00312.

(37) Nguyen, L. T.; Mertens, C.; Du Prez, F. E. Aza-Michael Chemistry for PDMS-Based Covalent Adaptable Elastomers: Design and Dual Role of the Silica Filler. *Macromolecules* **2024**, *57* (10), 4817–4825. https://doi.org/10.1021/acs.macromol.4c00023.

(38) Kim, S.; Kang, S.; Kim, G.; Lee, Y. Copper-Catalyzed Aza-Michael Addition of Aromatic Amines or Aromatic Aza-Heterocycles to α,β-Unsaturated Olefins. *J. Org. Chem.* **2016**, *81* (10), 4048–4057. https://doi.org/10.1021/acs.joc.6b00341.

(39) Ying, A.; Li, Z.; Yang, J.; Liu, S.; Xu, S.; Yan, H.; Wu, C. DABCO-Based Ionic Liquids: Recyclable Catalysts for Aza-Michael Addition of α,β-Unsaturated Amides under Solvent-Free Conditions. *J. Org. Chem.* **2014**, *79* (14), 6510–6516. https://doi.org/10.1021/jo500937a.

(40) Desmet, G. B.; D'hooge, D. R.; Omurtag, P. S.; Espeel, P.; Marin, G. B.; Du Prez, F. E.; Reyniers, M.-F. Quantitative First-Principles Kinetic Modeling of the Aza-Michael Addition to Acrylates in Polar Aprotic Solvents. *J. Org. Chem.* **2016**, *81* (24), 12291–12302. https://doi.org/10.1021/acs.joc.6b02218.

(41) Desmet, G. B.; D'hooge, D. R.; Omurtag, P. S.; Espeel, P.; Marin, G. B.; Du Prez, F. E.; Reyniers, M.-F. Quantitative First-Principles Kinetic Modeling of the Aza-Michael Addition to Acrylates in Polar Aprotic Solvents. *J. Org. Chem.* **2016**, *81* (24), 12291–12302. https://doi.org/10.1021/acs.joc.6b02218.

(42) Taplan, C.; Guerre, M.; Du Prez, F. E. Covalent Adaptable Networks Using β-Amino Esters as Thermally Reversible Building Blocks. *J. Am. Chem. Soc.* **2021**, *143* (24), 9140–9150. https://doi.org/10.1021/jacs.1c03316.

(43) Lee, G.; Song, H. Y.; Choi, S.; Kim, C. B.; Hyun, K.; Ahn, S. Harnessing β-Hydroxyl Groups in Poly(β-Amino Esters) toward Robust and Fast Reprocessing Covalent Adaptable Networks. *Macromolecules* **2022**, *55* (23), 10366–10376. https://doi.org/10.1021/acs.macromol.2c01872.

(44) Fischer, S. M.; De Baere, I.; Nguyen, L. T.; Stecher, H.; Van Paepegem, W.; Du Prez, F. E. Scalable β-Aminoester-Based Covalent Adaptable Networks for Wind Turbine Blade Composites. *Macromolecules* **2025**, *58* (15), 7948–7956. https://doi.org/10.1021/acs.macromol.5c00958.

(45) Ivaldi, C.; Laguzzi, E.; Ospina, V. M.; Antonioli, D.; Chiarcos, R.; Campo, F.; Cuminetti, N.; De Buck, J.; Laus, M. Exploiting β-Amino Ester Chemistry to Obtain Methacrylate-Based Covalent Adaptable Networks. *Polymer* **2024**, *293*, 126636. https://doi.org/10.1016/j.polymer.2023.126636.

(46) Berne, D.; Coste, G.; Morales-Cerrada, R.; Boursier, M.; Pinaud, J.; Ladmiral, V.; Caillol, S. Taking Advantage of β-Hydroxy Amine Enhanced Reactivity and Functionality for the Synthesis of Dual Covalent Adaptable Networks. *Polym. Chem.* **2022**, *13* (25), 3806–3814. https://doi.org/10.1039/D2PY00274D.

(47) Izquierdo, S.; Cintas, P.; Durán-Valle, C. J.; De La Concepción, J. G.; López-Coca, I. M. Reinvigorating Aza-Michael Reactions under Ionic Liquid Catalysis: A Greener Approach. *Org. Biomol. Chem.* **2024**, *22* (12), 2423–2434. https://doi.org/10.1039/D3OB02006A.

(48) Baruah, R.; Kumar, A.; Ujjwal, R. R.; Kedia, S.; Ranjan, A.; Ojha, U. Recyclable Thermosets Based on Dynamic Amidation and Aza-Michael Addition Chemistry. *Macromolecules* **2016**, *49* (20), 7814–7824. https://doi.org/10.1021/acs.macromol.6b01807.

(49) Oba, Y.; Kimura, T.; Hayashi, M.; Yamamoto, K. Correlation between Self-Assembled Nanostructures and Bond Exchange Properties for Polyacrylate-Based Vitrimer-like Materials with a Trans- *N* -Alkylation Bond Exchange Mechanism. *Macromolecules* **2022**, *55* (5), 1771–1782. https://doi.org/10.1021/acs.macromol.1c02406.

(50) Lu, H.-F.; Wang, M.; Chen, X.-M.; Lin, B.-P.; Yang, H. Interpenetrating Liquid-Crystal Polyurethane/Polyacrylate Elastomer with Ultrastrong Mechanical Property. *J. Am. Chem. Soc.* **2019**, *141* (36), 14364–14369. https://doi.org/10.1021/jacs.9b06757.

(51) Konuray, A. O.; Fernández-Francos, X.; Serra, À.; Ramis, X. Sequential Curing of Amine-Acrylate-Methacrylate Mixtures Based on Selective Aza-Michael Addition Followed by Radical Photopolymerization. *European Polymer Journal* **2016**, *84*, 256–267. https://doi.org/10.1016/j.eurpolymj.2016.09.025.

(52) Taplan, C.; Guerre, M.; Du Prez, F. E. Covalent Adaptable Networks Using β-Amino Esters as Thermally Reversible Building Blocks. *J. Am. Chem. Soc.* **2021**, *143* (24), 9140–9150. https://doi.org/10.1021/jacs.1c03316.

(53) Izquierdo, S.; Cintas, P.; Durán-Valle, C. J.; De La Concepción, J. G.; López-Coca, I. M. Reinvigorating Aza-Michael Reactions under Ionic Liquid Catalysis: A Greener Approach. *Org. Biomol. Chem.* **2024**, *22* (12), 2423–2434. https://doi.org/10.1039/D3OB02006A.

(54) Berne, D.; Quienne, B.; Caillol, S.; Leclerc, E.; Ladmiral, V. Biobased Catalyst-Free Covalent Adaptable Networks Based on CF_3 -Activated

Synergistic Aza-Michael Exchange and Transesterification. *J. Mater. Chem. A* **2022**, *10* (47), 25085–25097. https://doi.org/10.1039/D2TA05067F.

(55) Nguyen, L. T.; Mertens, C.; Du Prez, F. E. Aza-Michael Chemistry for PDMS-Based Covalent Adaptable Elastomers: Design and Dual Role of the Silica Filler. *Macromolecules* **2024**, *57* (10), 4817–4825. https://doi.org/10.1021/acs.macromol.4c00023.